Orchestrating Smart Charging in mass Deployment

D4.6 Smart charging v2.0 and impact

Authors: Yunhe Yu, David Reihs, Saumitra Wagh, Aditya Shekhar, Gautham Ram, Pavol Bauer, Lehfuss Felix

Date: April 2021

"This project has received funding from the ERA-NET COFUND Electric Mobility Europe (EMEurope)"

Electric Mobility Europe

European Commission

CONTENTS

1. Introduction

1.1 Aim

The goal of this algorithm is to reduce the cost of charging EVs based on the renewable energy forecast, EV user preferences, offer of up and down regulation services and charging based on energy prices. A smart charging algorithm based on Mixed-Integer Programming (MIP) is proposed that controls the charging of an EV fleet based on the above applications.

1.2 Nomenclature

t, j, n – Optimization indices for time, electric vehicle (EV) at charger j, node index in the grid, respectively

ΔT – Time step (data resolution) (min)

T – Time duration of optimization horizon

t_{start} – Start time of the smart charging algorithm

t_{end} – End time of the smart charging algorithm

J – Number of EV chargers in the car park

$p_j^{e(ar)}$ – 'Average rate' charging power of j^{th} EV (kW)

C^{ev} – Charging costs for entire EV fleet (€)

S^{PV} – Revenue from sales of renewable power (€)

S^{as} – Revenue from sales of ancillary services (€)

C^{ar}, C^{imm}, C^{opt} – Net costs for average rate, immediate and optimized charging from PV (€)

1.3 Optimization input parameters

Electric vehicle & user parameters (index n,j: EV j at node n)

Parameter	Note	Source	Available/Protocol
$T_{n,j}^a$	– Arrival time of EV (h)	User	Elaad has prediction model Input from user (e.g. from app, considered as prediction): Not possible for now, but possible in the future; Actual arrival time can be informed to CSO through OCPP
$T_{n,j}^d$	– Departure time of EV (h)	User	Yes, at least through next version of 15118, the user can inform it, and the info will be transmitted via Electric Vehicle

			Communication Controller (EVCC, installed in EV) to the Supply Equipment Communication Controller (SECC, in EVSE)
$B^a_{n,j}$	– Energy in the battery of the j^{th} EV currently = Current SOC in terms of energy (kWh)	EV	Yes, in 15118
$B^d_{n,j}$	– Required energy in the battery of j^{th} EV at departure $T^d_{n,j}$ (kWh)	User	Same as below
$d_{n,j}$	– Charging energy demand of j^{th} EV, $(B^d_{n,j} - B^a_{n,j})$ (kWh)	User	Yes, in 15118
$C^p_{n,j}$	– Penalty for not meeting energy demand $d_{n,j}$ by departure time $T^d_{n,j}$ of j^{th} EV (€/kWh)	CSO	
$B^{min}_{n,j}, B^{max}_{n,j}$	– Minimum and maximum possible energy in the battery of the j^{th} EV, respectively (kWh)	EV &/or User	Yes, in 15118 new version, the mechanism is: Each car has an ID, which can map to all the car information. The card for charging payment will be no longer needed. Or via database (Indirect)
$p^{max}_{n,j}$	– Maximum charging power of j^{th} EV (kW) when its SOC is $S^{CV}_{n,j}$	EV	Yes, in 15118, in the form of: - Max V (RMS phase to neutral voltage) - Max and Min current But not sure if it's absolute Pmax, or the SOC dependent real-time Pmax. Or, Via database or Use data from past charging sessions – May not be accurate
$\eta^{ev}_{n,j}$	– Efficiency of charging of the battery of j^{th} EV including the losses in the battery, EVSE, on-board charger (kW)	EV	Via database or Use data from past charging sessions
$S_{n,j,t}$	SOC value of the battery	EV	
$S^{CV}_{n,j}$	SOC value when the battery charging	EV	

	process shifts from CC to CV stage of j^{th} EV		
$p_{n,j}^{CC0}$	Maximum charging power of j^{th} EV when the SOC is at its lowest level	EV	
$\Delta i_{n,j}^{e+}$	The minimum current step of adjustment Integer	EV&/or EVSE	
$B_{n,j}^{SC}$	– Minimum assure capacity in the battery of the j^{th} EV (kWh), only above which the smart charging activation is allowed	EV &/or User	

Charger parameters (index j,n)

Parameter	Note	Source	Protocol
$p_{n,j}^{EVr}$	– Rated power of the EV charger connected to the j^{th} EV (kW)	EVSE/CSO	Yes/Installation
	Location of the charger and the node	EVSE/CSO	Yes/Installation
	Voltage and frequency at the EV charger		Not possible to know at the moment, but a different smart meter protocol could achieve it in the future.

Local energy parameters (index t ,n; time t at node n^{th} where the car parker is connected to)

Parameter	Note	Source	Protocol
p_n^{PVr}	– Rated power of renewable power source connected to (or close to) the car park (kWp). If there is no local generation, P_n^{PVr} can be set to zero	CSO or User	Yes/Installation

$\eta_{n,t}^{inv}$	– Efficiency of the PV inverter (%)	EVSE	
$K_{n,t}^{PV}$	– Scaling factor to factor in the non-optimal generation of the renewable energy source (e.g., shading of PV panels)	CSO/ User	
C^{PV}	– Cost of obtaining PV energy (€/kWh)	CSO/ User	
$p_{n,t}^{PV(fc)}$	– Power generation forecast of renewable generation source installed at the car park (kW)	CSO/ User	BRP takes the prediction into consideration
${y_{n,t}}^{PV(fc)}$	– Maximum uncertainty in solar forecast data (%)	CSO/ User	
$p_{n,t}^{PV(meas)}$	– This is the real-time PV generation measurement (kW)		Real time meas. of loads, PV power every 5s
$p_{n,t}^{local}$	– This is the net value of the local loads (kW)		
$V_{n,t}$	- This is the voltage of node nth, it is assumed that everything connected to this node has the same voltage.		

ISO (TSO) & DSO parameters (index t)

Parameter	**Note**	**Source of parameter**	**Protocol**
$C_t^{e(buy)}$, $C_t^{e(sell)}$	– Market clearing price for buying and selling electricity from the grid respectively (€/kWh)	BRP	Yes, openADR, current & future Energy supplier, BRP and DSO send price signals, the DSO cam also send the available capacity signal.
$C_t^{r(up)}$, $C_t^{r(dn)}$	– Market clearing price for offering reserve capacity for up and down regulation respectively (€/kW)	TSO	Maybe, challenge for FCR is reliability & time lag
$p_{n,t}^{G+}$, $p_{n,t}^{G-}$	– Distribution network (Grid) capacity for drawing and	DSO	Command sent from back-end to the CSO, via openADR and OSCP: - OSCP, old version is mainly

	feeding power to car park respectively (kW)		for EV applications, the new version will have broader in general applications. - OpenADR: might be applied in OSCD project ('capacity guard' profile)

* The market price is set as all the same for one grid, but the grid capacity limitation is local congestion based thus the grid power limitation has the index "n".

Note – EV chargers are not controlled in real time from the CSO end. Charging plans are sent to charge with profile for the rest of the day. If there is a change/update, a new plan is sent.

1.4 Optimization variables

All variables listed below are positive

$p_{n,j,t}^{e+}$ – Charging power of j^{th} EV which connected to the n^{th} node at time *t* (kW)

$i_{n,j,t}^{e+}$ – Charging current of j^{th} EV which connected to the n^{th} node at time *t* (kW)

$B_{n,j,t}$ – Battery energy of j^{th} EV battery which connected to the n^{th} node at time *t* (kWh)

$p_{n,t}^{PV}$ – Power generated by the renewable energy source at the car park at time *t*, n^{th} *node* (kW)

$p_{n,j,t}^{r(up)}, p_{n,j,t}^{r(dn)}$ – Reserve power capacity offered to grid for up and down regulation by j^{th} EV at time *t*, n^{th} *node* (kW)

$P_{n,t}^{g(imp)}, P_{n,t}^{g(exp)}$– Power imported and exported to grid by the EV car park at time *t*, respectively (kW)

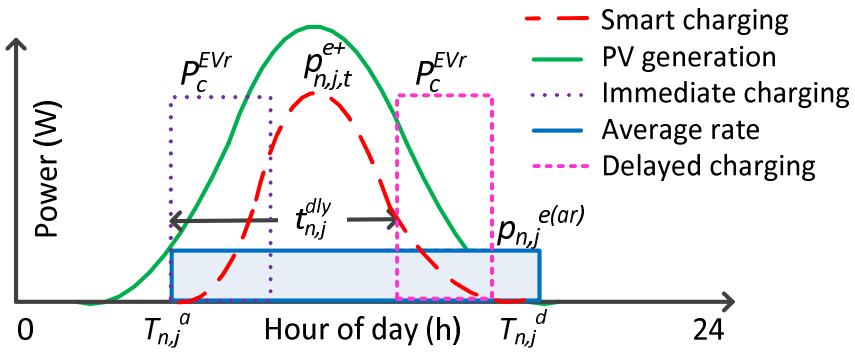

Figure 1 Immediate, average rate, randomly delayed and smart charging of EV

2. Smart charging of EVs

2.1 Control/Uncontrolled charging

Immediate and average rate charging

Today, when an EV arrives at the workplace and is connected to the electric vehicle supply equipment (EVSE), the EV starts charging essentially immediately at the nominal maximum EVSE power rating, p_c^{EVr}. The charging continues at approximately constant power until the battery is nearly full[1]. This is referred to as immediate charging (IMM) or uncontrolled charging [1]. This is the simplest form of charging requiring no information from the user or communication infrastructure and results in the lowest charging time. However, IMM typically results in a huge demand on the grid based on the EVSE, as shown in Figure 1.

At the same time, the long parking times of EVs at workplace offers the flexibility in scheduling the charging in terms of both charging power and duration. This means that EVs can be charged at a much lower power than the EVSE nominal rating if the EV user arrival time, T_j^a, departure time, T_j^d and required energy demand, d_j are known. One approach is the "Average Rate" (AR) charging policy [1], where the charging power $p_j^{e(ar)}$ is the minimum of the EVSE capacity, p_c^{EVr}, and the ratio of the energy demand divided by the parking time of the EV[1]:

$$p_j^{e(ar)} = Min.\left\{\frac{d_j}{T_j^d - T_j^a}, p_c^{EVr}\right\} \qquad \forall\, t \in [T_j^a; T_j^d] \qquad (1)$$

The advantage of the AR policy is that the charging of the fleet is spread throughout the day instead of being concentrated around the arrival time (typically early morning), as seen in Figure 1.

Smart charging

The optimal way to charge EVs is hence to schedule the charging by taking into consideration the EV user preferences, local renewable generation, distribution network and energy prices from the market. Figure 1 shows an example of smart charging where the EV charging follows the PV generation. Further, EVs can have an extremely fast ramp up and ramp down rate. CHAdeMO and Combo EV charging standards for DC charging stipulate response time of 200ms for power changes [2]. This makes EVs ideal candidates for providing ancillary services in the form of frequency regulation and voltage regulation services to the grid [3]–[6].

[1] The analysis does not consider the duration in the constant-voltage (CV) charging mode, which occurs typically when EV battery is above 80% SOC and the maximum charging power is limited [12].

Following the formulation in [4], [7], an Energy Services Company (ESCo) company acts as an intermediary between the wholesale market operated by the Independent System Operator (ISO) and the EV end-users (Transmission system operator, TSO in case of Europe). The ESCo operates at the car park where people charge their EVs, and the location has local renewable energy generation like overhead PV installation. The motive of the ESCo is to schedule the charging of the EV and feeding of PV power to the grid in such a way that EV charging costs are lowered, regulation services are offered to the ISO, and at the same time, the income from PV is increased. ESCo achieves this motive by using an Energy Management System (EMS) to schedule the EV based charging on a multitude of inputs:

1. Information from the EV user about EV type, arrival and departure times, the state of charge (SOC) of EV battery and energy demand.
2. Settlement point prices for buying and selling electricity from the grid at time *t* ($C_t^{e(buy)}$, $C_t^{e(sell)}$).
3. Clearing prices for capacity for offering frequency regulation reserves to the ISO for up and down regulation. ($C_t^{r(up)}$, $C_t^{r(dn)}$).
4. Distribution network (Grid) limits for drawing and feeding power between the EV car park and the grid (p_t^{G+}, p_t^{G-}). These values can be adjusted to implement demand side management (DSM).
5. Renewable energy forecast information to help reduce the uncertainties due to variability in generation on diurnal and seasonal basis ($p_t^{PV(fc)}$). Focus here is on PV, but it can be other forms of generation as well.

The main contributions of the work reported below include:

- Proposing an integrated model that captures charging of EV from PV, use of dynamic grid prices, using EV to offer ancillary services, and considering distribution network capacity constraints as a single Mixed-Integer Programming (MIP) formulation. The algorithm demonstrates that the integrated formulation results in large cost savings, which is much higher than what has been achieved earlier. This is due to the addition of benefits from each application, such that the net benefit is economically attractive. With the prior approaches, the economic benefits were too small to warrant mass adoption of smart charging
- The integrated scheduling of EV and PV makes PV an economically controllable commodity with respect to feeding power to the grid, which would not be possible otherwise. Depending on grid energy prices, PV energy can be diverted either to the EV or to the grid or curtailed.

2.2 EMS Architecture and market structure

EV and user input

Each EV arrives at the car park which has PV panels and connected to the nth node with a battery of energy content $B_{n,j}^a$ at time $T_{n,j}^a$. The EV owners provide the information to the EMS

about their expected departure time $T^d_{n,j}$ and charging energy demand $d_{n,j}$. This means that the departure energy content of the vehicle $B^d_{n,j}$ is:

$$B^d_{n,j} = B^a_{n,j} + d_{n,j} \quad (2)$$

If the required SOC is not reached by the departure time, the EV owner will be compensated by the ESCo at the rate of $C^p_{n,j}$ €/kWh. The users can enter the maximum and minimum allowed energy of the EV battery ($B^{min}_{n,j}, B^{max}_{n,j}$) and the maximum charging power ($p^{max}_{n,j}$) respectively. The efficiency of the EV battery for charging ($\eta^{ev}_{n,j}$) is either obtained from the EV or stored in a database within the EMS for different EV models.

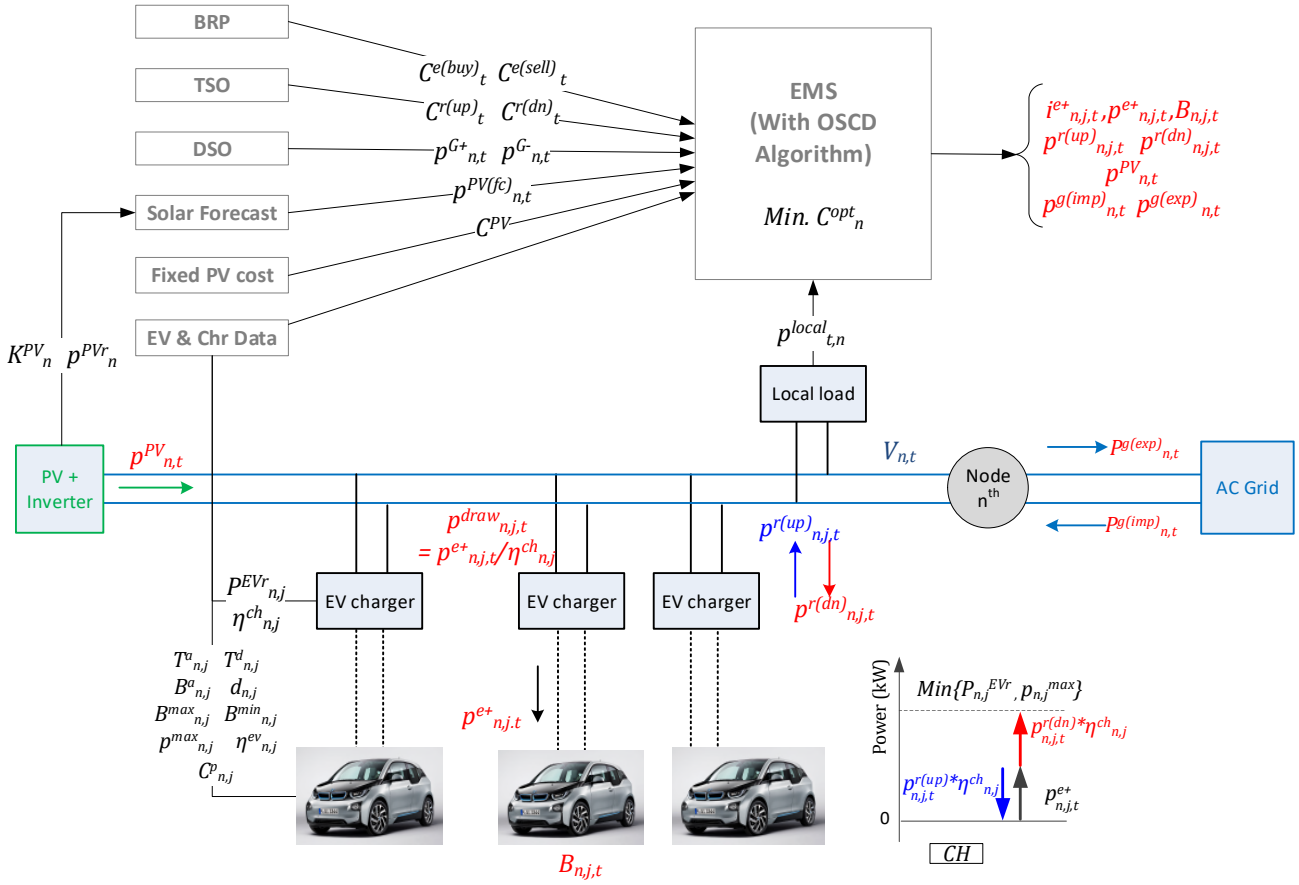

Figure 2 Schematic of the Energy Management System for the solar powered EV parking lot consisting of several EV chargers as shown above.

EV charger

Each location of the EV park (node n[th]) is connected to a PV array of rated power p^{PVr}_n via a maximum power point tracking (MPPT) DC/DC converter [8]. The EV charger has an efficiency of $\eta^{ch}_{n,j}$, which for AC chargers is close to 100%. Each EV charger draws $P^{draw}_{n,j,t}$ power from the EV car park as determined by the EMS. Different EV chargers can exchange power within the car park from the PV and these are 'intra-park' power exchanges. When the net

'intra-park' energy exchanges are non-zero, the EV park at node n[th] imports or exports power with the external grid referred to as $P_{n,t}^{g(imp)}$, $P_{n,t}^{g(exp)}$respectively.

Trading energy and reserves in the energy market

The ESCo uses the EMS to control the solar powered EV car park for energy trading with the grid. Since $p_{n,t}^{g(imp)}$, $p_{n,t}^{g(exp)}$ are small relative to the power traded in the market, the ESCo is a price taker and does not influence the market clearing prices. It uses the settlement point prices for trading power in the market and reserve capacity prices for offering up and down regulation services. Markets like the Electric Reliability Council of Texas (ERCOT) provide different prices for offering capacity reserves for up and down regulation (asymmetric, $C_t^{r(up)} \neq C_t^{r(dn)}$). However, other US markets such as PJM trade up and down regulation as a single product (symmetric). In order to make the EMS flexible and work with both types of markets, it is designed to take different inputs for $C_t^{r(up)}$ and $C_t^{r(dn)}$ and allow for a requirement that up and down regulation quantities could be equal.

2.3 Receding horizon model predictive control

There are two sources of variability in the EV-PV system. The first is the diurnal and seasonal variation in PV generation due to changes in weather. The EMS uses solar forecast information as an input to predict the PV variation. Any solar forecast data source can be used for the given MIP formulation. For example, the online short-term solar power forecasting [9], the autoregressive integrated moving average (ARIMA) models [10] or any of the methods listed in [11]. $p_{n,t}^{PV(fc)}$ is power generation forecast for an optimally orientated 1kW$_p$ PV array at the car park location connected to node n[th] with a maximum uncertainty in forecast of y_{PV}^{fc}. It is vital to recognize that all forecasting methods will have forecasting errors in terms of temporal and spatial resolution. The second variability is the variation in the arrival and departure patterns of the EV user and the EV parameters like charging powers limits, efficiency of the battery and SOC.

The EMS is implemented as a receding horizon model predictive control with a time step ΔT to manage these two variations. The horizon for the model is flexible and can be triggered and reset by events or with fixed reset cycle. The event could be new arrival cars, the sudden change of certain system parameters e.g. the solar radiation, the earlier departure car than predicted. This means whenever there is an event happens or when it is the time to reset, the EMS can utilize updated forecast information and input parameters, perform the optimization and plan the EV charging for the rest of the day. Hence, the receding horizon implementation helps in minimizing forecasting errors and model inaccuracies with a reasonable frequency.

3. MIP formulation

This section describes the objective function and constraints for the MIP formulation of the EMS. It is important to note that all optimization variables considered are positive.

3.1 Decision variables

These variables are expected outcomes of the algorithm

$p_{n,j,t}^{e+}$ – Charging power of *j*th EV which connected to the nth node at time *t* (kW)

$i_{n,j,t}^{e+}$ – Charging current of *j*th EV which connected to the nth node at time *t* (kW)

$B_{n,j,t}$ – SOC of *j*th EV battery which connected to the nth node at time *t* (kWh)

$p_{n,t}^{PV}$ – Power generated by the renewable energy source at the car park at time *t, node n* (kW)

$p_{n,j,t}^{r(up)}, p_{n,j,t}^{r(dn)}$ – Reserve power capacity offered to grid for up and down regulation by *j*th EV at time *t, node n* (kW)

$P_{n,t}^{g(imp)}$, $P_{n,t}^{g(exp)}$– Power imported and exported to grid by the EV car park at time *t,* respectively (kW)

3.2 Objective function

Main function

$$Min.\quad C_n^{opt} = \sum_{j=1}^{J}\left(B_{n,j}^{a} + d_{n,j} - B_{n,j,T_j^d}\right)C_{n,j}^{p} + \Delta T\sum_{t=1}^{T} p_{n,t}^{PV}\,C^{PV} + \Delta T\sum_{t=1}^{T}\left(p_{n,t}^{g(imp)}C_t^{e(buy)} - p_{n,t}^{g(exp)}C_t^{e(sell)}\right) - \Delta T\sum_{t=1}^{T}\sum_{j=1}^{J} p_{n,j,t}^{r(up)}C_t^{r(up)} + p_{n,j,t}^{r(dn)}C_t^{r(dn)} \quad (3)$$

The objective function is to minimize the total costs C_n^{opt} of EV charging, feeding PV power and offering reserves at node nth. The formulation is such that the C_n^{opt} can be positive or negative. It has five components, namely:

- The penalty to be paid to the user if the energy demand $d_{j,n}$ is not met by the departure time $T_{j,n}^{d}$. $C_{j,n}^{p}$ is EV user specific and the penalty can be different for each user based on EV battery size, tariff policy and customer 'loyalty' program.
- PV power that is used to charge the EV need not always be free of cost. If the PV is installed by a third-party, it can be obtained at a pre-determined contractual cost of C^{PV}.
- The cost of buying and selling energy from the grid based on the settlement point prices $C_t^{e(buy)}$, $C_t^{e(sell)}$. The market dynamics will ensure that $C_t^{e(buy)} \geq C_t^{e(sell)}$

- Income S^{as} obtained from offering reserve capacity $p_{t,j,n}^{r(up)}, p_{t,j,n}^{r(dn)}$ to the TSO.

Apart from that, the green part in the equation represents the variables and the rest are the input parameters.

Sub-functions

This section explained how the parameters/variables are defined or how are they related to each other.

Equations(4)-(5) are used to set the initial capacity of the EV battery and estimate the capacity of the battery $B_{n,j,t}$ based on the charging efficiency ($\eta_{n,j}^{ev}$) and power $p_{n,j,t}^{e+}$ respectively. It is assumed that the net energy delivered/absorbed by the EV over one time period due to offer of reserves is zero [4], [7]. Hence, $p_{n,j,t}^{r(up)}, p_{n,j,t}^{r(dn)}$ do not appear in Equation (4),(5) for SOC estimation.

Equation (6) shows how is the charging current calculated from the charging power and the node voltage, and Equation (7) shows how the state of the charge of the battery is calculated.

$$B_{n,j,t} = B_{n,j}^{a} + \Delta T \sum_{T_j^a}^{t} \left(p_{n,j,t}^{e+} \, \eta_{n,j}^{ev}\right) \qquad \forall\, t \in n,j,\left[T_{n,j}^{a}; T_{n,j}^{d}\right] \qquad (4)$$

$$B_{n,j,T_{n,j}^{d}} = B_{n,j}^{a} + \Delta T \sum_{t}^{T_j^d} \left(p_{n,j,t}^{e+} \, \eta_{n,j}^{ev}\right) \qquad \forall\, t \in n,j,\left[T_{n,j}^{a}; T_{n,j}^{d}\right] \qquad (5)$$

$$p_{n,j,t}^{e+} = i_{n,j,t}^{e+} \times V_{n,t} \qquad \forall\, t \in n,j,\left[T_{n,j}^{a}; T_{n,j}^{d}\right] \qquad (6)$$

$$S_{n,j,t} = \frac{B_{n,j,t} - B_{n,j}^{min}}{\left(B_{n,j}^{max} - B_{n,j}^{min}\right)} \qquad \forall\, t \in n,j,\left[T_{n,j}^{a}; T_{n,j}^{d}\right] \qquad (7)$$

3.3 Acceptance criteria

Charger accepts EV

When an EV arrives at the EV car park connected to node n, it is connected to one of the chargers. The user links to the EMS and the EMS instructs the user on which EV charger he/she must connect to, based on two 'acceptance criteria'. The first criteria is that the energy demand $d_{n,j}$ and parking time, $\left(T_{n,j}^{d} - T_{n,j}^{a}\right)$ of all the EVs connected to a EV charger must be within the power limits of the charger, (8). The second criteria is that the arrival energy content of the vehicle must be above the minimum limit as set by the user, (9). This is to ensure that constraint (16) is satisfied.

If the input from the user are not satisfied with the condition, especially the energy demand and the departure time, then user will be asked to re-input its requirements and the car information.

$$\frac{d_{n,j}}{T^d_{n,j} - T^a_{n,j}} \leq Min.\{p^{EVr}_{n,j}, p^{max}_{n,j}\} \qquad \forall\, n,j \qquad (8)$$

$$B^{min}_{n,j} \leq B^a_{n,j} \qquad \forall\, n,j \qquad (9)$$

Smart charging availability

There is another acceptance criteria which allows the EMS to decide if the smart charging algorithm can be activated and applied on certain EV. The condition is the SOC of the EV $B_{n,j,t}$ has to be no less than the emergency SOC value $B^{SC}_{n,j}$, as indicated in Equation (10).

$$B_{n,j,t} \geq B^{SC}_{n,j} \qquad \forall\, n,j \qquad (10)$$

3.4 Constraints

Constraints: EV and user inputs

The EMS at node n controls the charging power $p^{e+}_{n,j,t}$, up and down regulation reserve capacity $p^{r(up)}_{n,j,t}$, $p^{r(dn)}_{n,j,t}$ of each EV at time *t*. $p^{e+}_{n,j,t}$ have to be within the power limits of the EV charger $p^{EVr}_{n,j}$ and the charging power limits as set by the EV, respectively, as shown in equations (11)-(13).

The maximum charging powers are also dependent on the SOC of the EV battery as shown in (12)-(13). For example, during the constant current (CC) charging stage, the voltage of the battery is gradually increase with the rising SOC value. Therefore the maximum charging power is also increase along with the SOC from $p^{CC0}_{n,j}$ until it reaches the maximum charging power $p^{max}_{n,j}$. It is assumed that the power increase during CC stage is linear. Then, fast charging of EV battery (CC stage) cannot be done beyond 80% SOC of the battery [12]. Here, it is assumed that the maximum charging power linearly reduces from $p^{max}_{n,j}$,to zero when the battery is charged beyond 80% SOC till 100% ($S^{CV}_{n,j}$=0.8). Even though the exact dependence of battery power on the SOC is non-linear, this is not considered here as it is beyond the scope of the chapter and would prevent us from casting the problem into an MIP formulation. The curve of how the maximum charging power changing with the SOC value is in Figure 3

Equation (10) is the simplified equation of how the maximum charging power varies with SOC value during constant current (CC) charging stage, where m is assumed as a constant value in this project.

$$p^{e+}_{n,j,t} \leq P^{EVr}_{n,j} \qquad \forall\, t \in n,j,[T^a_{n,j}; T^d_{n,j}] \qquad (11)$$

$$p^{e+}_{n,j,t} \leq \frac{p^{max}_{n,j} - p^{CC0}_{n,j}}{S^{CV}_{n,j}} * S_{n,j,t} + p^{CC0}_{n,j} \qquad \forall\, t \in n,j,[T^a_{n,j}; T^d_{n,j}]\ \&\ S_{n,j,t} \leq S^{CV}_{n,j} \qquad (12)$$

$$p^{e+}_{n,j,t} \leq \frac{p^{max}_{n,j}}{(1 - S^{CV}_{n,j})}(1 - S_{n,j,t}) \qquad \forall\, t \in n,j,[T^a_{n,j}; T^d_{n,j}]\&\ S_{n,j,t} > S^{CV}_{n,j} \qquad (13)$$

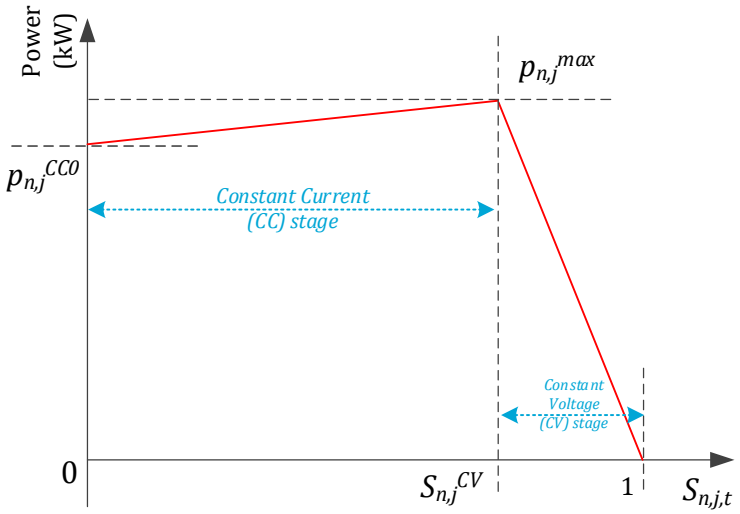

Figure 3 Maximum charging power varies with SOC value

The EMS restricts the capacity of the battery to be within the limits $B_{n,j}^{min}, B_{n,j}^{max}$ as set by the EV and/or user. The battery capacity is controlled to not exceed the initial battery capacity $B_{n,j}^{a}$ plus the required energy $d_{n,j}$ as showed in equation (15). Besides, all the charging related variables are set to zero when it is out of the charging sessions, as listed in Equation (17)

When EV is connected:

$$B_{t,j,n} \geq B_{j,n}^{a} \qquad \forall\, t \in n,j,\left[T_{n,j}^{a}; T_{n,j}^{d}\right] \qquad (14)$$

$$B_{t,j,n} \leq Min\left\{d_{j,n} + B_{j,n}^{a},\ B_{j,n}^{max}\right\} \qquad \forall\, t \in n,j,\left[T_{n,j}^{a}; T_{n,j}^{d}\right] \qquad (15)$$

$$B_{t,j,n} \geq B_{j,n}^{min} \qquad \forall\, t \in n,j,\left[T_{n,j}^{a}; T_{n,j}^{d}\right] \qquad (16)$$

When the EV is not connected:

$$i_{n,j,t}^{e+},\ p_{n,j,t}^{e+}, p_{n,j,t}^{r(up)}, p_{n,j,t}^{r(dn)}, B_{n,j,t} = 0 \qquad \forall\, t < T_{n,j}^{a}\ \&\ t \geq T_{n,j}^{d} \qquad (17)$$

Constraints: EV charger, PV and car park

For each EV charger, if the charging process is on then the lowest allowed charging current is 6A and the current value should be integer with step of 1A.

$$\left(i_{n,j,t}^{e+} = 0\right) OR \left(i_{n,j,t}^{e+} \geq 6\right) \qquad \forall\, t \in n,j,\left[T_{n,j}^{a}; T_{n,j}^{d}\right] \qquad (18)$$

Therefore, the maximum charging power is also limited by the current constraints and the updated curve is shown in Figure 4.

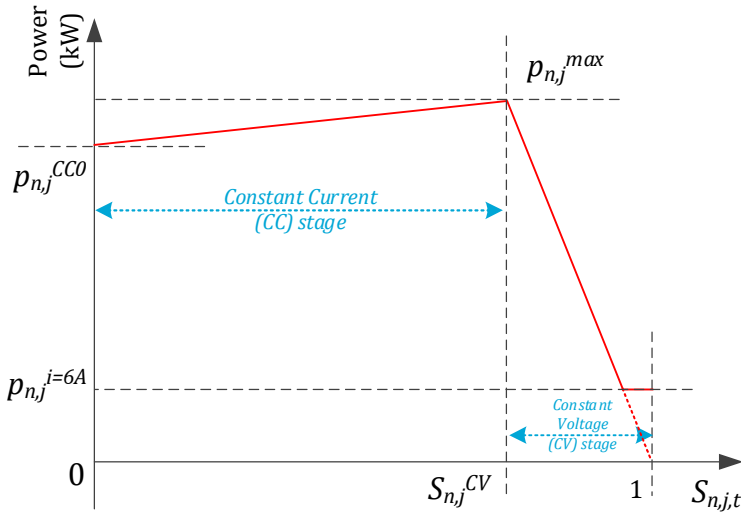

Figure 4 Adjusted maximum charging power varies with SOC value

Under normal operation, the PV converter extracts maximum power from the PV array using MPPT as shown in right side of equation (19). The PV power is dependent on the scaling factor $K_{n,j}^{PV}$ which scales the installation characteristics (e.g. azimuth, tilt, module parameters) of the PV array connected with respect to the 1kWp reference array used for the forecast data $p_{n,t}^{PV(fc)}$ and the efficiency of the PV inverter η_n^{inv}

The AC grid is used for power exchanges between the EV, PV, the local loads and the grid. The intra-car park power exchanges between different EV chargers and PV are related to the power exchanged with the external grid $p_t^{g(imp)}, p_t^{g(exp)}$ using (20). Both $p_t^{g(imp)}, p_t^{g(exp)}$ will not have finite values at the same time because of the way the objective function is formulated and because $C_t^{e(buy)} \geq C_t^{e(sell)}$ at all times.

$$p_{n,t}^{PV} \leq K_{n,t}^{PV} p_n^{PVr} p_{t,n}^{PV(fc)} \eta_n^{inv} \qquad \forall\, n,t \qquad (19)$$

$$\sum_{j=1}^{j=J} \left(p_{n,j,t}^{e+}/\eta_{n,j}^{ch}\right) + p_{n,t}^{local} - p_{n,t}^{PV} = p_{n,t}^{diff} = p_{n,t}^{g(imp)} - p_{n,t}^{g(exp)} \qquad \forall\, n,j,t \qquad (20)$$

$$p_{n,t}^{g(imp)} = \left\{p_{n,t}^{diff} \middle| p_{n,t}^{diff} > 0\right\} \qquad \forall\, n,j,t \qquad (21)$$

$$p_{n,t}^{g(exp)} = -1 * \left\{p_{n,t}^{diff} \middle| p_{n,t}^{diff} < 0\right\} \qquad \forall\, n,j,t \qquad (22)$$

Next, the up and down regulation offered $p_{n,j,t}^{r(up)}, p_{n,j,t}^{r(dn)}$ should be within the power limitations of the EV and the EV charger $p_{n,j}^{EVr}$ as shown in Equation (23)-(26) . From the EV charger perspective, the regulation power offered must be within the power rating of the grid connection and the SOC of the EV battery (like (12)-(13))). This is summarized in equations below. While asymmetric reserve offers are assumed here ($p_{n,j,t}^{r(up)} \neq p_{n,j,t}^{r(dn)}$), symmetric reserves can be achieved by including $p_{n,j,t}^{r(up)} = p_{n,j,t}^{r(dn)}$ to the constraints.

$$p_{n,j,t}^{r(up)} \leq p_{n,j,t}^{e+}/\eta_{n,j}^{ch} \qquad \forall\, n,j,t \qquad (23)$$

$$p_{n,j,t}^{e+} + p_{n,j,t}^{r(dn)}\eta_{n,j}^{ch} \leq p_{n,j}^{EVr} \qquad \forall\, n,j,\left[T_{n,j}^{a};T_{n,j}^{d}\right] \qquad (24)$$

$$p_{n,j,t}^{e+} + p_{n,j,t}^{r(dn)}\eta_{n,j}^{ch} \leq \frac{p_{n,j}^{max} - p_{n,j}^{CC0}}{S_{n,j}^{CV}} * S_{n,j,t} + p_{n,j}^{CC0} \qquad \forall\, n,j,t \in \left[T_{n,j}^{a};T_{n,j}^{d}\right] \,\&\, S_{n,j,t} \leq S_{n,j}^{CV} \qquad (25)$$

$$p_{n,j,t}^{e+} + p_{n,j,t}^{r(dn)}\eta_{n,j}^{ch} \leq \frac{p_{n,j}^{max}}{\left(1 - S_{n,j}^{CV}\right)}\left(1 - S_{n,j,t}\right) \qquad \forall\, n,j,t \in \left[T_{n,j}^{a};T_{n,j}^{d}\right] \,\&\, S_{n,j,t} > S_{j,n}^{CV} \qquad (26)$$

$$\sum_{j=1}^{j=J} \frac{p_{n,j,t}^{e+}}{\eta_{n,j}^{ch}} + p_{n,t}^{local} - p_{n,t}^{PV} = p_{n,t}^{diff} = p_{n,t}^{g(imp)} - p_{n,t}^{g(exp)} \qquad \forall\, n,j,t \qquad (27)$$

$$p_{n,t}^{g(imp)} = \left\{p_{n,t}^{diff} \middle| p_{n,t}^{diff} > 0\right\} \qquad \forall\, n,j,t \qquad (28)$$

$$p_{n,t}^{g(exp)} = -1 * \left\{p_{n,t}^{diff} \middle| p_{n,t}^{diff} < 0\right\} \qquad \forall\, n,j,t \qquad (29)$$

$$\sum_{j=1}^{j=J}\left(\frac{p_{n,j,t}^{e+}}{\eta_{n,j}^{ch}} + p_{n,j,t}^{r(dn)}\right) + p_{n,t}^{local} - p_{n,t}^{PV} \leq p_{n,t}^{G+} \qquad \forall\, n,j,t \qquad (30)$$

$$p_{n,t}^{PV} - \sum_{j=1}^{j=J}\left(\frac{p_{n,j,t}^{e+}}{\eta_{n,j}^{ch}} - p_{n,j,t}^{r(up)}\right) - p_{n,t}^{local} \leq p_{n,t}^{G-} \qquad \forall\, n,j,t \qquad (31)$$

Finally, $p_{n,t}^{g(imp)}, p_{n,t}^{g(exp)}$ should be within the distribution network capacity $p_{n,t}^{G+}, p_{n,t}^{G-}$ as shown in (32)-(33). $p_{n,t}^{G+}, p_{n,t}^{G-}$ are used as a thermal proxy for all potential limitations in the distribution network including voltage limits, line limits and transformer capacity. The values can come from the distribution system operator (DSO), ISO or ESco based on loading and voltage in the network and can be set at every time step in the receding horizon implementation.

$$p_{n,t}^{g(imp)} \leq p_{n,t}^{G+} \qquad \forall\, n,t \qquad (32)$$

$$p_{n,t}^{g(exp)} \leq p_{n,t}^{G-} \qquad \forall\, n,t \qquad (33)$$

4. Algorithm Implementation considerations

In this section, the practical aspects of implementing this optimization are analysed.

4.1 Adaptability

It must be kept in mind that even though wholesale DAM prices and small EV fleet have been used in this study, the formulation is generic to be used with large EV fleet, real-time market (RTM) and retail electricity prices as well. The parameters listed in the nomenclature section can be adapted for different markets, PV, EV types and to different smart charging scenarios as highlighted by the six case studies done for Austin.

4.2 Capital cost and sharing of benefits

The capital cost of building the proposed EV-PV integrated charging facility will be cheaper than a non-integrated system due to:

- The use of rolling horizon implementation as opposed to stochastic optimization to handle forecasting errors and uncertainties simplifies the formulation and reduces the computational complexity; hence less powerful and cheaper hardware can be used.
- The integrated scheduling of EV-PV--regulation reduces the net costs on an average by 158%, and this could provide a revenue stream to recover the capital cost [13].

The EV-PV car park has several players involved namely the owner of PV and parking area, the ESCo, the ISO EV user and in a general scenario, the charging station operator (CSO), e-mobility service provider (eMSP) and the DSO. The capital investment of the EV-PV charging facility and the benefit of the net cost reduction will ultimately have to be shared amongst all these parties. This will be dependent on the contractual business agreement between the parties.

4.3 Scalability

Similar to any MIP problem, the problem size will grow with the number of EV. At the same time, different parking locations are decoupled by their EV, PV and distribution constraints and hence the model dimension is naturally limited to the size of a single parking lot, about 5 to 1000 EVs. Thus, the MIP's dimensionality is limited to problem sizes that are tractable by the current technology and therefore fairly scalable. Further, the receding horizon implementation makes the problem more scalable in terms of computational complexity when compared to stochastic optimization.

Stochastic optimization is an alternative to the receding horizon approach. But it was not considered here for two reasons. First, the given problem has a lot of stochastic variables, making it computationally intensive and hence less scalable. This is especially a problem as the number of EV grows to above 50 in a parking lot. The MIP formulation with receding horizon approach makes it computationally easier. Second, stochastic optimization requires the generation of probabilistic data for all inputs and creating different scenarios for PV, EV, and market. Due to limited EV penetration, there is insufficient data now on EV and EV user patterns creating lots of dimensions of uncertainty. If such limited data is used as input, it is difficult to get reliable and useful results.

4.4 Interaction with de-regulated energy markets

With up to 1000 EVs and 10kW EV charger, the total car park is handling 10MW power at maximum. This is small in relation to the power scales in the energy market. Hence, no perturbations will be observed on the market prices and no feedback on prices would be required for this system. At the same time, the net car park power can be occasionally lower than the minimum bid required by ISOs to participate in regulation services (for example, 0.1MW for PJM, 0.1MW for ERCOT and typically 1MW in other ISOs) It is expected that ISOs around the world would lower the minimum bid requirements in the future to allow EVs to participate in ancillary services.

5. Implementation of Smart Charging 2.0 algorithm

To eliminate implementation effects and enable an implementation independent analysis of the presented smart charging algorithm, the implementation of the optimization algorithm was done at AIT and TU Delft independently using the description of the algorithm provided by TU Delft.

5.1 TU Delft implementation specifics

System implementation of the algorithm in distribution grid

The pre-described algorithm is on node level and it is expected that there is a central entity who is responsible for collecting the congestion information of the whole grid. This central entity will then give a limit of how much power can each node exchange with the grid to each node accordingly, as shown in Figure 5. Since the function of central coordinator is out of scope of this project, a very simple rule based central coordination is implemented for demonstration.

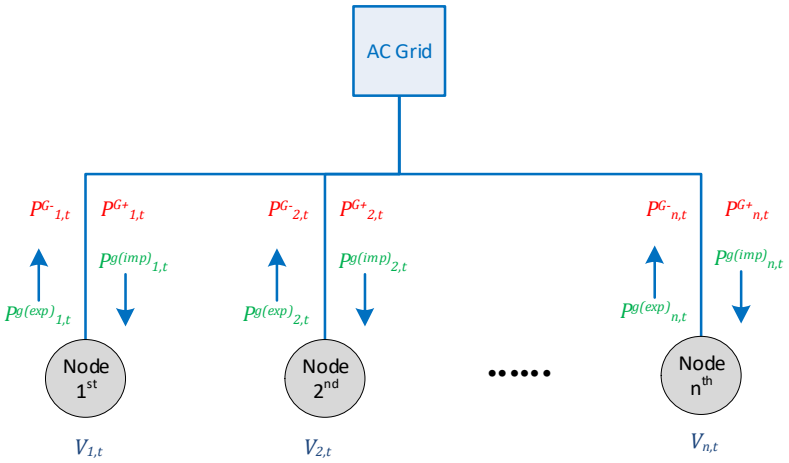

Figure 5 Schematic of the system implementation

This simple central coordination does not have real-time congestion detection function, it only evenly distributes a pre-set grid limit value to all the nodes where there is EV connecting. Take the grid import limit for each node as an example. This pre-set grid limit is the total allowed power for all EV charging in the whole grid and it is equally shared to all EV-connecting nodes depends on the number of connecting EVs at that moment.

$$p^{G+}_{m,t} = \frac{P^{lim}}{\sum_{n=1}^{N} J^{c}_{n,t}} * J^{c}_{m,t} \tag{34}$$

The import power limit $p^{G+}_{m,t}$ of node m at time t is calculated in this way: the pre-set grid limit P^{lim} divided by the total number of connecting EVs $\sum_{n=1}^{N} J^{c}_{n,t}$ at time t, then multiply with the number of connecting EVs $J^{c}_{m,t}$ at node m, as shown in equation (34). The schematic of this central coordination is presented in Figure 6. The uncontrolled charging results of Dutch grids (which can be found in deliverable 1.2) show no excessive exporting power problem at all, thus the export power limit is not specifically set for the smart charging simulations.

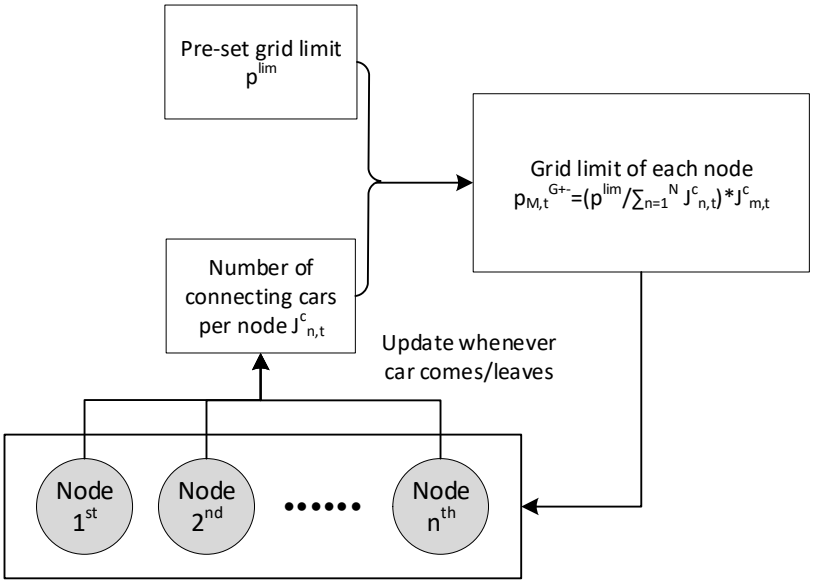

Figure 6 Simple rule based central coordination

In the simulation, the transformer capacity is selected as the limit for sum of EV charging power in the whole grid, which is 400kW for each grid. The results with a tighter grid limitation are also presented and compared.

Structure and time scale of the distribution algorithm

The algorithm consists of a simulator and the MIP optimisation, and the formulation of the MIP optimisation is explained in the previous sections. The simulator is to mimic the real application environment, to adjust the system parameters and to execute the MIP optimisation. The function of this simulator includes analysing both the input, output data, set the moving horizon T, and then trigger the MIP optimisation. There are several rounds of the MIP optimisation from the beginning until the end of the whole optimisation duration. The whole optimisation duration originally refers to the one winter or one summer week defined in the scenario definition document. However, the optimisation duration in this algorithm is not limited by this period length that it can be set from one day to as many days if there is sufficient input data. The structure of the algorithm is plotted in Figure 7, and the time scale concept of the algorithm is shown in Figure 8.

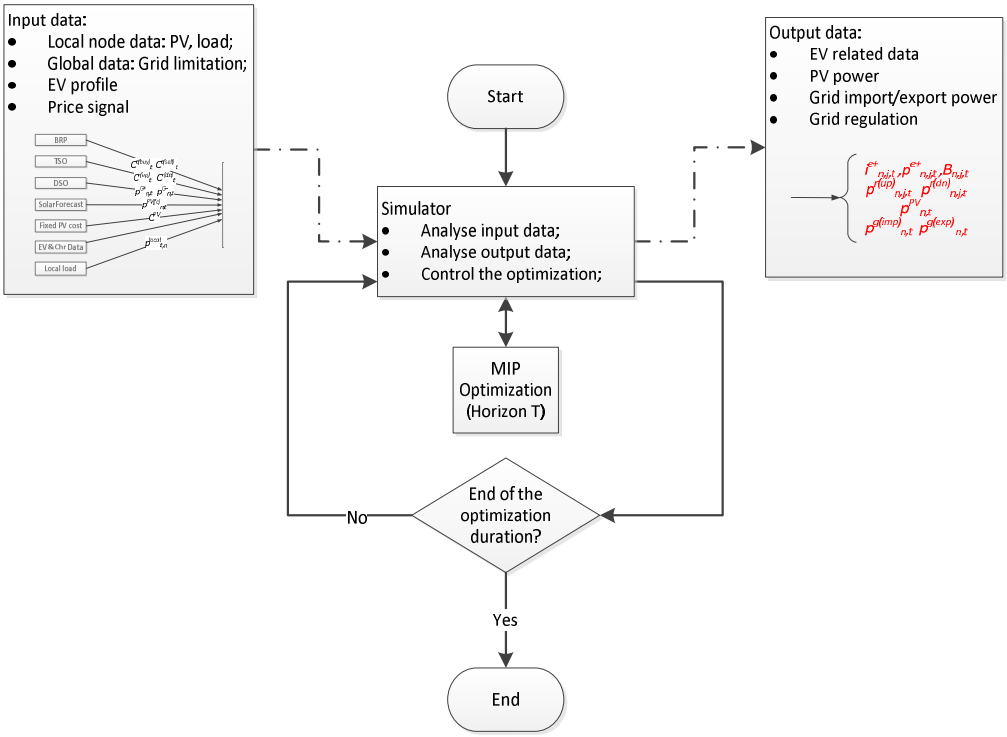

Figure 7: Structure schematic of the SCv2.0 implementation with YUD

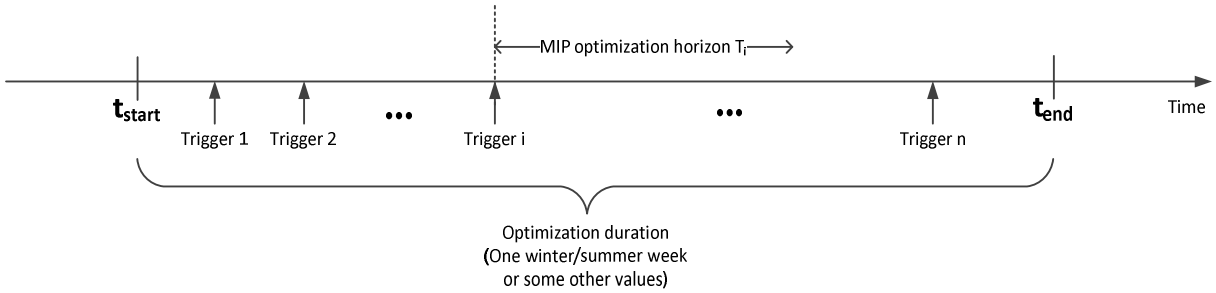

Figure 8 Time scale schematic of the OSCD smart charging algorithm

The MIP optimisation is triggered by certain events or with fixed time cycle, the implementation of SCv2.0 in OSCD project takes the new coming cars as the only trigger of the optimisation. Which means whenever there are new coming cars, the algorithm will reset the horizon and then run the MIP optimisation.

Moving and flexible receding horizon

Assume at node n there is a charging park equipped with four chargers (J = 4) with the algorithm is operating as shown in Figure 19. In this figure, each coordinate represents one charger; each block represents a car. In each coordinate, the X-axis represents the parking time of each car and the Y-axis shows the connectivity status of each car.

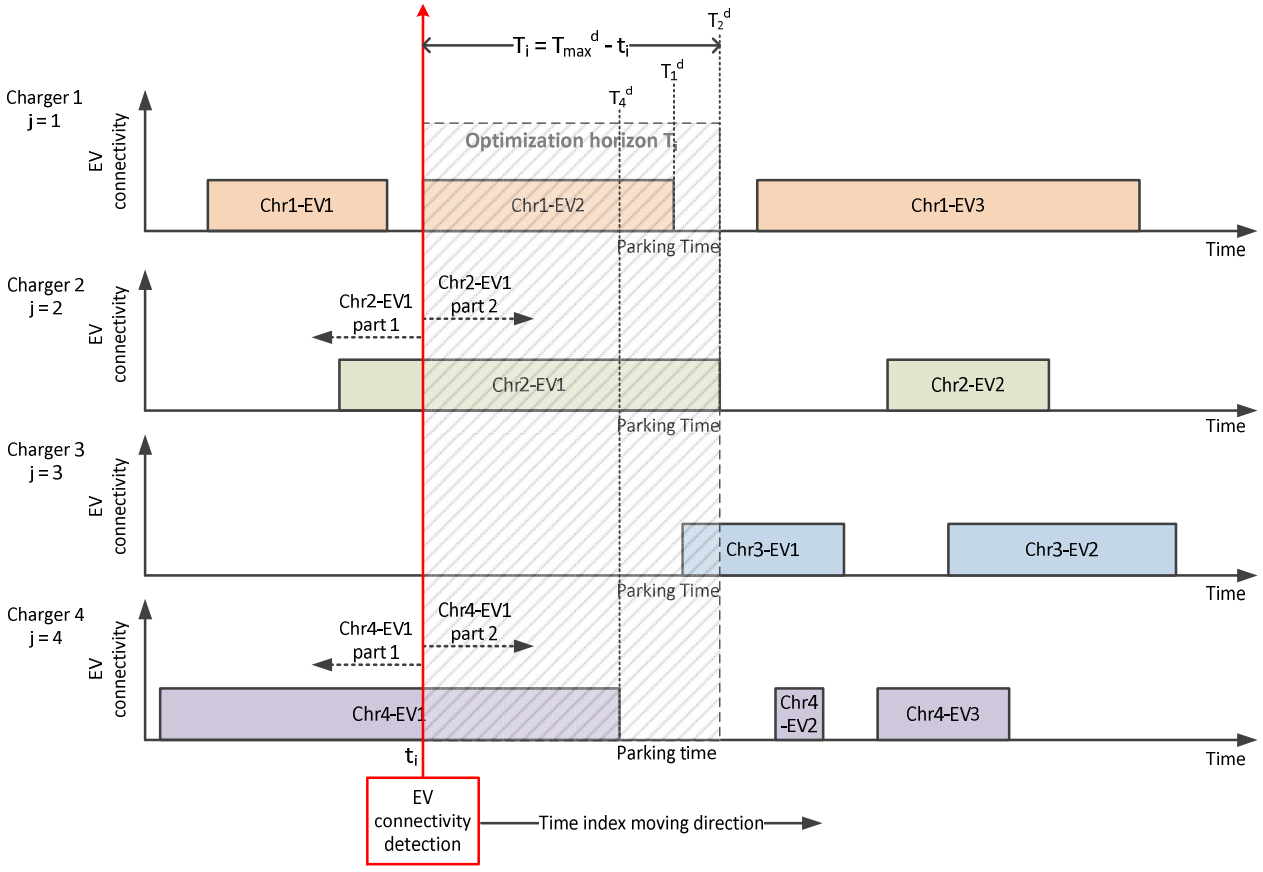

Figure 9 Illustration of the optimisation horizon determination

The algorithm detects if there is any new arrival/departure car or existing connected cars at every time step. At an arbitrary time t_i, there is a new car (Chr1-EV2) arrives at charger 1 while charger 2 and charger 4 already have car connected with separately, and the charger 3 is empty. The algorithm identifies all EVs from the charger's perspective. That is to say, even if there are only three cars connected at time t_i, J still equals to 4, but the parameters of each j is different. For example, at j = 3, which is the empty charger 3, all of the EV related parameters are either empty or equal to the default value. The algorithm then compares the departure time of cars connected to all four chargers (including one charger with an empty value) and select the latest departure time $T_{max}^d = Max\{T_j^d | j \in J\}$. The optimisation horizon T_i at time t_i is then determined as $T_i = T_{max}^d - t_i$.

Parameter updates and results output

The new arrival car triggers one new round of MIP optimisation, and what has happened in the past will not be included in the optimisation of the future. Thus the parameters of the connecting cars will be divided into "the past"(part 1 in Figure 19) and "the future" (part 2 in Figure 19) two parts and updated for the new round of optimisation. For instance, when car Chr1-EV2 arrives at time t_i , the parameters like arrival time, energy demand, SOC of car Chr2-EV1 and Chr4-EV1 need to be updated. The "future" part including the remaining parking time, remaining energy demand will be added into the new round of optimisation. The "past" part including the charged energy, the SOC will be stored temporarily and combined with the output data from MIP optimisation after the new round finished or when the car is leaving.

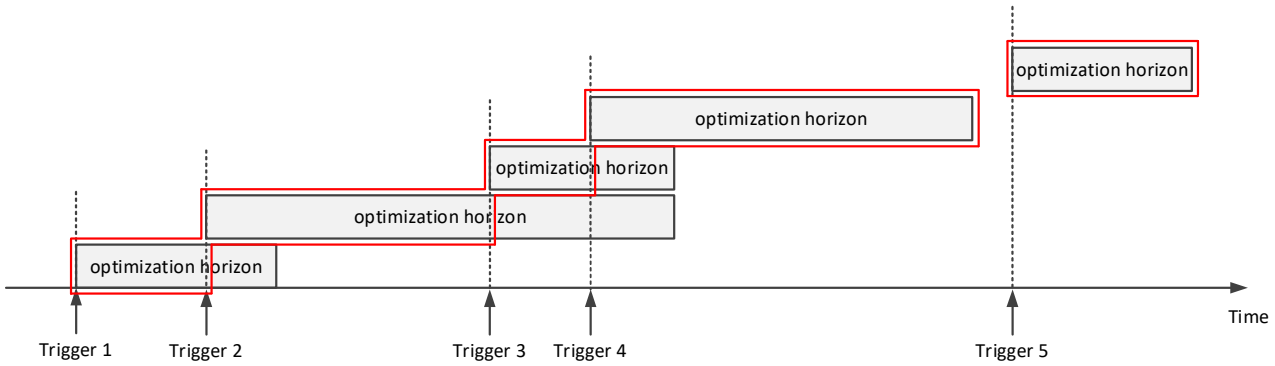

Figure 10 Schematic of the update of the output data

When this new round of MIP optimisation finished, its results will overwrite the output of previous optimisation rounds if there is overlap of horizon from time t_i to $t_i + T_i$. The schematic of the update of the output data is shown in Figure 23, and the final output data is highlighted with red lines. It is assumed that the PV prediction and load prediction have 100% accuracy, and the algorithm only works on the EV charging process in this first draft version of algorithm. Therefore, the algorithm does not work when there is no EV connected to the charger and thus the output of the optimisation will be the system default value, as the gap before "Trigger 5" plotted in Figure 23.

Assume the user of the algorithm is CSO, the CSO can set the algorithm start/end time t_{start}/t_{end}, which is when the algorithm is switched on/off. The timestep ΔT, which is the data resolution, can also be set by the CSO.

Simulation environment and parameter setups

For smart charging simulation, the platforms applied are Python and DIgSILENT PowerFacotry, and the MILP solver is GUROBI. The duration of the whole simulation is 4 days with 5 minutes resolution. The input data for PV, local load and grid models are the same as described in scenario definition and uncontrolled simulation. The price signal which is implemented is Day Ahead Market price (DAM) for the Netherland from year 2018. The DAM market price for both selling and buying are the same, however, in order to distinguish the difference between the energy being sold and purchased, also to include the losses during grid power Import and export, we set the sell price for electricity as 90% of the DAM buying price.

The implementation of a detailed regulation service procedure is also out of the scope of project, thus a simple version of implementation for demonstration is implemented in the simulation. It is assumed that the regulation service price the symmetrical, but the service offer can be asymmetrical, and the offer can be updated every 5 minutes.

Both DAM and FCR price are obtained from entsoe platform (https://transparency.entsoe.eu/) and the price of 4 winter days is shown in Figure 11.

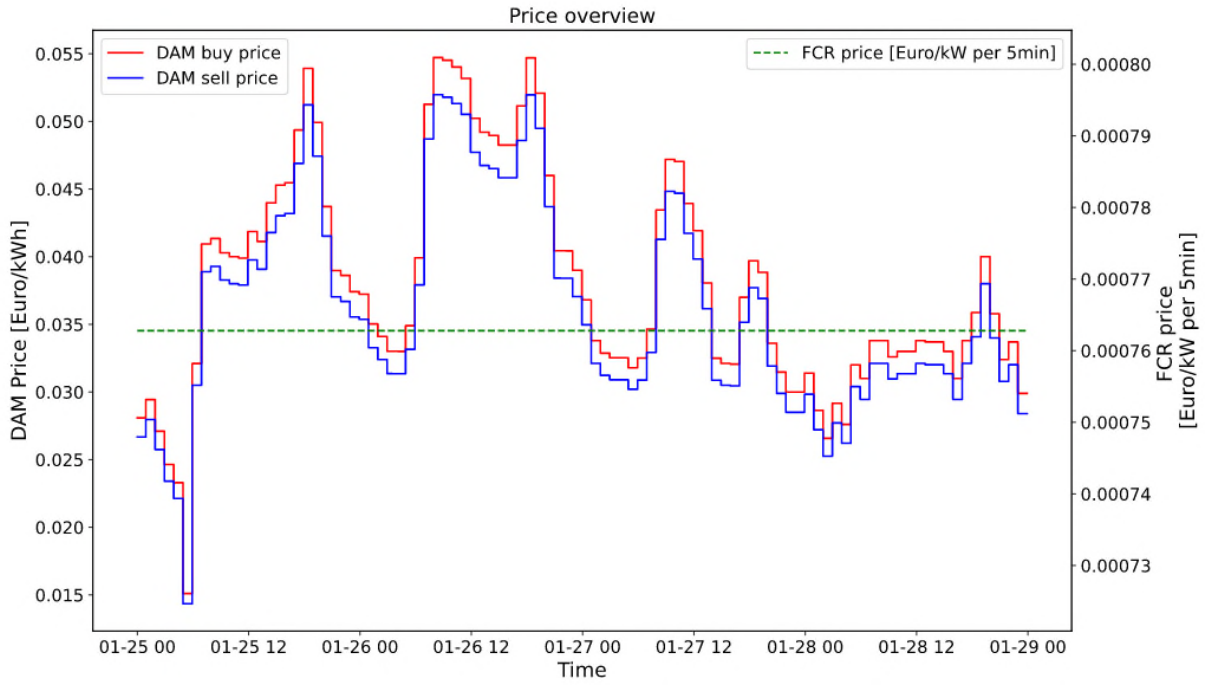

Figure 11 Sample DAM and FCR price data or Netherland in Winter

5.2 AIT implementation specifics

AIT specific assumptions

For the implementation AIT used the mathematical programming framework JuMP (Dunning, Huchette, & Lubin, 2017). The open source MILP (mixed integer linear programming) solver CBC (johnjforrest, et al., 2020) was used as a solver.

The prices that were used as input for the optimization problem were historical intraday prices from the EPEX spot market for the year 2018.

To keep the smart charging implementation within the grid limits (ie. Voltage minimum, line loading and transformer loading) an iterative process was implemented. Within the control loop a preliminary load flow calculation is executed with the previously determined maximum charging power for each charger. If one the implemented limits is exceeded, all involved chargers are sent new limits for charging power, and a new optimization process is started for these chargers. With the new power limits, another load flow calculation is done, this process is done iteratively until no limit transgressions were found anymore. For line and voltage limit transgressions, at first the reduction was done only for the affected feeder, if that was not able to fix the limit transgressions, charging for all chargers in the whole grid was reduced. For transformer loading transgressions all charging in the whole grid was reduced from the start.

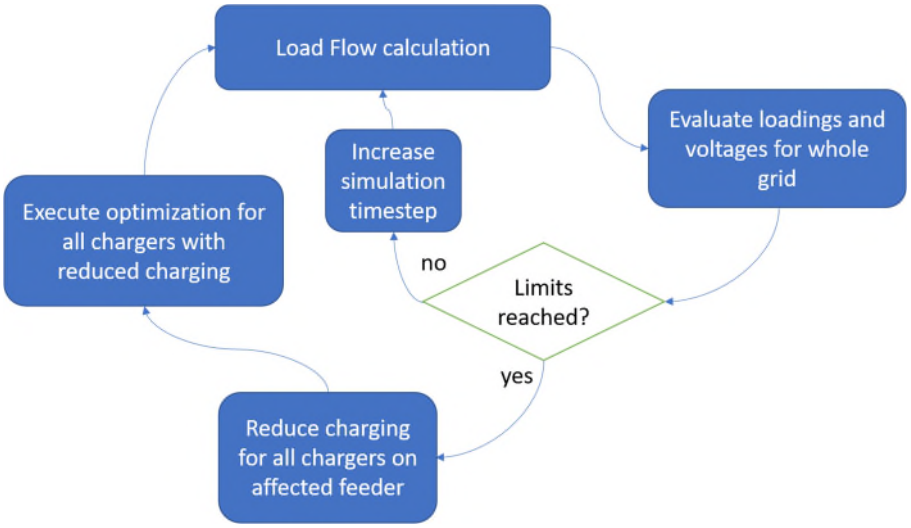

Figure 12: Exemplary depiction of central grid resource management mechanism

As for the simple smart charging algorithms, during the simulation with the smart charging algorithm the maximum reduction of charging current, was to reduce the charging to the minimal charging current that is defined by IEC 61851 as 6A. (International Electrotechnical Commission, 2017).

No interruption of charging processes was possible due to overstepped limits. TThe limits that were chosen for the central grid capacity management are shown in the following table.

Minimum voltage	Maximum line loading	Transformer loading
0.95 per unit	90% of rated current	90% of rated power

The AIT implementation of the smart charging algorithm did not include the balancing energy consideration from the SCv2.0 algorithm description, as it proved too time consuming to implement a realistic balancing energy market, and no sufficient data was available to do so.

All results presented in the following sections have been conducted for winter scenarios. The plots of the results for the summer simulations can be found in the appendix.

AIT specific simulation setup

The following graphics have already been presented for the uncontrolled charging scenario in deliverable D2.1 and are shown here to reintroduce some of the AIT specific simulation environment characteristics. As these plots are per charging algorithm, presenting them for every simulated scenario and each algorithm individually would require too much space. the plots in later sections show a statistical analysis of the results of several simulations.

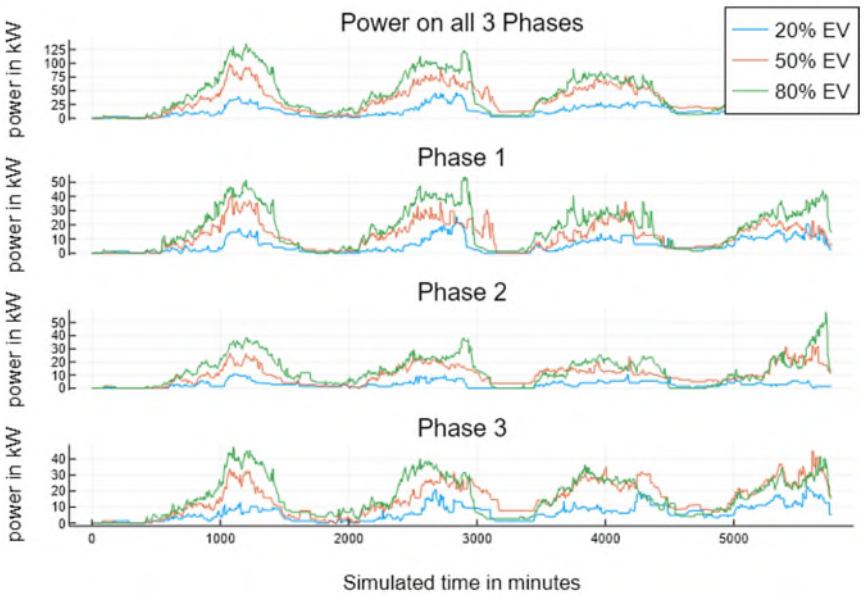

Figure 13: Phase distribution of charging power from all chargers throughout the grid and simulation for different EV penetration scenarios for Austrian Grid 8, winter

Figure 13 shows an exemplary distribution of charging power on different phases as well as the overall power for one time based simulation. This shows the asymmetry between the 3 phases that occurs because of different chargers as well as cars using different phase configurations. Even though the peaks match up, there is a phase asymmetry of several kW throughout the grid. The effect seems to become less apparent at higher penetrations, which is to be suspected. Such asymmetries could prove to be problematic when a single phase of a grid is critical to begin with.

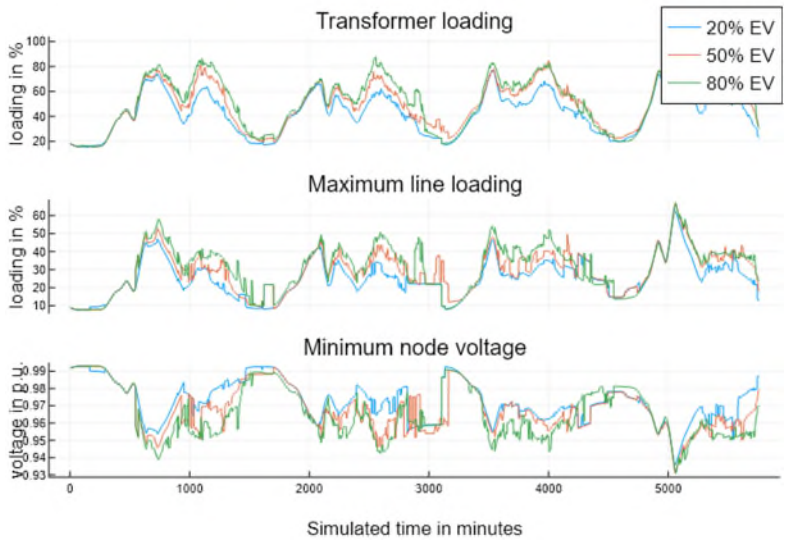

Figure 14: Time based simulation results depicting grid KPIs for smart charging Austrian Grid 8, winter

Figure 14 shows an exemplary plot of time based grid loading. The assumption of letting every EV charge whenever it arrives at a location with an EV charger leads to there being a large amount of charging events throughout the simulation, but few charging events for short periods of time. This can be seen by the fluctuating curves depicting grid performance indicators.

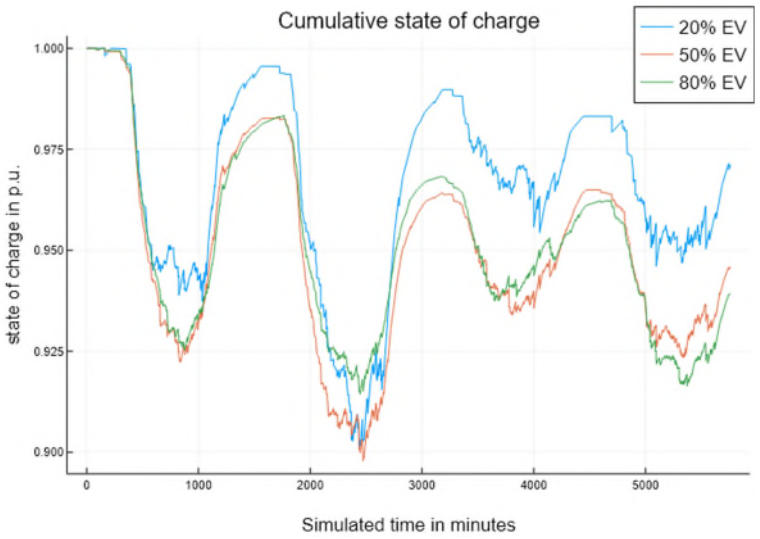

Figure 15: Time based simulation results showing accumulated state of charge of all vehicles within the simulation, Austrian Grid 8, winter

Figure 15 shows the accumulated state of charge of all simulated EVs over the simulated time.

During the day the energy content of EVs declines when they are being used for trips. In the afternoon and in the night EVs are mostly connected and the collective state of charge increases again. An interesting effect that can be seen on this graph is the fact that not all vehicles are recharged by the end of the simulation. This is mostly the case because the vehicles have travelled to a location where they are not able to charge. As the mobility data is generated through statistical evaluation of a mobility survey, this effect should reflect situations in real distribution grids well.

6. Simulation Results - Netherlands

To evaluate the multi-actor-optimised smart charging algorithm the same grids are used to evaluate the effects of uncontrolled charging and simple smart charging as in D2.1 and D2.2 respectively.

Table 1 Dutch rural Grid parameters

Grid type	Rural Grid 1	Rural Grid 2
Transformer capacity	400kVA	400kVA
No. of loads	3	138
Number of households	0	133
Average line length[m]	22.837	7.908
Longest feeder length	367.812	452.206
Yearly energy demand [MWh]	97.954	486.782

Table 2 Dutch suburban Grid Parameters

Grid type	Suburban 1	Suburban 2
Transformer capacity	400kVA	400kVA
No. of loads	480	266
Number of households	475	266
Average line length[m]	7.350	8.072
Longest feeder length	566.034	546.630
Yearly energy demand [MWh]	1394.143	800.796

Table 3 Parameters for Simulated Urban Grids

Grid type	Urban Grid 1	Urban Grid 2
Transformer capacity	400kVA	400kVA
No. of loads	296	123
Number of households	283	122
Average line length[m]	4.441	10.252
Longest feeder length	332.547	360.425
Yearly energy demand [MWh]	1680.224	261.036

6.1 Grid performance

In this section, for different scenarios the results of uncontrolled charging are compared with those of three simple smart charging techniques (price, based, average rate. Voltage based) and with the proposed smart charging algorithm. The observed changes in transformer loading, line loading and nodal voltages are compared.

Accumulative results

Figure 16 shows the box plot of transformer loading, maximum loading, and minimal node voltage at 80% EV penetration during Winter. he results of uncontrolled charging are compared with those of three simple smart charging techniques (price, based, average rate. Voltage based) and with the proposed smart charging algorithm.

- Grid loading results of SCv2.0 are more compact compared to other methods and the medium values are also better, especially for heavily loaded grids e.g. suburban grids. This shows SCv2.0 does improve the grid performance.
- Only two suburban grids are overloaded with peak values, the other grids have no problem at all.
- A short moment of e.g. transformer loading breach is not a problem, so this plot does not necessarily point to a negative sign for the smart charging.
- It is important to recognize that SCv2.0 does not always decrease the grid peak loadings or prevent grid overloading. This is because, due to the distributed nature of the algorithms' implementation, it heavily relies on the grid import/export limitations as set by the grid coordinator. This is hence a key control variable that strongly influences the charging profile and meeting the EV energy demand.
- To improve the algorithm's performance, it is important to have a suitable central coordination entity to set the grid limits for import and export. The coordination entity needs to look at all the nodes with and without EVs. But also, at current and expected future loading patterns.

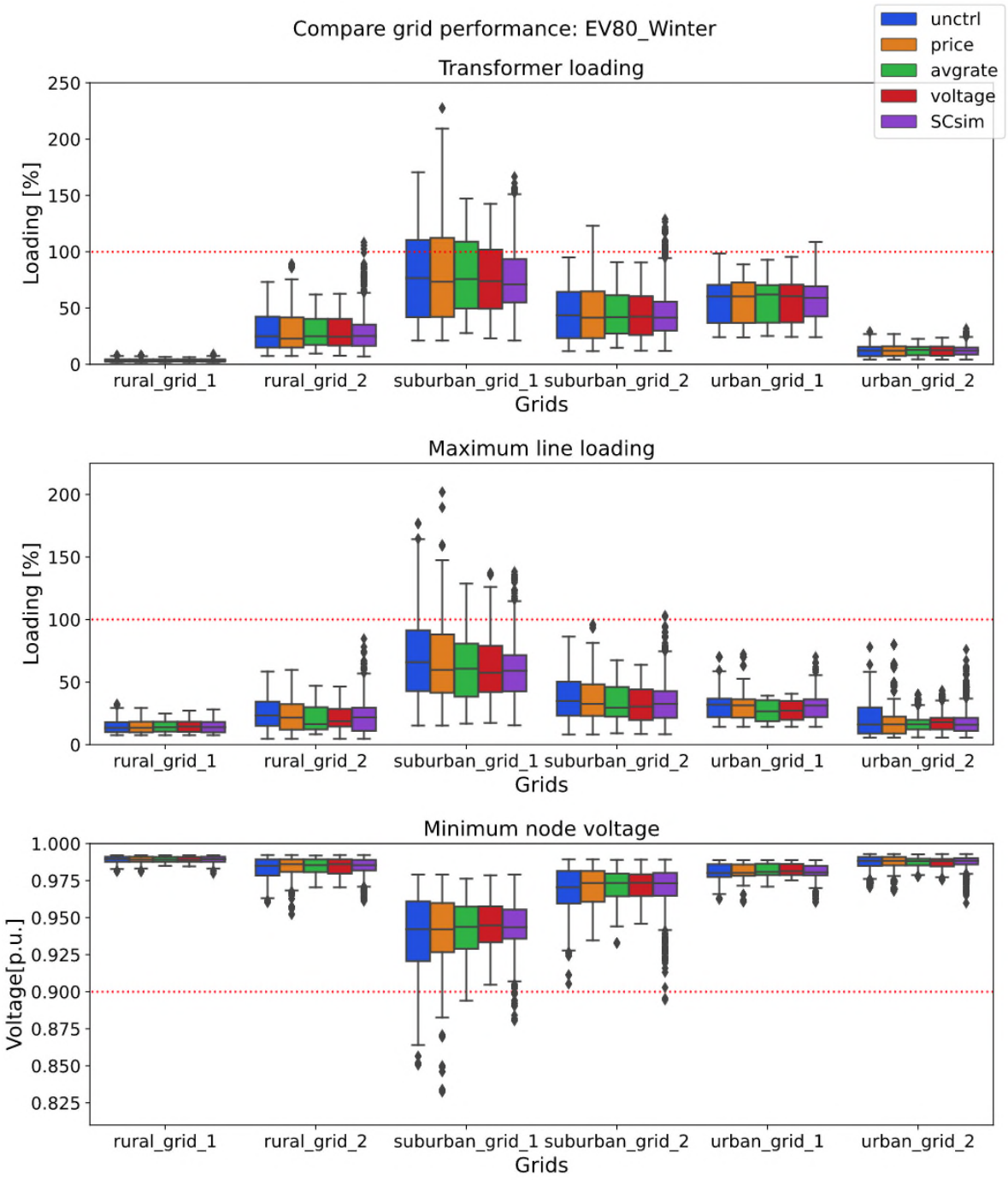

Figure 16 Box plot of transformer loading, maximum loading and minimal node voltage at 80% EV penetration in Winter

Time based plots

Figure 17, Figure 18, Figure 20 shows the time-based Grid transformer loading, maximum line loading amongst all lines and minimum nodal voltage amongst all nodes for the case of 80% EV penetration in Winter. We can observe that

- The SCv2.0 helps in reducing the peak loading compared to other methods, especially for the heavily loaded grid suburban grid 1. Both the overloading duration and magnitude are decreased with SCv2.0.
- Most of the EV charging power is shifted to the "free capacity" time window (or valley window) where the base load is low and the grid has more free capacity as seen in Figure 17. This concept is further shown in Figure 19 where we define the free capacity as: the available grid capacity apart from existing base load;
- It is preferable to charge EVs in this way because it does not add too much burden unlike the other methods which charging power are add on top of existing peaks;
- This is further elaborated in Figure 21 which shows the percentage of EV charging energy that falls into free capacity windows. The plot proves indeed the SCv2.0 helps use the grid capacity in the most efficient ways;
- If eventually the free capacity is used up, then the grid needs to be reinforced by increasing the capacity of transformers and lines.

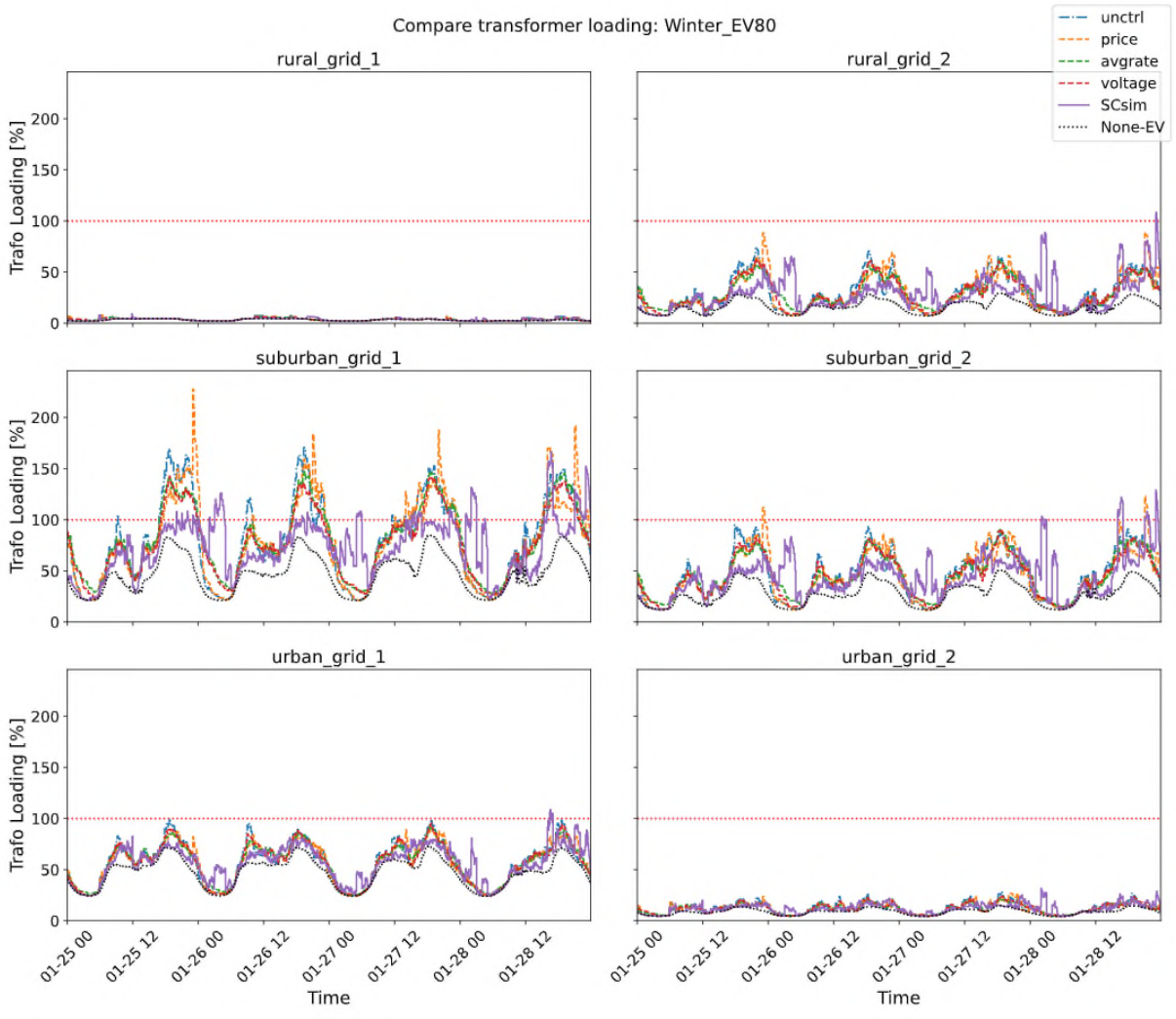

Figure 17 Grid transformer loading versus time at 80% EV penetration in Winter

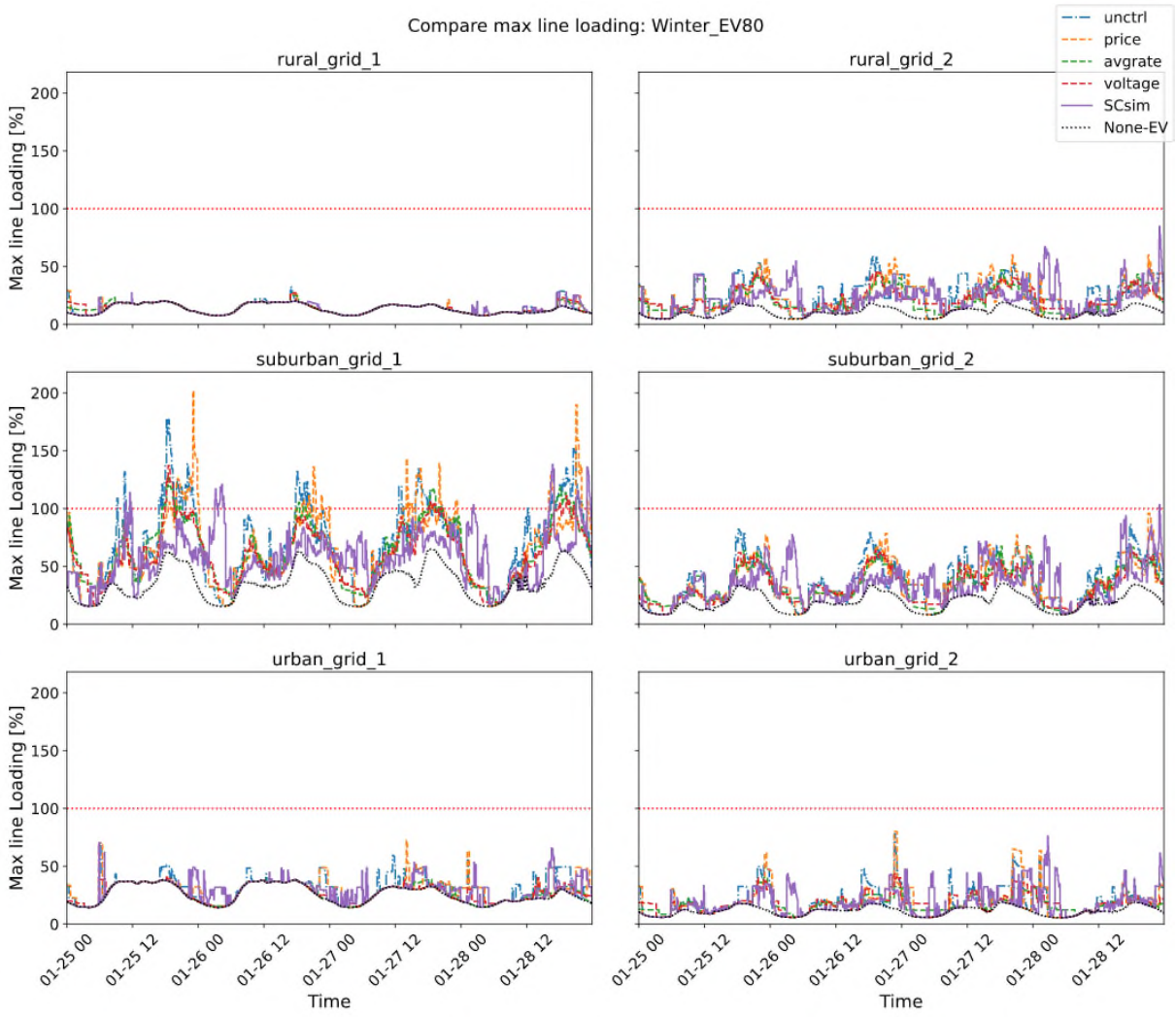

Figure 18 Loading of maximum loaded line of the grid versus time at 80% EV penetration in Winter

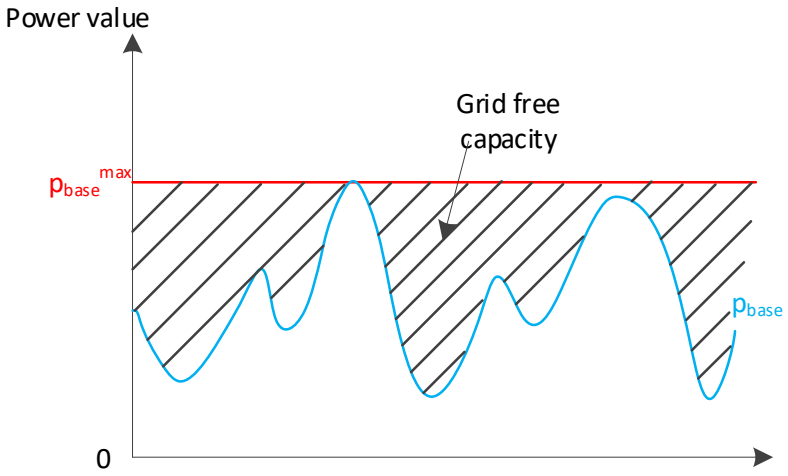

Figure 19 Schematic of grid free capacity for EV charging

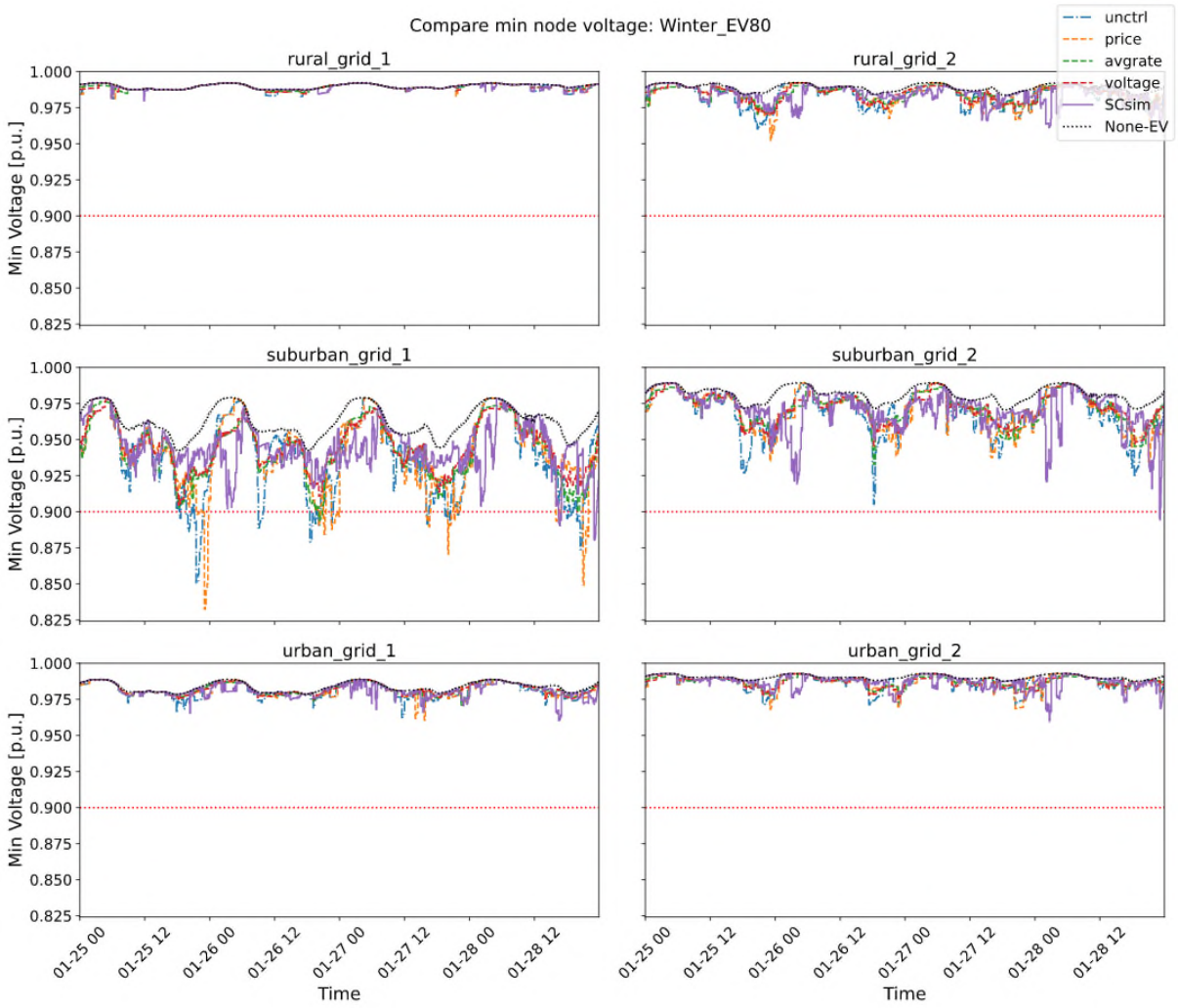

Figure 20 Minimal node voltage of the grid versus time at 80% EV penetration in Winter

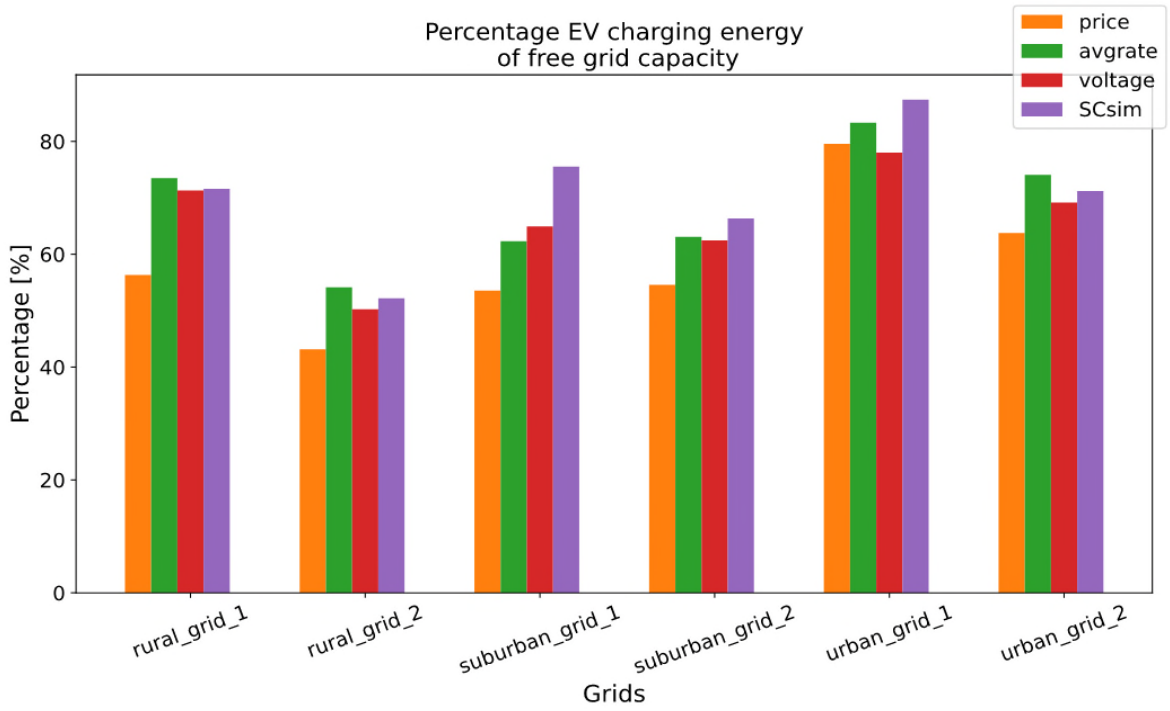

Figure 21 Percentage of EV charging energy that falls into free capacity windows

6.2 Charging satisfaction and cost

This paragraph compares the results between the charging techniques adjusted for normalised charging costs, charging accomplishments at the pre-set grid charging limit (400kW), as described in Section 5.1

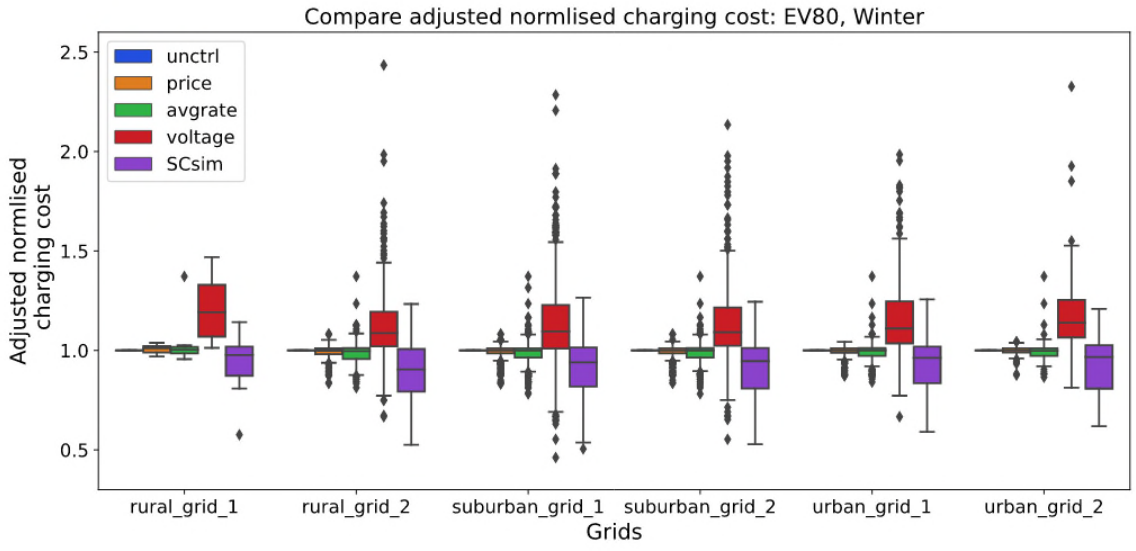

Figure 22 Adjusted normalised charging cost comparison for EV 80% penetration in Winter

Figure 22 compares the adjusted normalised charging costs of the different charging techniques for all the charging sessions. For each charging event, the cost of different simple and smart charging methods is normalised with the uncontrolled charging costs and then corrected for the charge satisfaction using the formula (35) below:

$$Adjusted\ normalised\ charging\ cost = \frac{C_{SCC}/C_{unctrl}}{E_{charged}/E_{request}} \quad (35)$$

Where C_{SCC} is the charging cost of cost of different simple and smart charging methods, C_{unctrl} is the cost of uncontrolled charging, $E_{charged}$ the actual charged energy and $E_{request}$ is the charging energy demand.

The figure shows a significant decrease in charging costs for the SCv2.0.

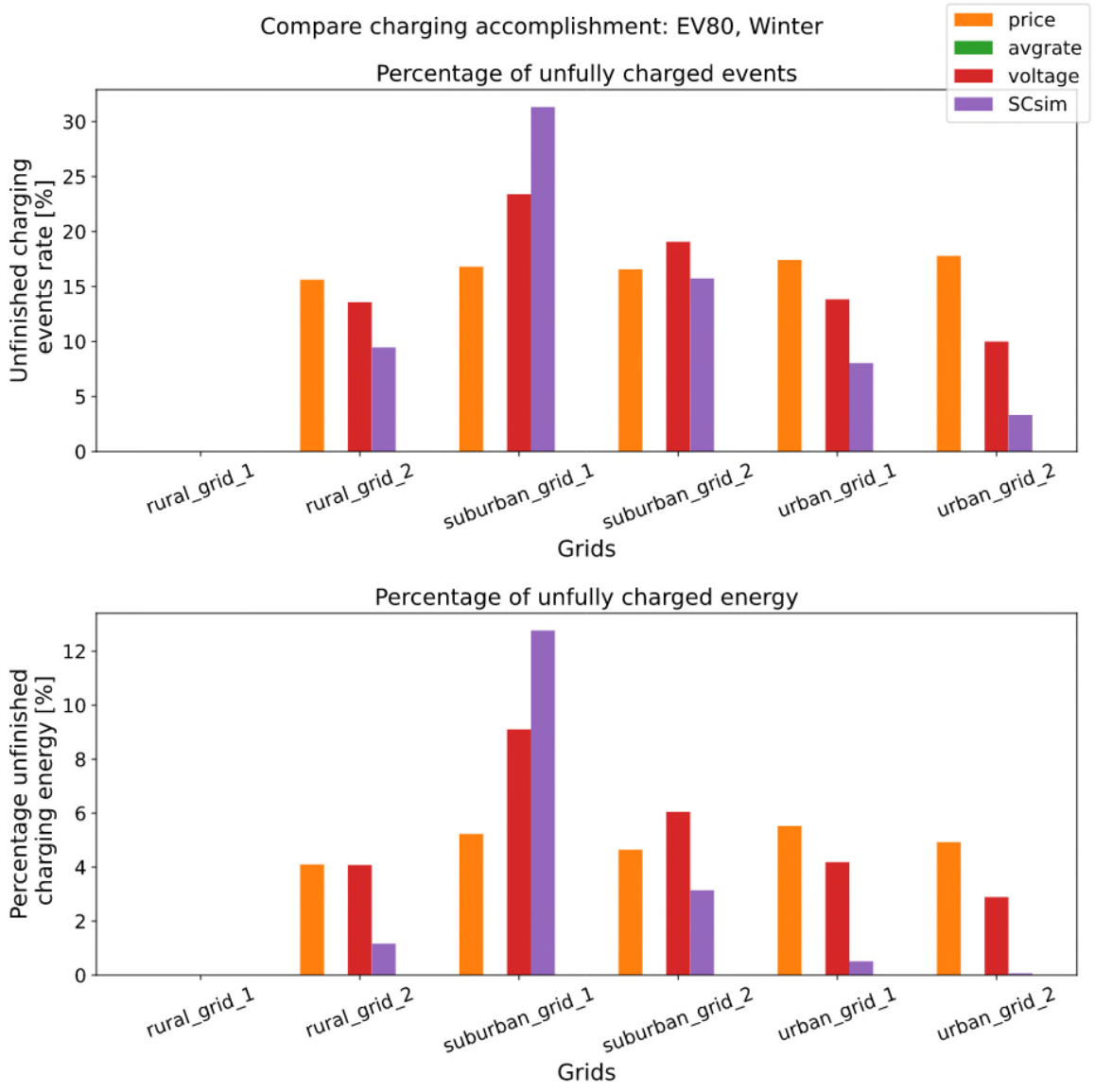

Figure 23 Level of charging accomplishment comparison for EV 80% penetration in Winter

The charging level accomplishments are greatly improved by the SCv2.0 both in number of events and fulfilled charge requests, for all grids except for suburban grid as shown in Figure 23. This is because in this specific situation where grid overloading is the major problem for suburban grid 1, the priority of the algorithm is to mitigate the grid congestion rather than to meet the charge request.

This also explains why some of the other grids have higher peak loadings with SCv2.0 in Figure 17, Figure 18 and Figure 20. As in these cases the algorithm prioritises EV charge accomplishments within the grid capacity limitations.

- SCv2.0 improves both charging accomplishment regarding both the number of events and requested energy for all the other grids except suburban grid 1.
- That is because suburban 1 has great overloading issue thus the priority of the algorithm is to prevent grid congest rather than fulfil all the charging requests
- As for other grids, this results also explains why some other grids have higher grid peak loading with SCv2.0. That is because the algorithm tries to charge all the EV as much as possible within available grid capacity limitations.

6.3 Influence of central coordination alterations

The current central coordination method is very basic. It evenly distributes the pre-set grid EV charging limit (in this case the transformer capacity is used to set the value) to the EV connected nodes dynamically based on the number of connecting EVs. This method does not incorporate the base load of the whole grid, nor does it consider the EV charging demand variation and the other grid performance indices (line loading, node voltage). The only value that can be altered to change the power limit to each node is the pre-set grid EV-charge limit. As a result, it is important to see how the variation of pre-set grid limits of the central coordination influences the outcome of SCv2.0.

In this section, the pre-set grid limit is tightened from 400 kW to 300 kW on the grids that show congestions problems (i.e., rural 2, suburban 1 and suburban 2).

Grid performance with tightened pre-set grid limit

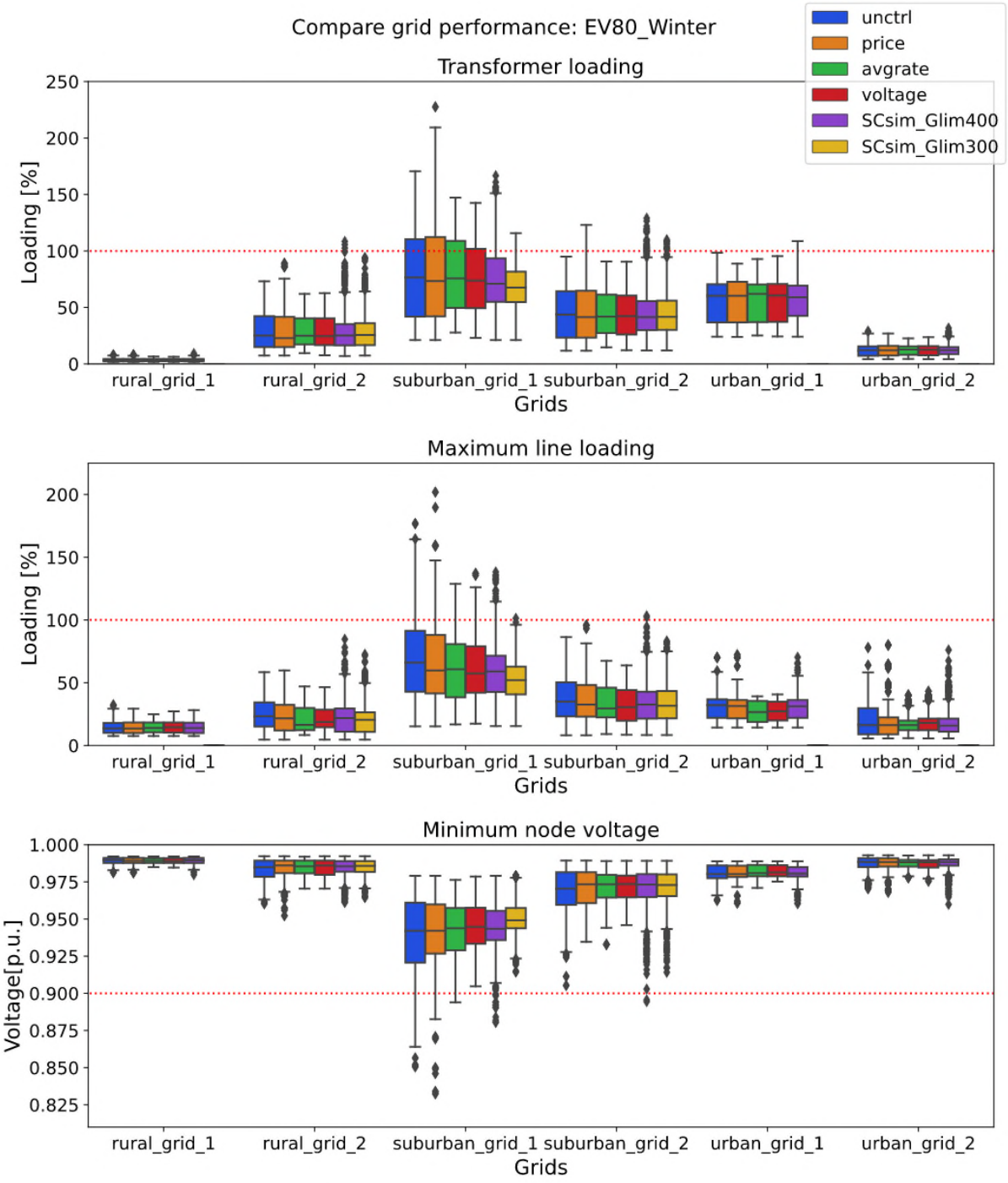

Figure 24 Grid performance including two grid limitations for SCv2.0

Grid performance is significantly improved by SCv2.0 in grids that have a lot of congestions, as shown by the Figure 24. Short moments of transformer or line overloading will not lead to grid disruptions.

Figure 25, Figure 26 and Figure 27 show the time-based grid transformer loading, maximum line loading and minimum node voltage for 80% EV penetration in Winter as in paragraph **Fehler! Textmarke nicht definiert.** with the addition of the reduced grid EV-charge limit. This shows that increasing the grid EV-charge limit improves performance in grids that have congestions problems.

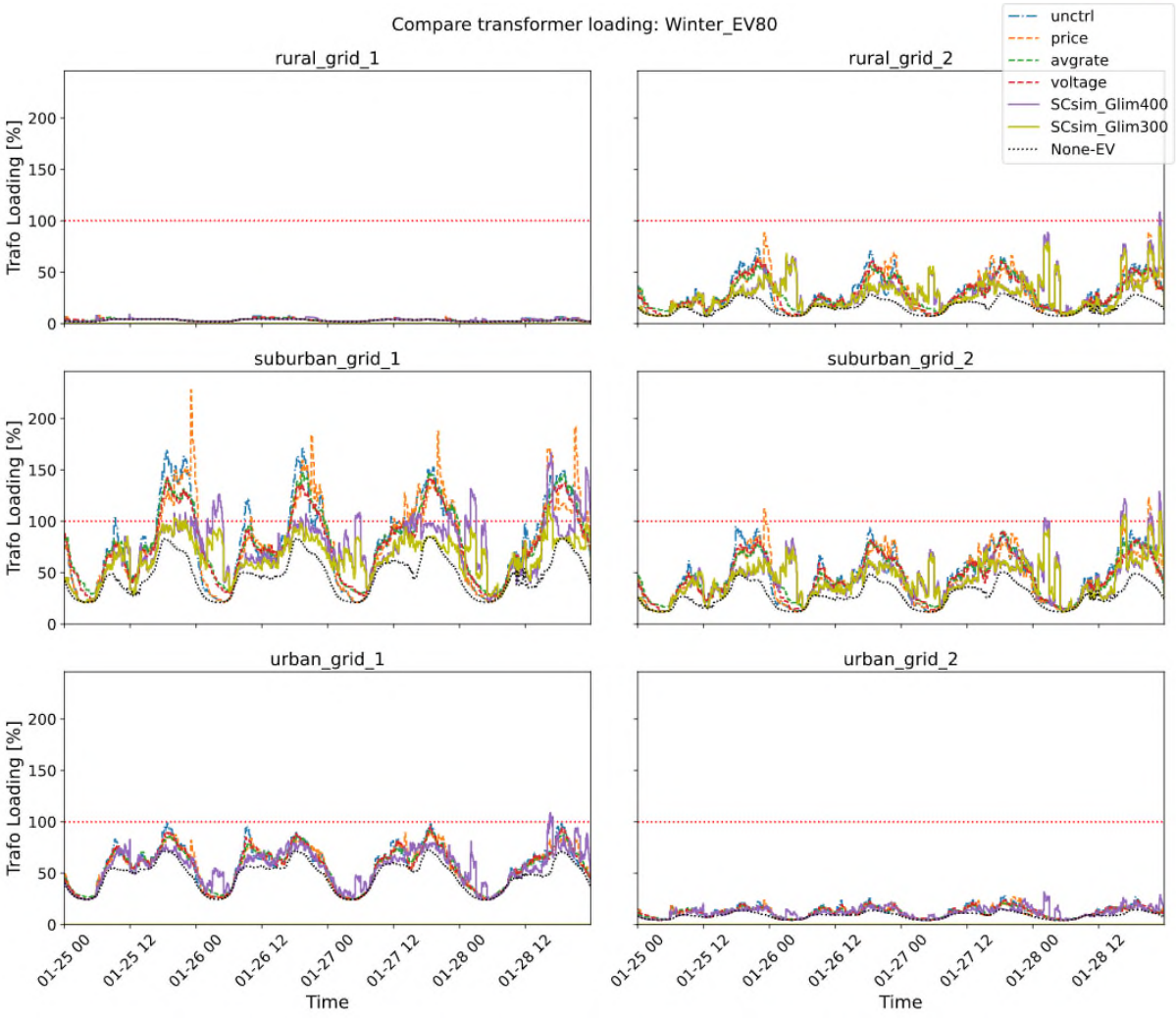

Figure 25 Grid transformer loading versus time at 80% EV penetration in Winter with reduced grid EV-charge limit

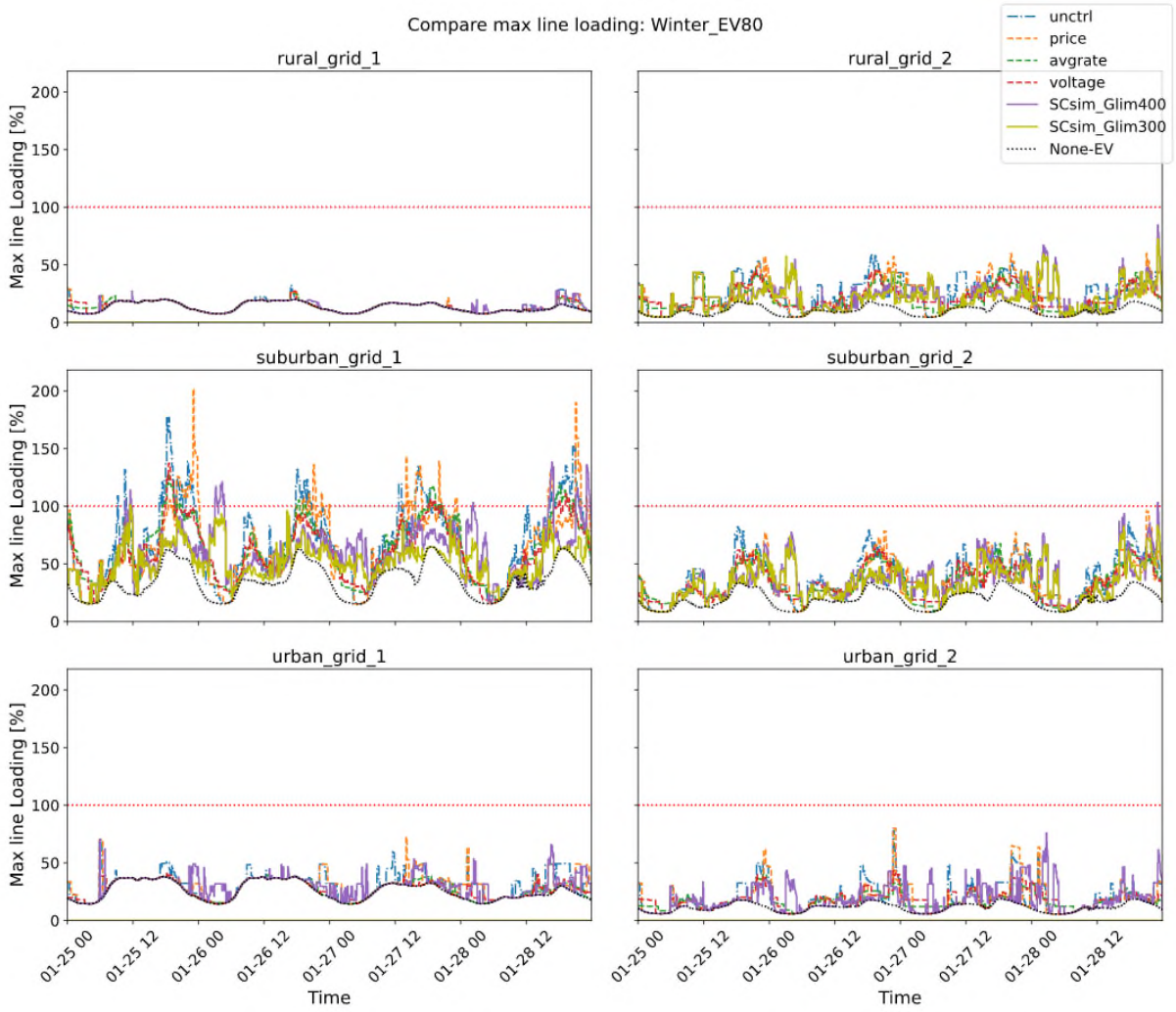

Figure 26 Loading of maximum loaded line of the grid versus time at 80% EV penetration in Winter with

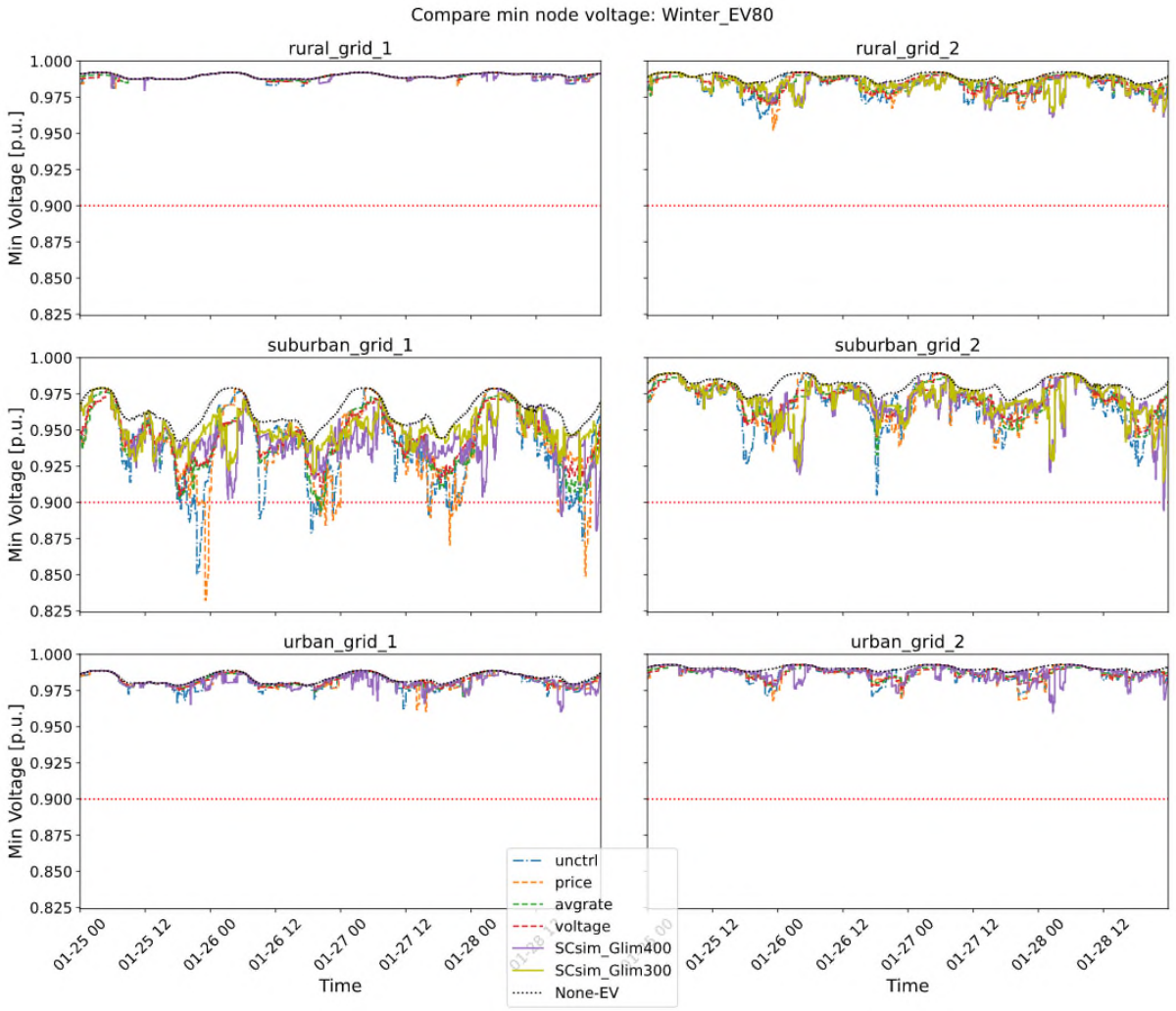

Figure 27 Minimal node voltage of the grid versus time at 80% EV penetration in Winter with reduced grid EV-charge limit

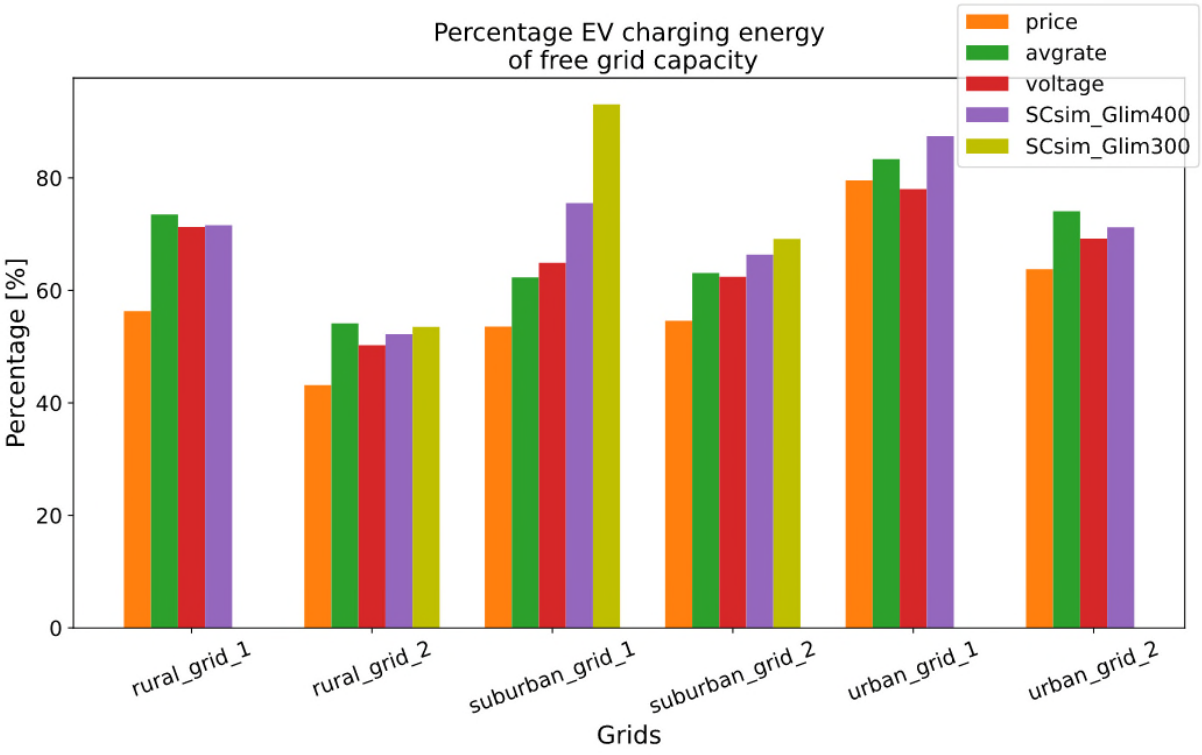

Figure 28 Level of charging accomplishment comparison for EV 80% penetration in Winter with reduced grid EV-charge limit

The power and energy plots show that heavy congested grids (i.e., suburban grid 1) can highly benefit from tightened grid EV-charge limits. Other less congested grids advantage less in decreasing congestion and could even unnecessarily sacrifice EV-charge demand, this is explained in the next section.

Charging cost and satisfaction with tightened pre-set grid limit

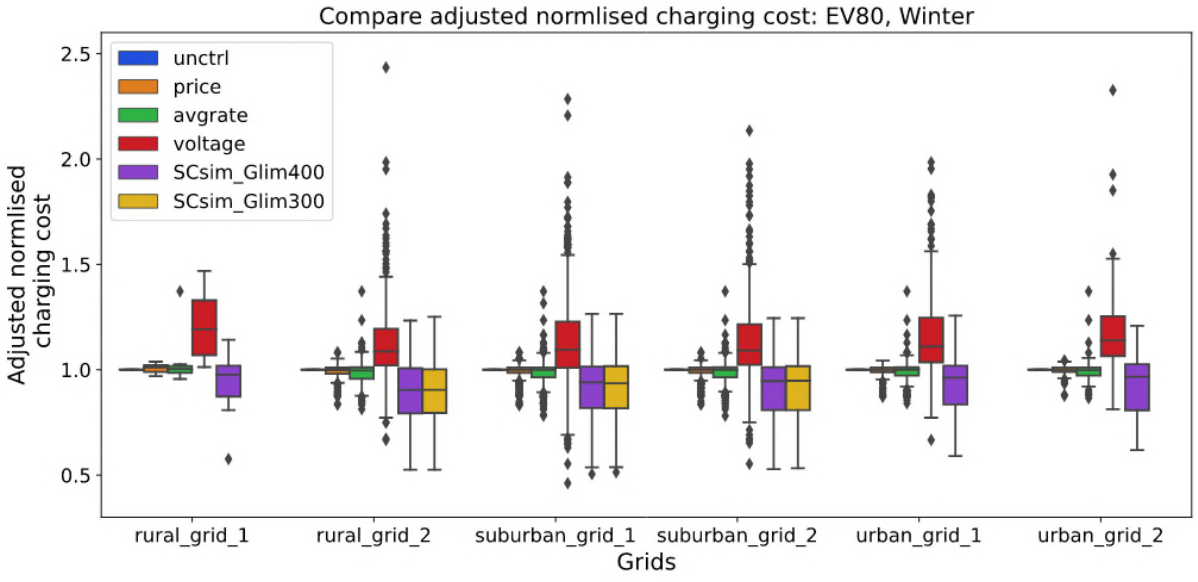

Figure 29 Adjusted normalised charging costs SCv2.0 with grid EV-charge limitation

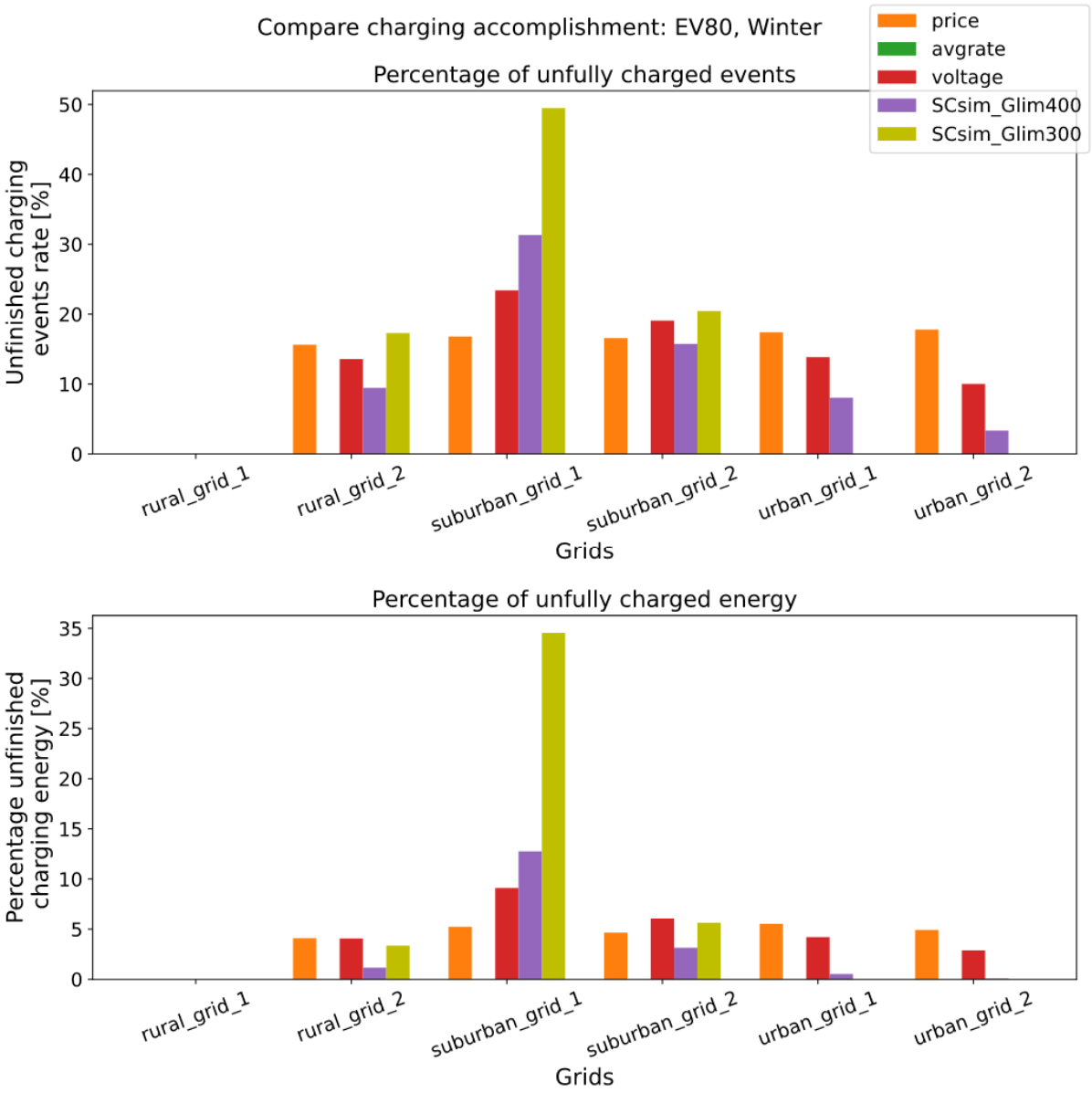

Figure 30 Level of charging accomplishment comparison for EV 80% penetration in Winter with different grid EV-charge limitation

As shown in Figure 29 tightening the grid EV-charge limitation does not influence the cost at all. It does lead to higher unfinished charging events as seen in Figure 30, especially for rural 2 and suburban 2. The grid performances are not significantly better, but less cars are charged to satisfaction. Because the EV-charge limitation is evenly distributed between connected nodes, some charge request might not be met while other nodes have unused capacity. Dynamic redistribution of available capacity between connected nodes, based on demand, would solve this.

This means that for each grid type the grid congestion level needs to be evaluated before setting a grid EV-charge limitation as there is a trade-off between grid performance and EV user satisfaction.

7. Simulation Results - Austria

To evaluate the multi-actor-optimised smart charging algorithm the same grids are used to evaluate the effects of uncontrolled charging and simple smart charging as in D2.1 and D2.2 respectively.

7.1 Rural Grids

For the Austrian simulation setup 2 Rural Grids were investigated. The key parameters identifying the grids are shown in the following table.

Rural Austrian Grids		
Grid	Austrian Grid 1	Austrian Grid 2
Problems expected	yes	no
Annual electricity demand	1121 MWh	384 MWh
Transformer capacity	1*630 kVA	1*250 kVA
Number of nodes	154	62
Number of households	280	77
Average line length	51 m	49 m
Total length longest feeder	1134 m	1312 m
Number of nodes equipped with PV	23	2
Total installed PV power	148 kVA	12 kVA

Figure 31 and Figure 32 show the simulation results with regards to minimal voltage reached throughout the simulations for the Austrian Grid 1 and 2 respectively. It can be seen that the smart charging algorithm "SCv2.0" shows the best results together with the average rate charging.

Figure 33 and Figure 34 shows the maximum line loading throughout the simulations with different control algorithms for the EV chargers. No critical situations were reached, but the smart charging algorithm seems to be performing the best with regards to line loading.

Figure 35 and Figure 36 show the results with regards to transformer loading for the Rural Austrian Grids 1 and 2 respectively. No critical situations can be highlighted. All charging control schemes performed well.

Figure 37 and Figure 38 show the average price in € per kWh per charging event for each of the simulations with Austrian Grid 1 and 2 respectively. There is not a lot of difference between the prices that can be achieved using the different algorithms if access to the intraday market is available. If the prices were compared to standard fixed tariff energy prices, 18.5486 €c per kWh including taxes and grid tariffs (Energie, 2020). In comparison with that a considerable advantage can be achieved with smart charging algorithms. This requires access to these dynamic markets, which will probably only be possible with a centrally controlled smart charging algorithm in place.

Figure 39 and Figure 40 show the comparison of the average state of charge at the end of charging events, where an advantage of the smart charging algorithm over the average rate algorithm can clearly be seen.

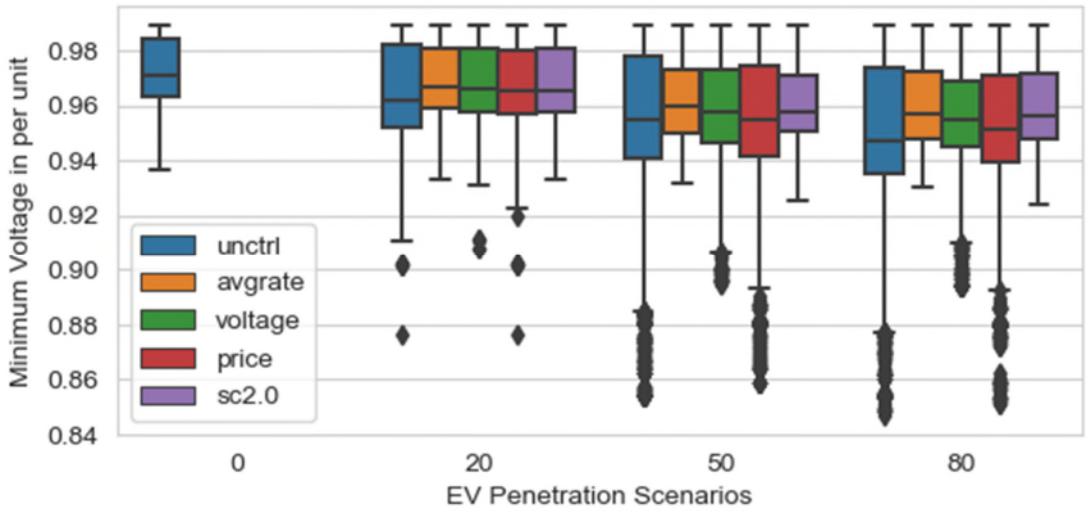

Figure 31: Comparison of minimum voltage per simulation time step for all penetration scenarios and control algorithms Austrian Grid 1, winter.

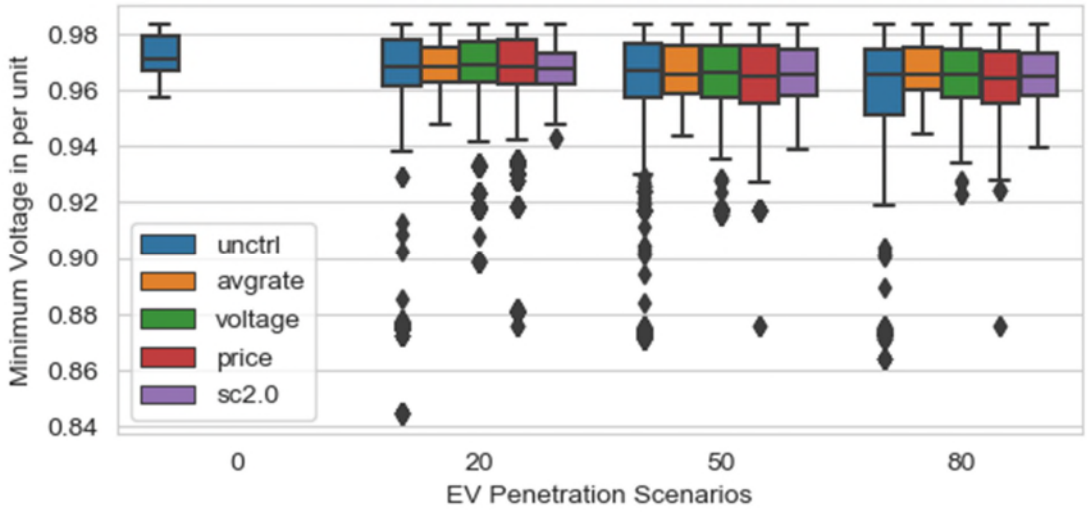

Figure 32: Comparison of minimum voltage per simulation time step for all penetration scenarios and control algorithms Austrian Grid 2, winter.

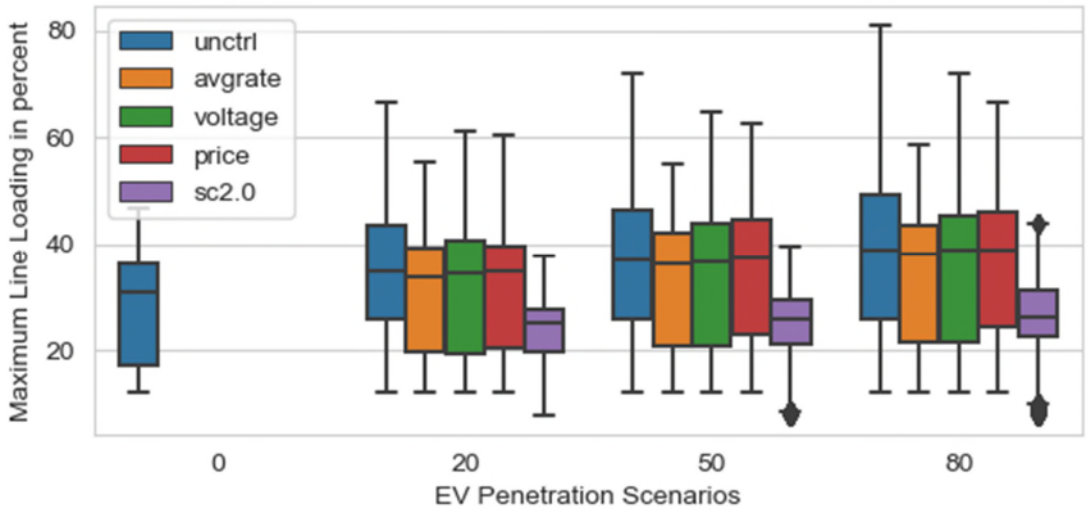

Figure 33: Comparison of maximum line loading per simulation time step for all penetration scenarios and control algorithms Austrian Grid 1, winter.

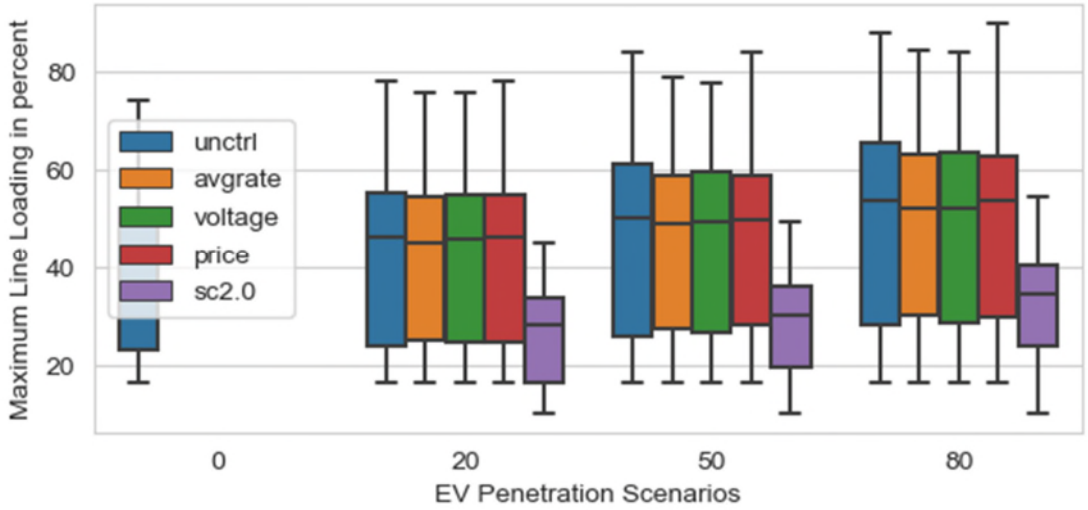

Figure 34: Comparison of maximum line loading per simulation time step for all penetration scenarios and control algorithms Austrian Grid 1, winter.

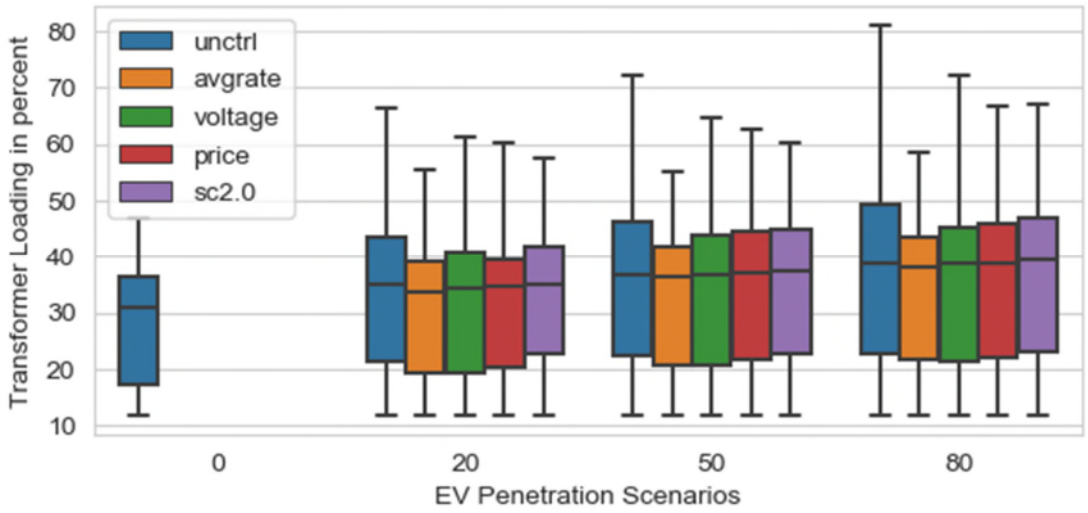

Figure 35: Comparison of transformer loading per simulation time step for all penetration scenarios and control algorithms Austrian Grid 1, winter.

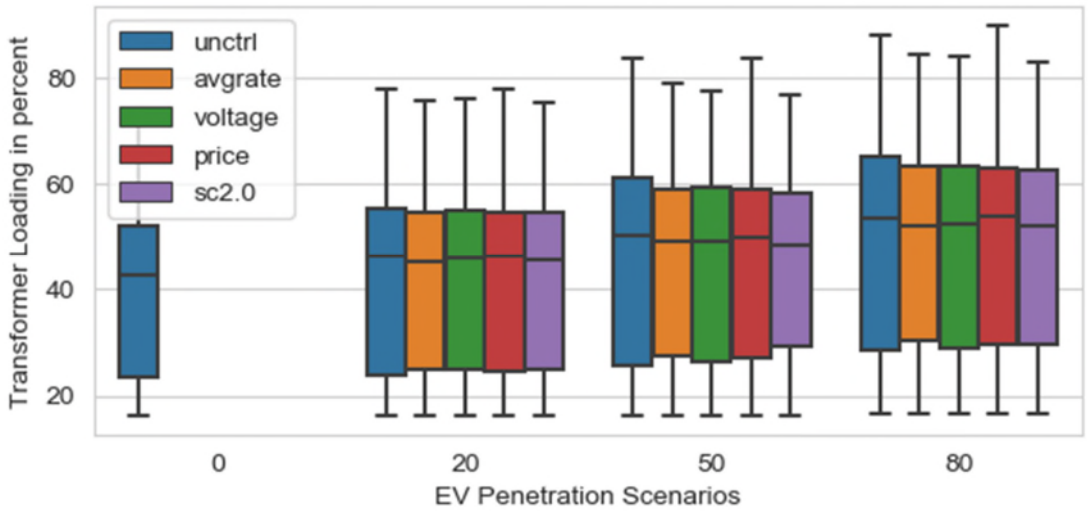

Figure 36: Comparison of transformer loading per simulation time step for all penetration scenarios and control algorithms Austrian Grid 2, winter.

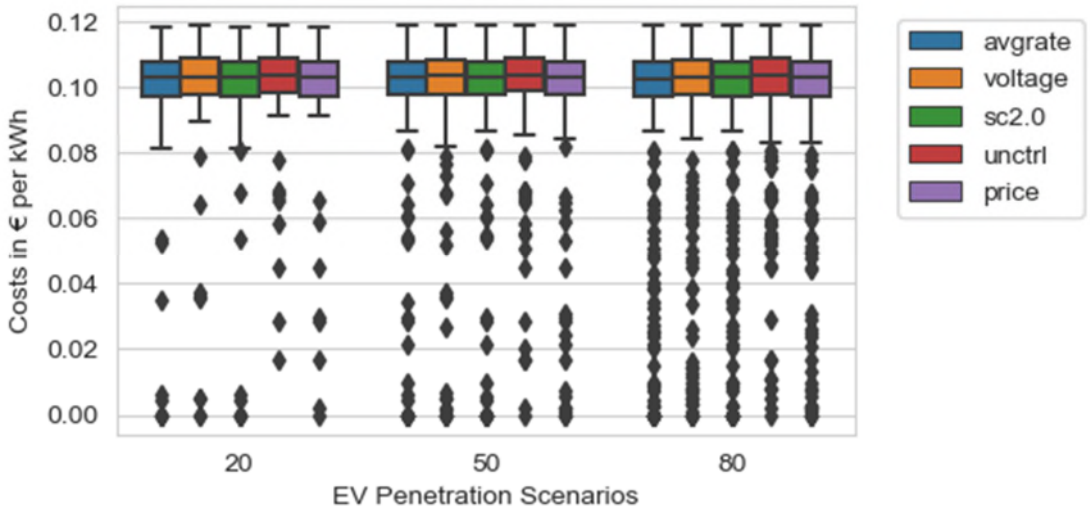

Figure 37: Comparison of charging costs per charging event for all penetration scenarios and control algorithms Austrian Grid 1, winter.

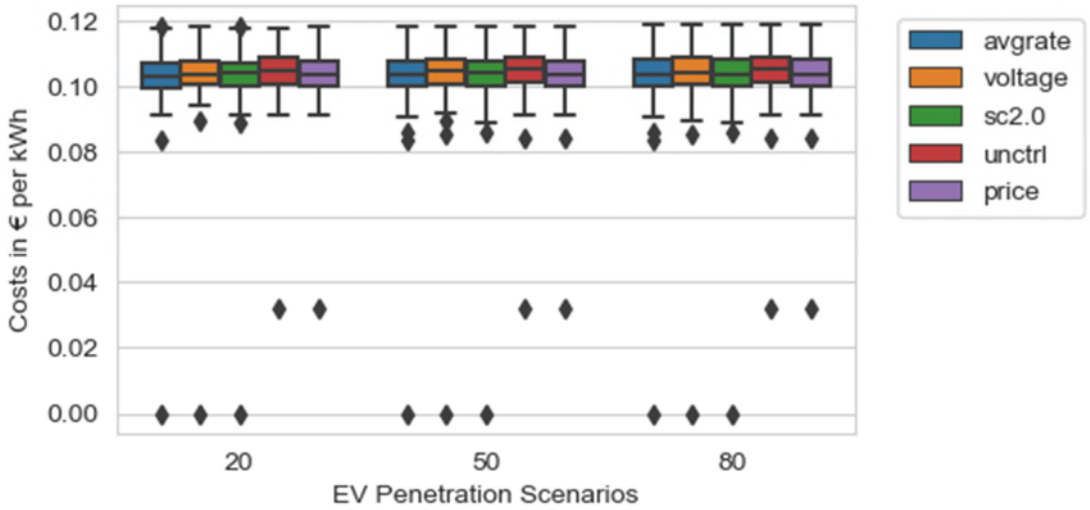

Figure 38: Comparison of charging costs per charging event for all penetration scenarios and control algorithms Austrian Grid 2, winter.

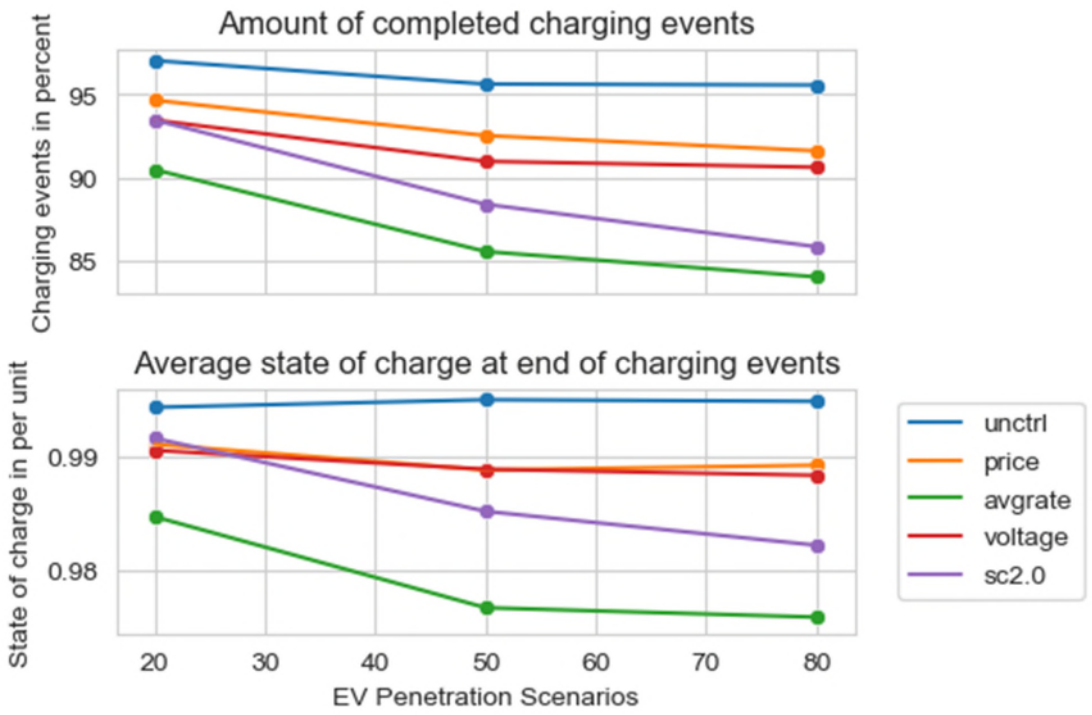

Figure 39: Comparison of completed charging events and average state of charge at the end of charging events for all penetration scenarios and control algorithms Austrian Grid 1, winter.

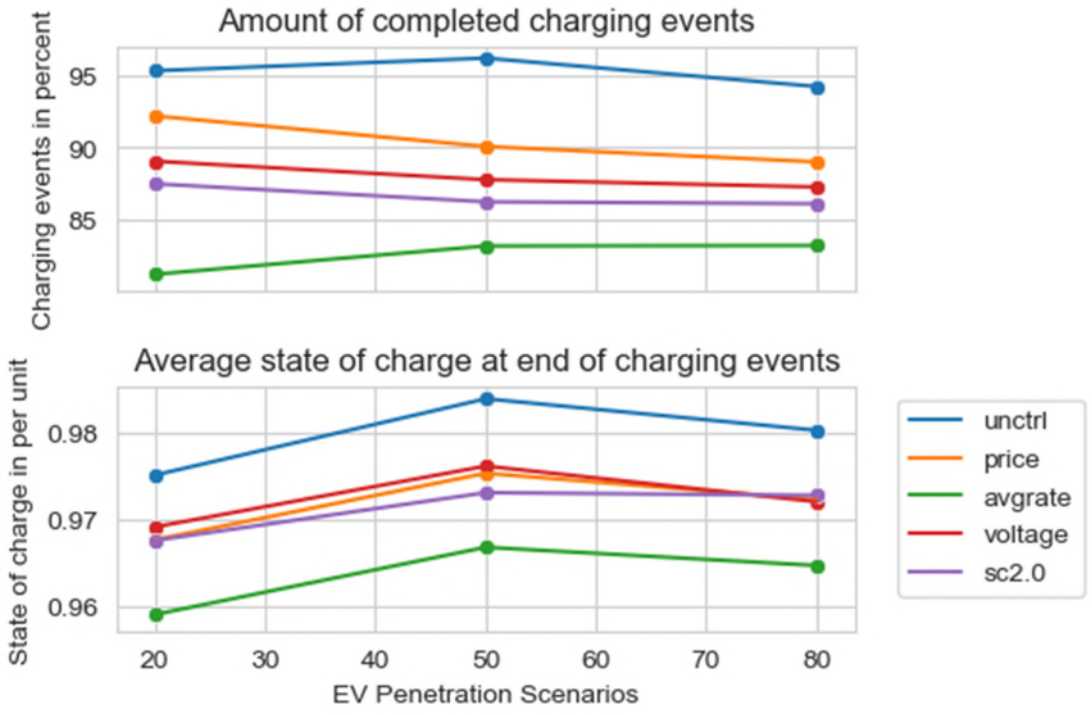

Figure 40: Comparison of completed charging events and average state of charge at the end of charging events for all penetration scenarios and control algorithms Austrian Grid 2, winter.

7.2 Suburban Grids

For the investigation of suburban grids in Austria 4 grids were implemented in the co-simulation environment. The key parameters for the different grids are summarised in the following table.

Suburban Austrian Grids				
Grid	Austrian Grid 3	Austrian Grid 4	Austrian Grid 8	Austrian Grid 9
Problems expected	yes	no	-	-
Annual electricity demand	1651 MWh	1213 MWh	760 MWh	1222 MWh
Transformer capacity	2*400 kVA	1*400+1*630 kVA	1*400 kVA	1*400 kVA
Number of nodes	205	51	147	141
Number of households	410	321	345	319
Average line length	37 m	34 m	22 m	31 m
Total length longest feeder	590 m	280 m	457 m	678 m
Number of nodes equipped with PV	14	3	19	7
Total installed PV power	107 kVA	13 kVA	111 kVA	45 kVA

Figure 41 to Figure 44 show the minimum voltages observed throughout the simulations for the different simple smart charging schemes and for different EV penetration scenarios. For all the grids the minimum observed voltage gets lower with higher EV penetration.

The multi-actor optimized smart charging algorithm performed equally good as the average rate charging algorithm, because at critical voltage situations a reduction of charging rate is implemented as described on Page 26. In none of the charging algorithms an interruption of the charging process is considered, the maximum charging reduction is to the minimum allowed charging power of 6A per phase as introduced in the IEC 61851 conductive charging standard (International Electrotechnical Commission, 2017). The information from the DSO proved to be correct for Austrian Grid 3 & 4, the problems that were observed with respect to voltage levels were far more severe for Austrian Grid 4 where the DSO expects problems with further integration of EVs in the future.

In Figure 44 for the EV system penetration of 50 percent a lower minimum voltage is reached than for the EV system penetration of 80 percent. This occurs during the price based and uncontrolled charging control. While this might seem odd at first, the behaviour is specific to the way the simulation was set up and can easily be explained. The grid as well as the chargers were simulated with 3 phases. Some of the vehicles however, do not charge using

all 3 phases. Some vehicles charge using only 1 phase or 2 phases. To accommodate for this fact at chargers that have several slots, like semi-public chargers in multi home car parks or public charging stations, each charging slot was assigned a particular single phase and 2 phase configurations (using for instance phase 1 for all single-phase charging events or using phase 2 and 3 for all 2 phase charging events) for all simulations. Now with higher penetration of EVs a situation can occur where a charging slot is already occupied when a vehicle arrives resulting in an arriving vehicle to charge in a different slot for a higher EV penetration. This can result in a beneficial voltage effect if an already affected phase is not used because of an already occupied charging slot. This behaviour is not a mistake in the simulation setup, but rather a feature of it, showing that it can highlight problems occurring down to node level for a very realistic setup.

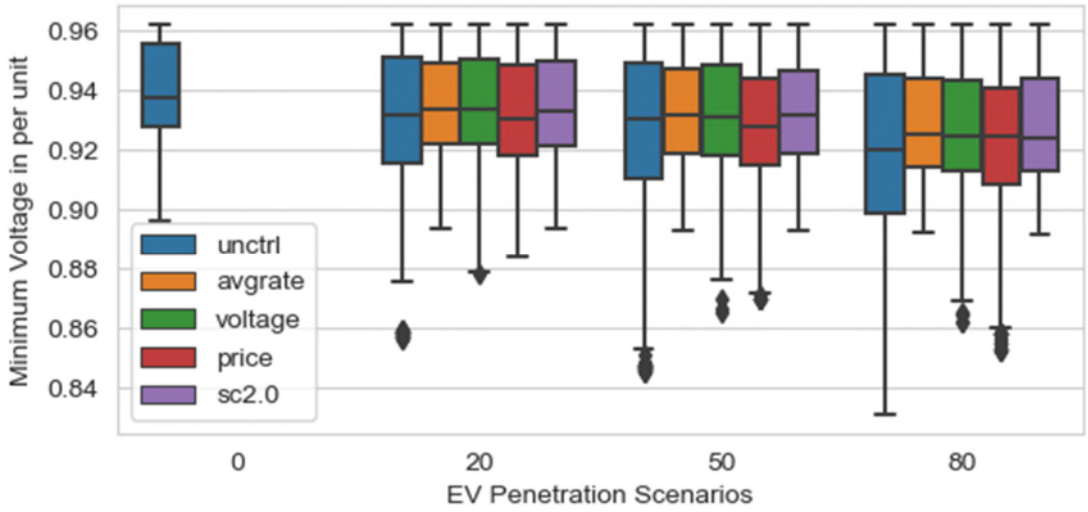

Figure 41: Comparison of minimum voltage per simulation time step for all penetration scenarios and control algorithms Austrian Grid 3, winter.

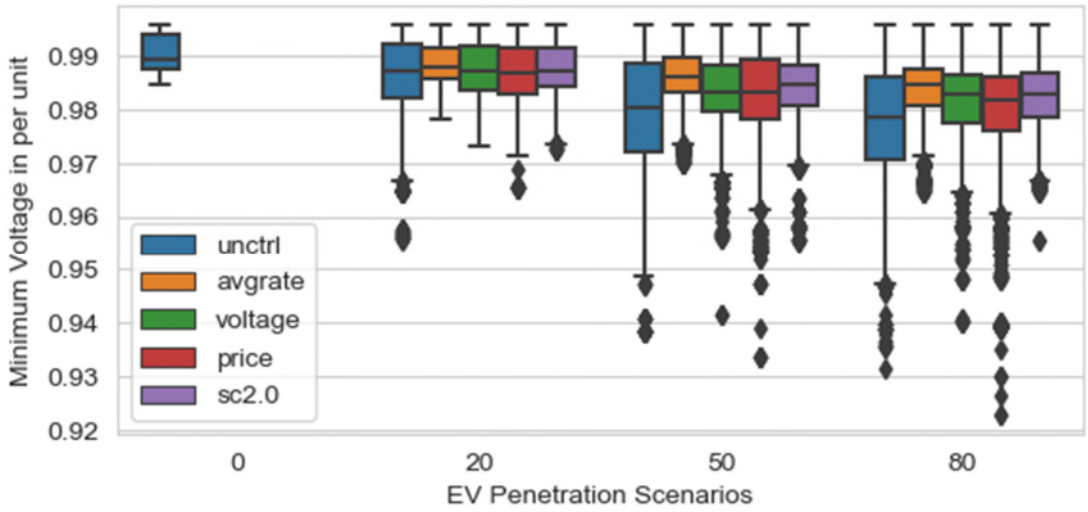

Figure 42: Comparison of minimum voltage per simulation time step for all penetration scenarios and control algorithms Austrian Grid 4, winter.

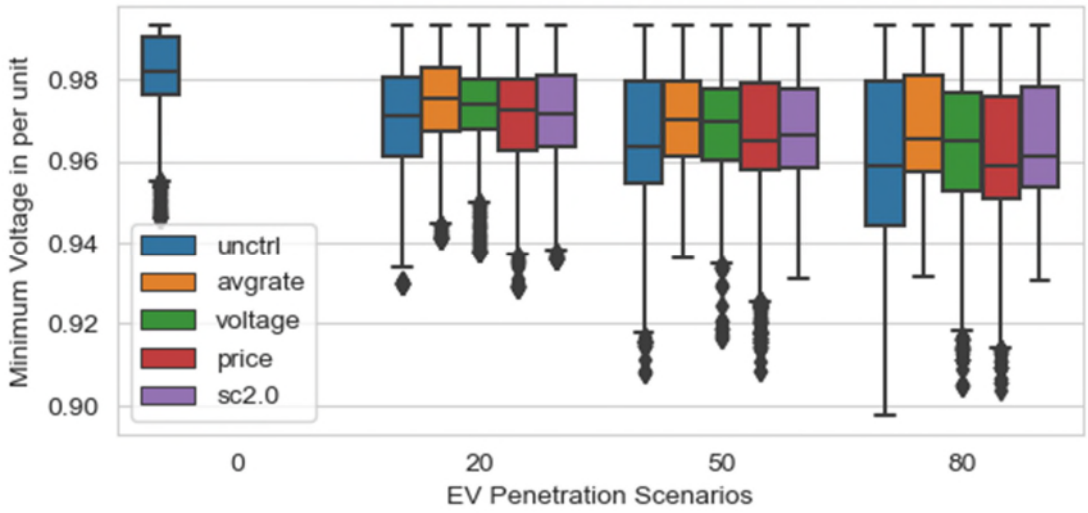

Figure 43: Comparison of minimum voltage per simulation time step for all penetration scenarios and control algorithms Austrian Grid 8, winter.

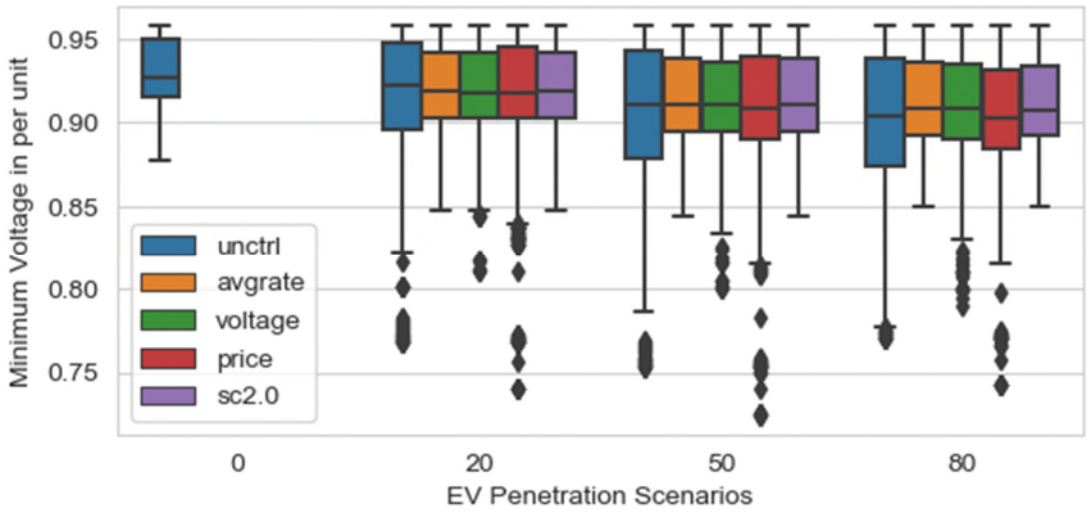

Figure 44: Comparison of minimum voltage per simulation time step for all penetration scenarios and control algorithms Austrian Grid 9, winter.

Figure 45 to Figure 48 show the maximum line loading throughout the simulations for the suburban Austrian Grids. There is some improvement for most of the simple smart charging algorithms, but the improvement is rather small in most cases. As the maximum line loading already seems high in the cases of Austrian Grid 3, 8 and 9, even without any charging EVs, it is reasonable to assume that there might be some bottlenecks in the grid infrastructure that will have to be reinforced in any case.

The smart charging algorithm SCv2.0 provided the best results of all investigated charging schemes. It was the only algorithm that was able to reduce critical situations for almost all grids. Only for Austrian Grid 9 there were critical situations, but these occurred in the case without any vehicles as well and the algorithm was not able to mitigate this behaviour.

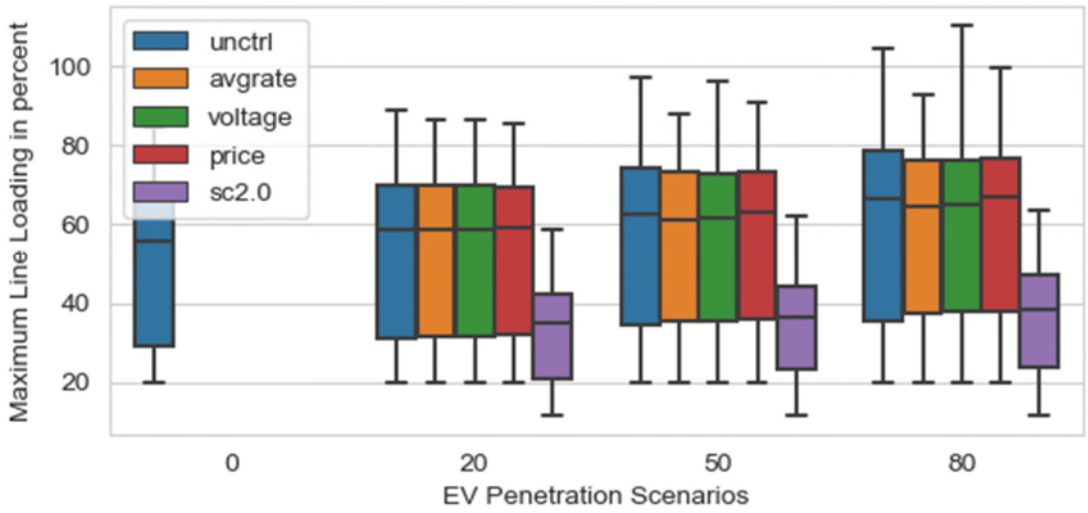

Figure 45: Comparison of maximum line loading per simulation time step for all penetration scenarios and control algorithms Austrian Grid 3, winter.

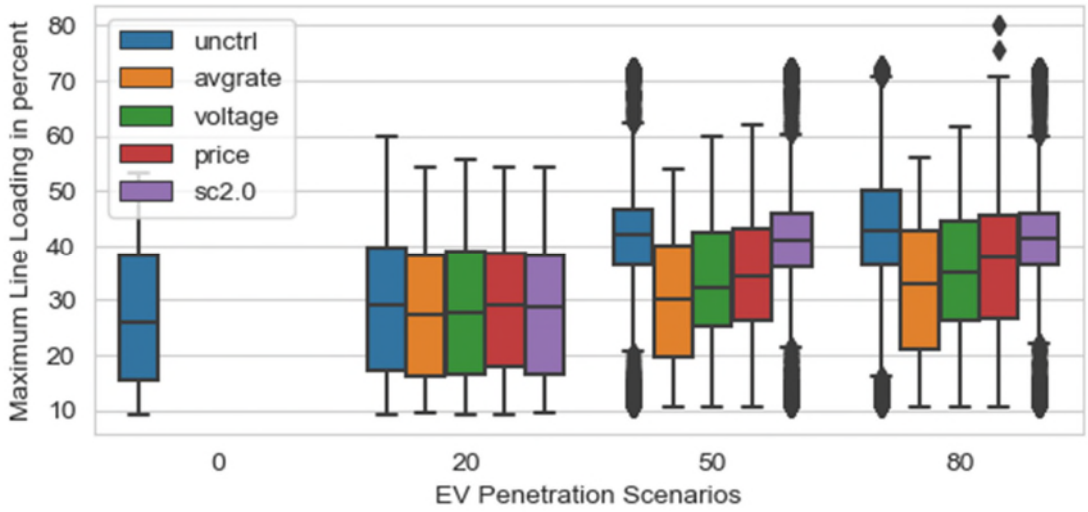

Figure 46: Comparison of maximum line loading per simulation time step for all penetration scenarios and control algorithms Austrian Grid 4, winter.

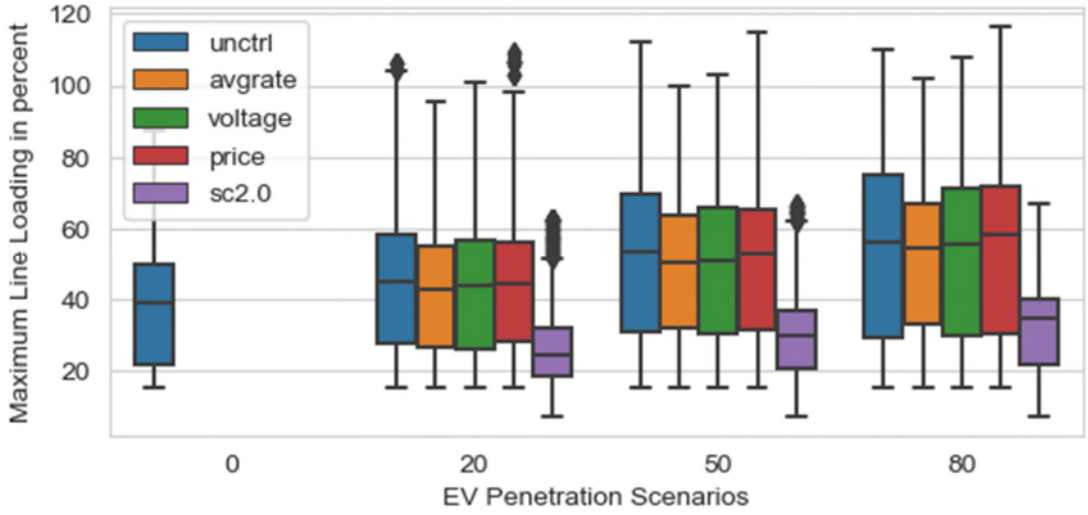

Figure 47: Comparison of maximum line loading per simulation time step for all penetration scenarios and control algorithms Austrian Grid 8, winter.

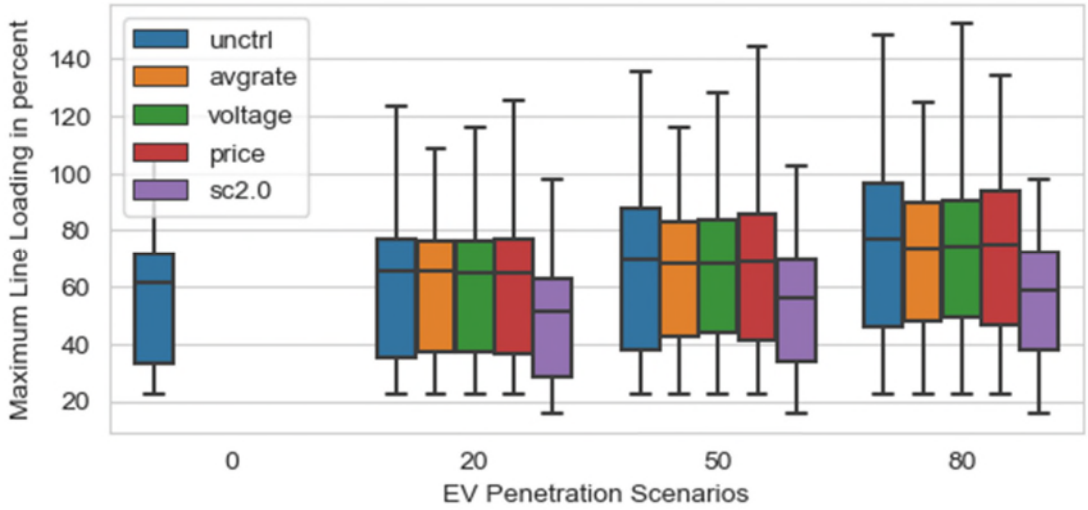

Figure 48: Comparison of maximum line loading per simulation time step for all penetration scenarios and control algorithms Austrian Grid 9, winter.

Figure 49 to Figure 52 shows the transformer loading throughout the simulations for the suburban grids in Austria. For the transformer loading, the situation is similar to the situation for the maximum line loading. There is an increase in loading visible in higher EV penetration scenarios, but it is not as critical as node voltage levels. The average rate algorithm and the smart charging algorithm v2.0 offer the best results. For Austrian Grid 3, 4 and 9 the price-based algorithm observes the second-best results, with the voltage-based algorithm fairing the worst. This seems surprising, because the price-based algorithm should lead to more EVs charging at the same time when prices are lower. The differences however are not huge and are probably down to several charging events being delayed due to low voltage levels in parts of the grid, resulting in higher EV charging load when more charging events are taking part simultaneously.

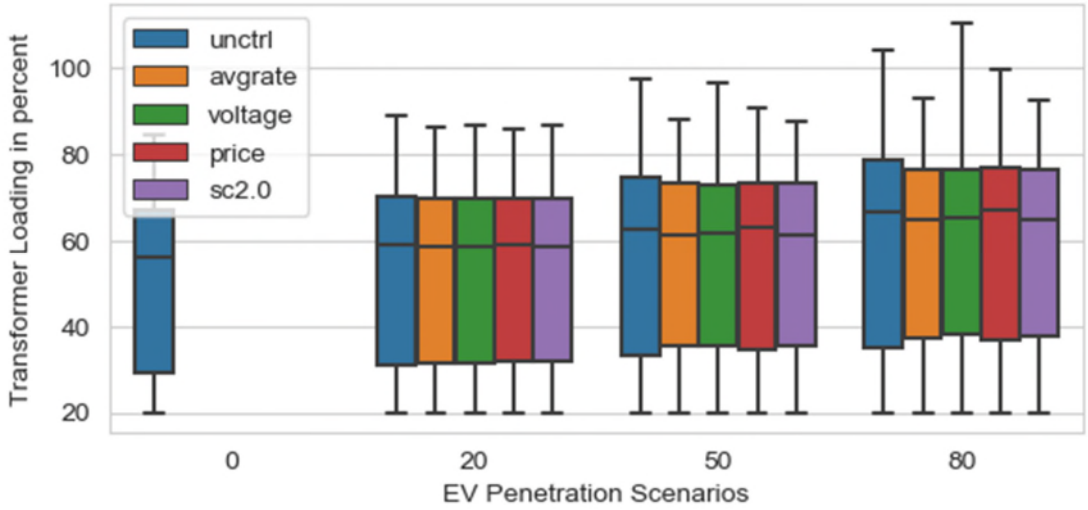

Figure 49: Comparison of transformer loading per simulation time step for all penetration scenarios and control algorithms Austrian Grid 3, winter.

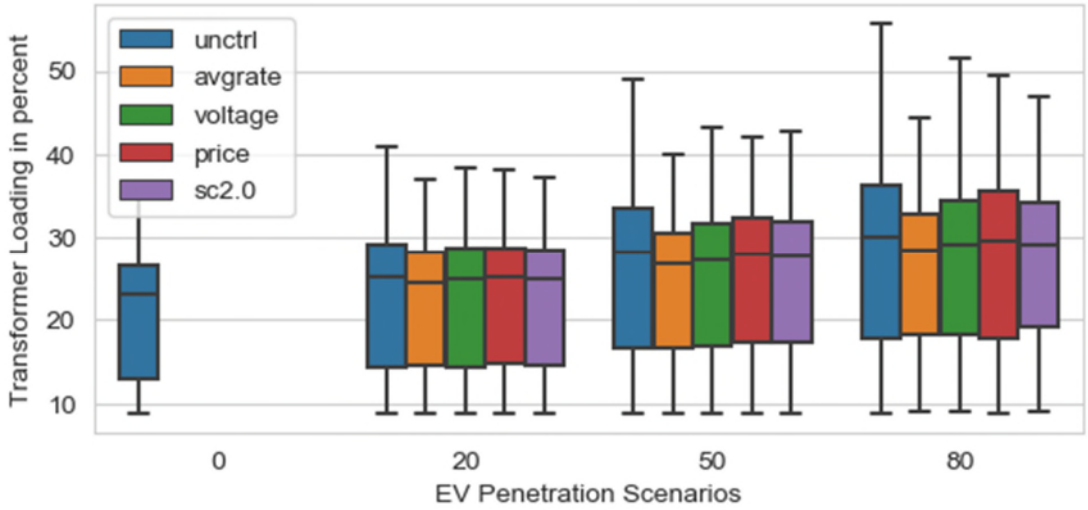

Figure 50: Comparison of transformer loading per simulation time step for all penetration scenarios and control algorithms Austrian Grid 4, winter.

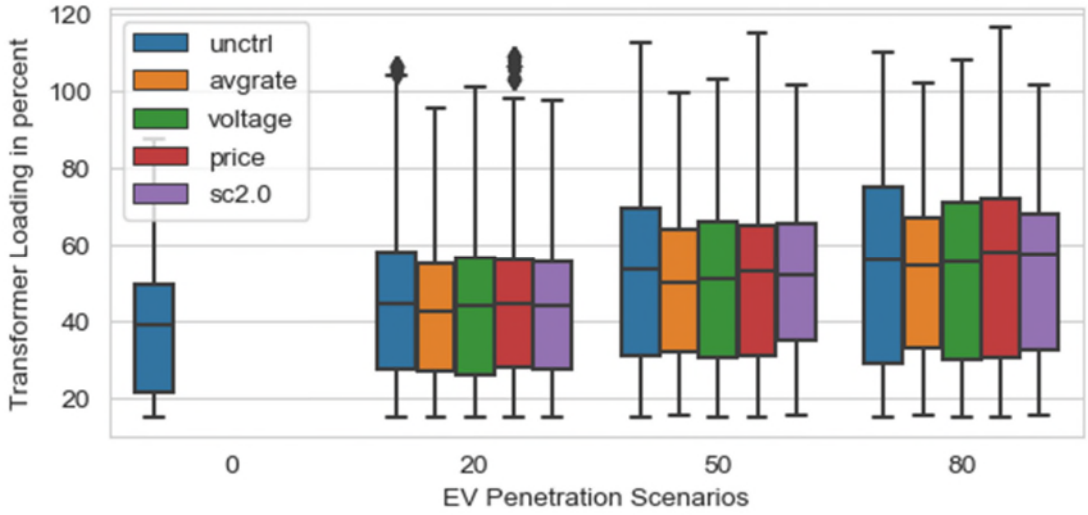

Figure 51: Comparison of transformer loading per simulation time step for all penetration scenarios and control algorithms Austrian Grid 8, winter.

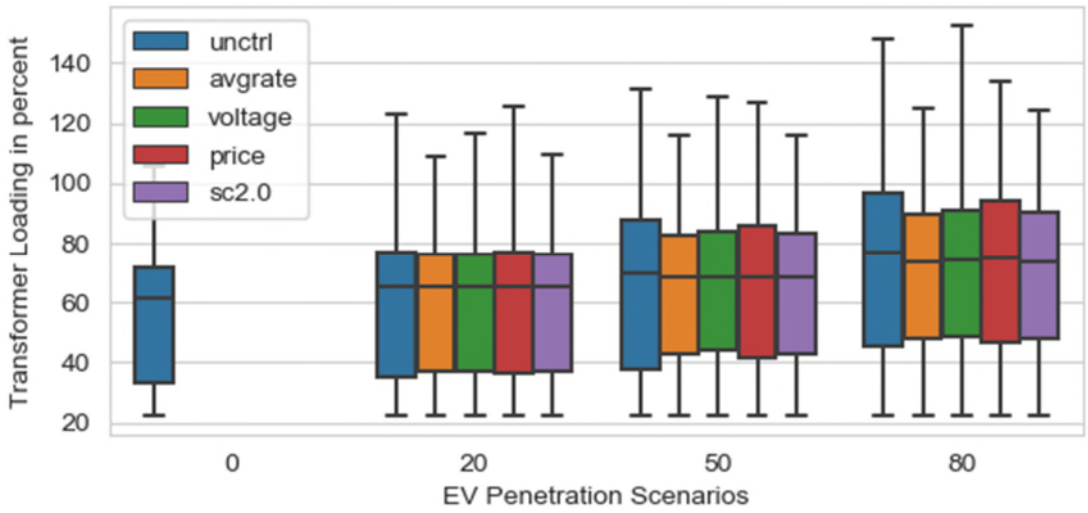

Figure 52: Comparison of transformer loading per simulation time step for all penetration scenarios and control algorithms Austrian Grid 9, winter.

Figure 53 to Figure 56 show the achieved charging even prices throughout all simulations using the suburban Austrian grids. It can be seen that the achieved prices are mostly very similar, but considering that no other algorithm than the smart charging algorithm could in reality have access to the prices at an intraday market that were used to accumulate the price results presented here, there is an inherent advantage of the smart charging algorithm over the simple smart charging algorithms, being able to achieve better energy prices for the charging EVs.

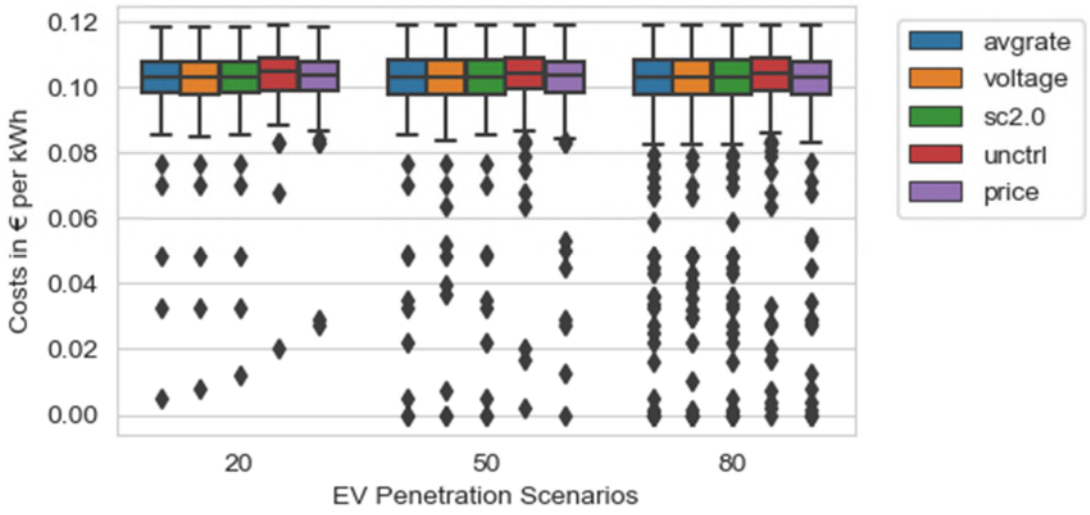

Figure 53: Comparison of charging costs per charging event for all penetration scenarios and control algorithms Austrian Grid 3, winter.

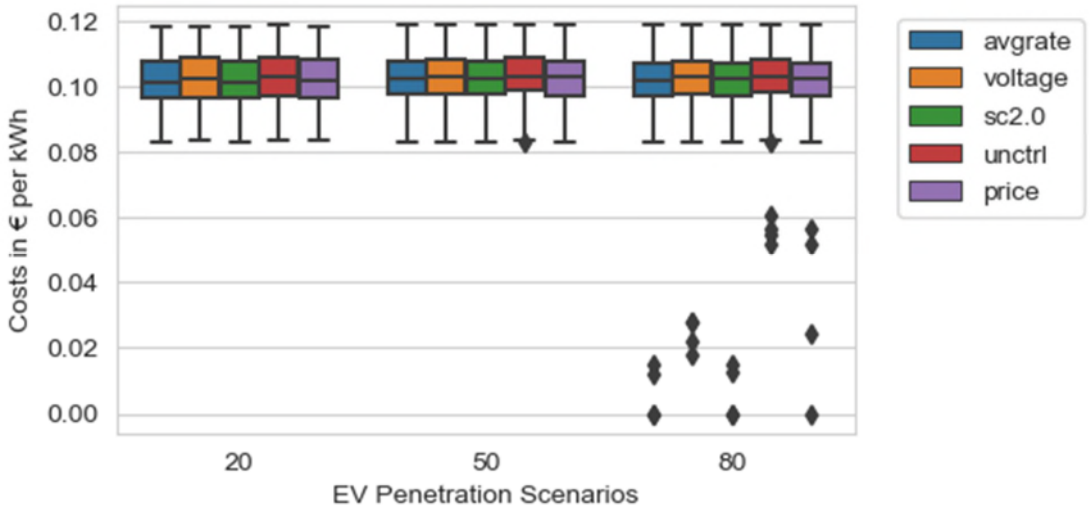

Figure 54: Comparison of charging costs per charging event for all penetration scenarios and control algorithms Austrian Grid 4, winter.

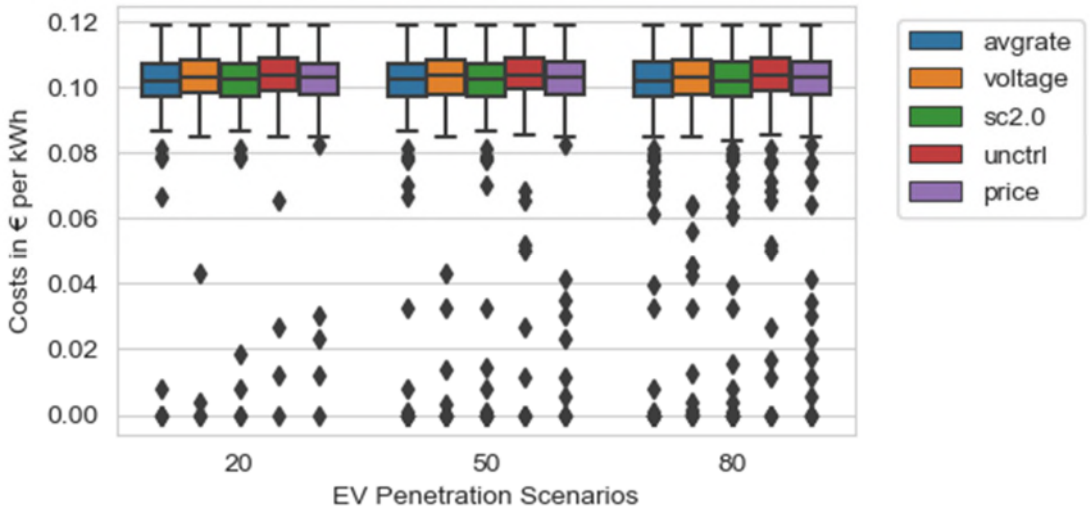

Figure 55: Comparison of charging costs per charging event for all penetration scenarios and control algorithms Austrian Grid 8, winter.

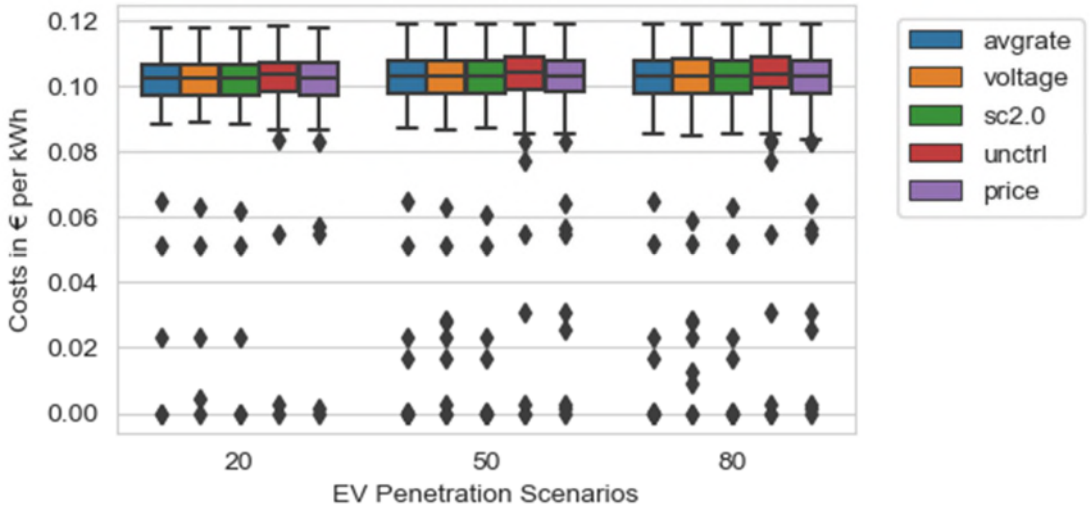

Figure 56: Comparison of charging costs per charging event for all penetration scenarios and control algorithms Austrian Grid 9, winter.

Figure 57 to Figure 60 show the amount of completed charging events and the average state at the end of each charging event for all suburban Austrian grids. It can be seen that all smart charging schemes perform worse than uncontrolled charging. The worst performing in terms of state of charge is the average rate charging control followed by the SCv2.0 smart charging. Considering the very good performance of SCv2.0 with regards to grid performance indicators it probably performs best considering both grid parameters and quality of service measured by the average state of charge.

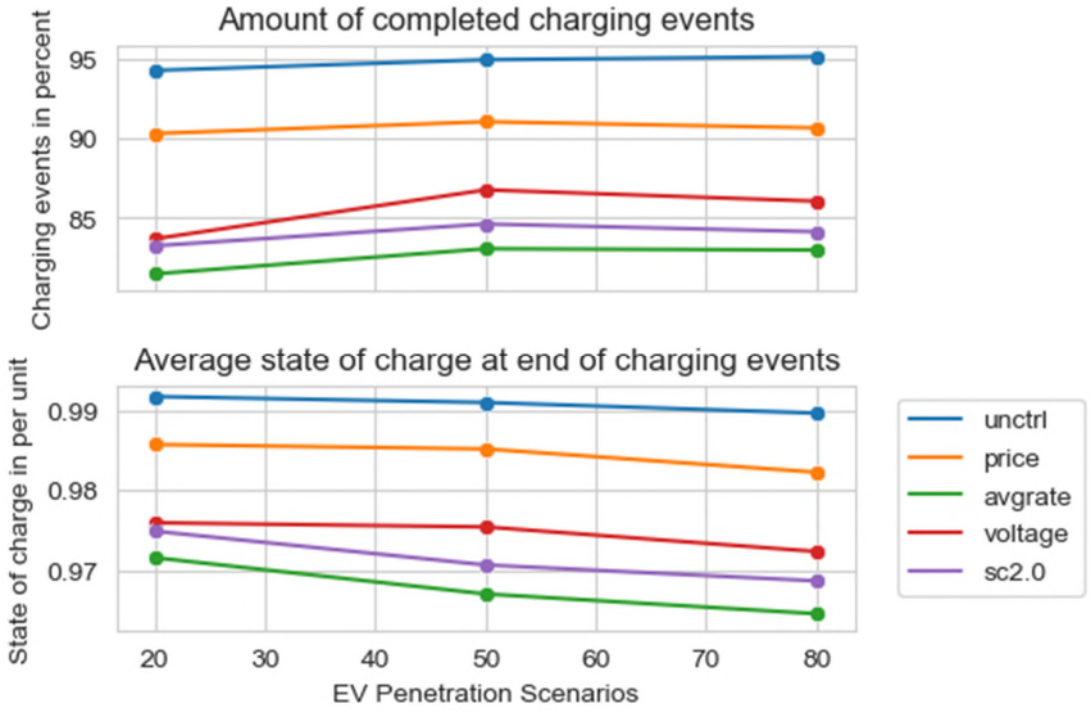

Figure 57: Comparison of completed charging events and average state of charge at the end of charging events for all penetration scenarios and control algorithms Austrian Grid 3, winter.

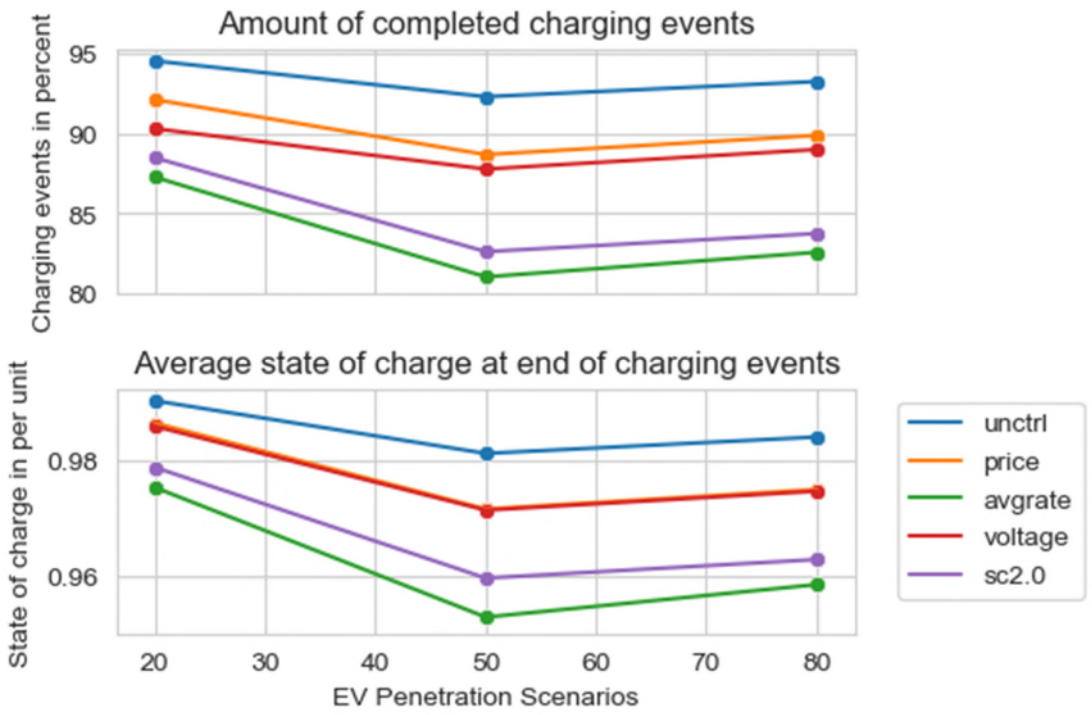

Figure 58: Comparison of completed charging events and average state of charge at the end of charging events for all penetration scenarios and control algorithms Austrian Grid 4, winter.

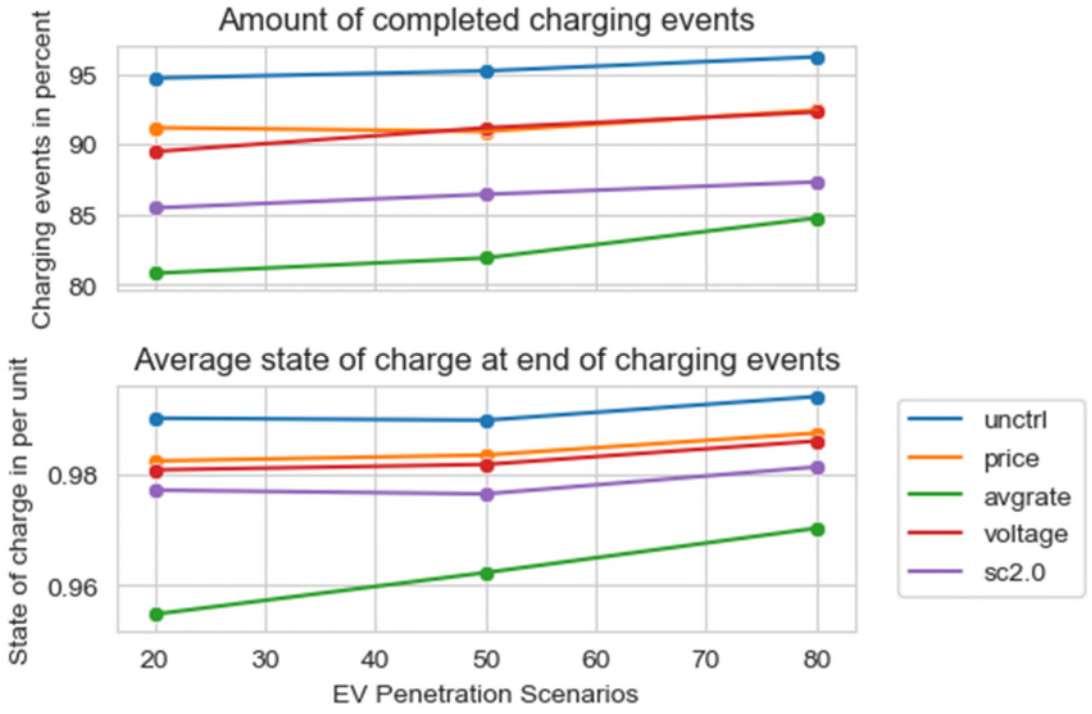

Figure 59: Comparison of completed charging events and average state of charge at the end of charging events for all penetration scenarios and control algorithms Austrian Grid 8, winter.

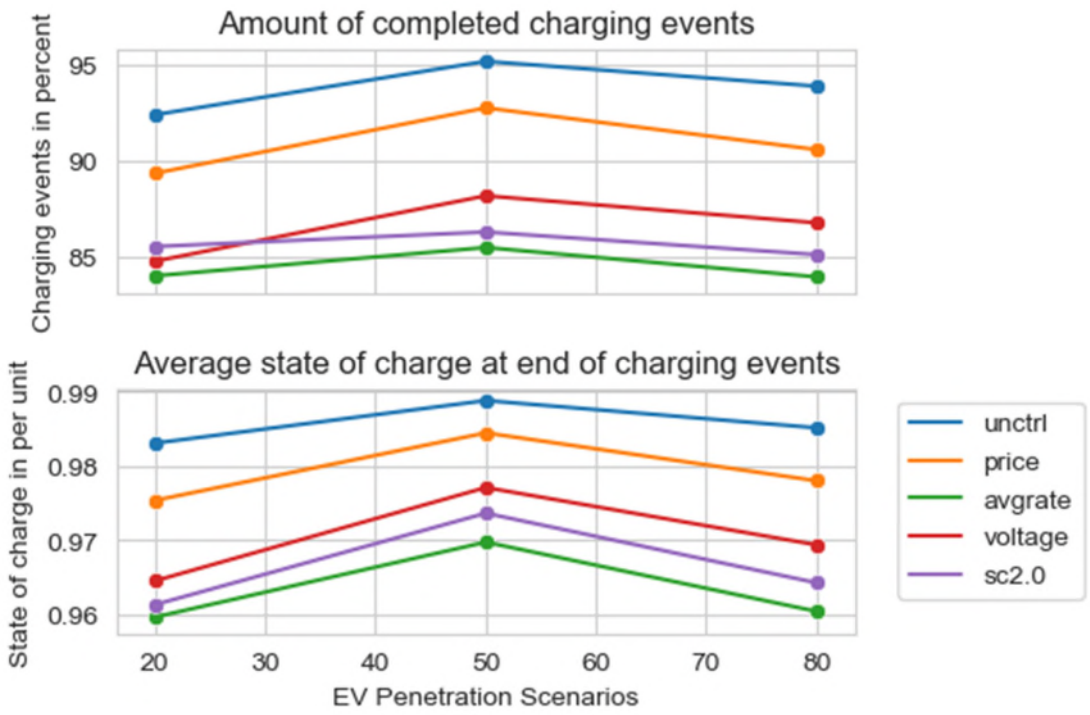

Figure 60: Comparison of completed charging events and average state of charge at the end of charging events for all penetration scenarios and control algorithms Austrian Grid 9, winter.

7.3 Urban Grids

For the investigation of urban grids in Austria 3 grids were used in the co-simulation setup. The key parameters for the different grids are summarised in the following table.

Urban Austrian Grids			
Grid	Austrian Grid 5	Austrian Grid 6	Austrian Grid 7
Problems expected	yes	no	-
Annual electricity demand	1379 MWh	1532 MWh	1052 MWh
Transformer capacity	2*630 kVA	2*630 kVA	1*400 kVA
Number of nodes	96	38	178
Number of households	451	344	274
Average line length	27 m	27 m	31 m
Total length longest feeder	491 m	314 m	431 m
Number of nodes equipped with PV	3	1	11
Total installed PV power	10 kVA	30 kVA	50 kVA

The observed minimum voltage throughout the respective grid are visualised in Figure 61 to Figure 63. For Austrian Grid 5, the minimum voltage was very similar for all charging methods and penetrations, with the smart charging algorithm and the average rate algorithm outperforming the other algorithms slightly. This could be accounted to the grid topology as well as the effect of the implemented 3 phase charger setup, described in the previous section. For the Urban grids, the voltage drop was smaller than for suburban and rural grids, this could be the result of the shorter average line lengths and shorter longest feeders relative to the suburban and rural grids. Overall the average rate and the smart charging algorithm version 2.0 proved to be the best control schemes. For smaller penetrations there is not a lot of difference between the different charging methods, but the differences become more apparent with higher EV penetrations.

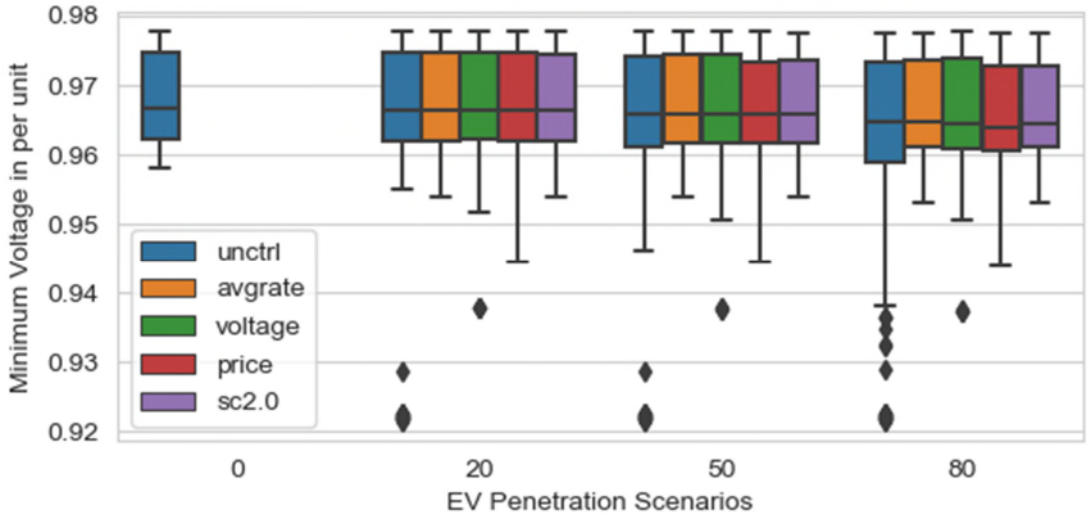

Figure 61: Comparison of minimum voltage per simulation time step for all penetration scenarios and control algorithms Austrian Grid 5, winter.

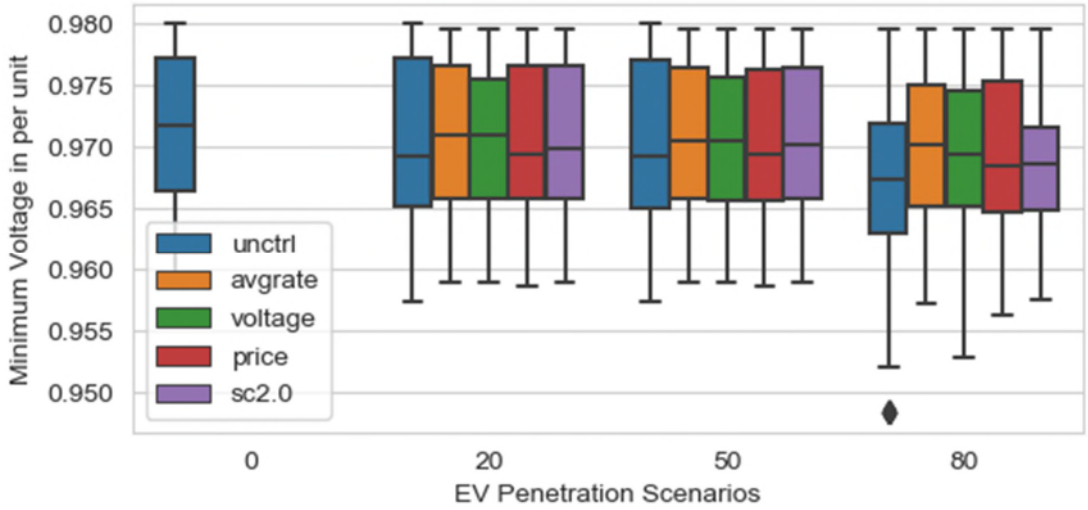

Figure 62: Comparison of minimum voltage per simulation time step for all penetration scenarios and control algorithms Austrian Grid 6, winter.

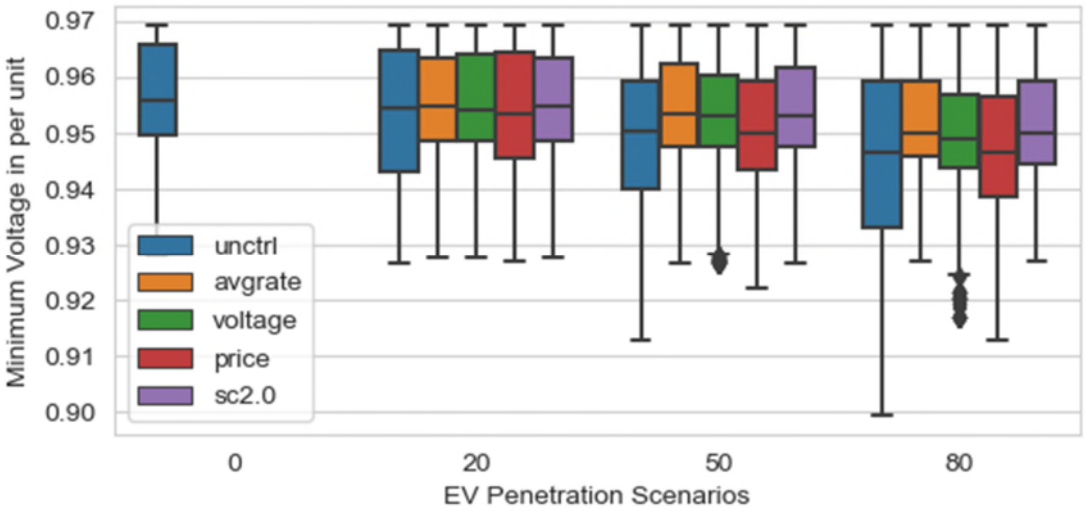

Figure 63: Comparison of minimum voltage per simulation time step for all penetration scenarios and control algorithms Austrian Grid 7, winter.

The observed maximum line loadings throughout the simulations for Austrian Grid 5, 6 and 7 are shown in Figure 64, Figure 65 and Figure 66 respectively. While some improvements over the uncontrolled charging scenario can be observed for Austrian Grid 5, for Austrian Grid 6 there is virtually no difference in terms of line loading. For Austrian Grid 7 the loading is reduced substantially through all simple smart charging schemes as well as the smart charging scenario.

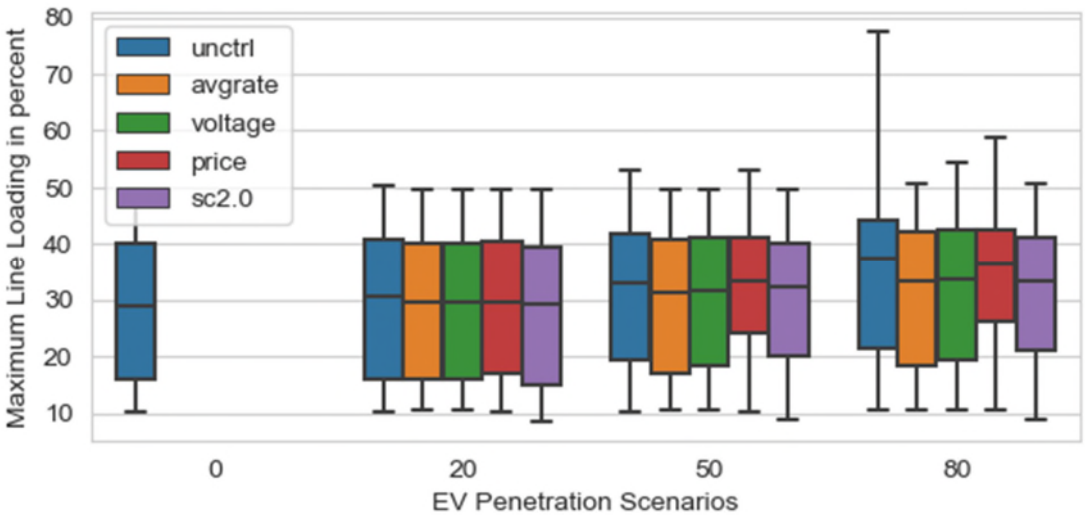

Figure 64: Comparison of maximum line loading per simulation time step for all penetration scenarios and control algorithms Austrian Grid 5, winter.

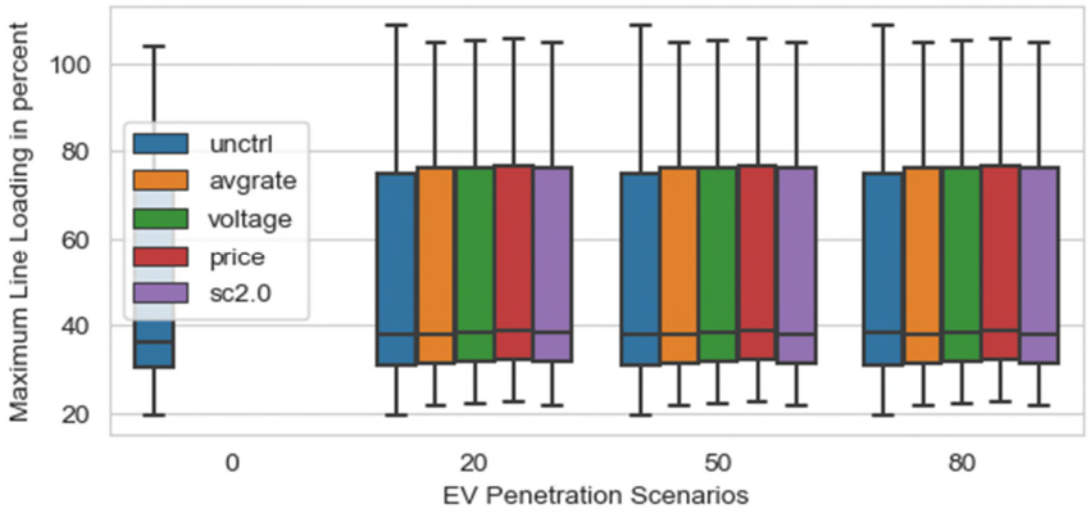

Figure 65: Comparison of maximum line loading per simulation time step for all penetration scenarios and control algorithms Austrian Grid 6, winter.

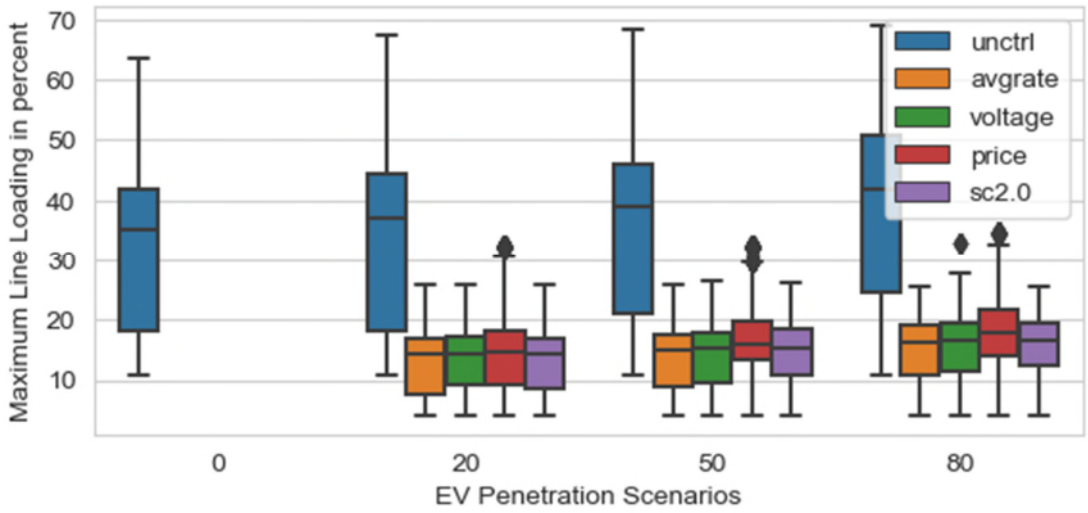

Figure 66: Comparison of maximum line loading per simulation time step for all penetration scenarios and control algorithms Austrian Grid 7, winter.

Figure 67 to Figure 69 show the transformer loading results for the Urban Austrian Grid simulations.

Like the line loading results, the results are not becoming a lot worse with increasing EV penetration. Therefor it can be concluded, that for the presented urban grids, transformer loading and line loading seem to be less critical grid related performance indicator.

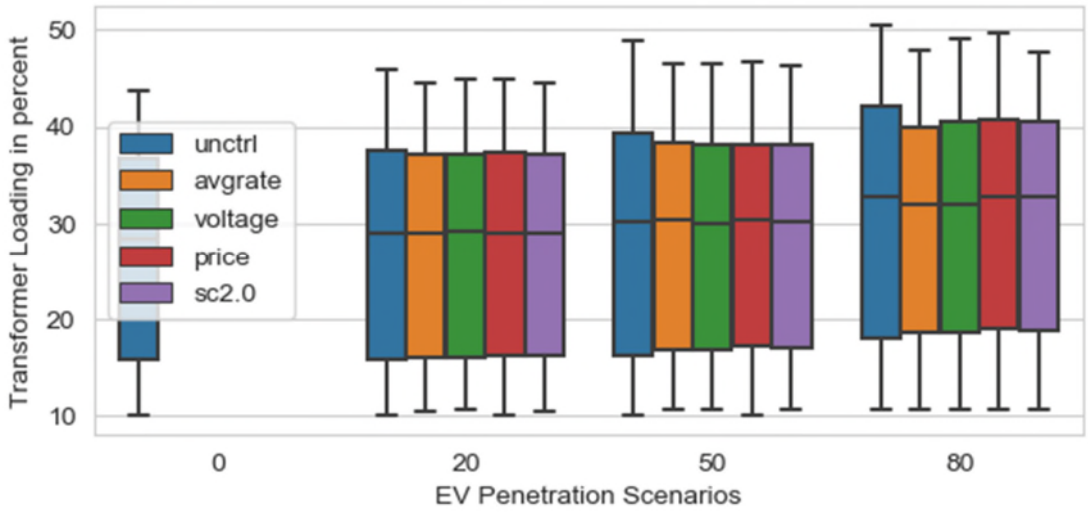

Figure 67: Comparison of transformer loading per simulation time step for all penetration scenarios and control algorithms Austrian Grid 5, winter.

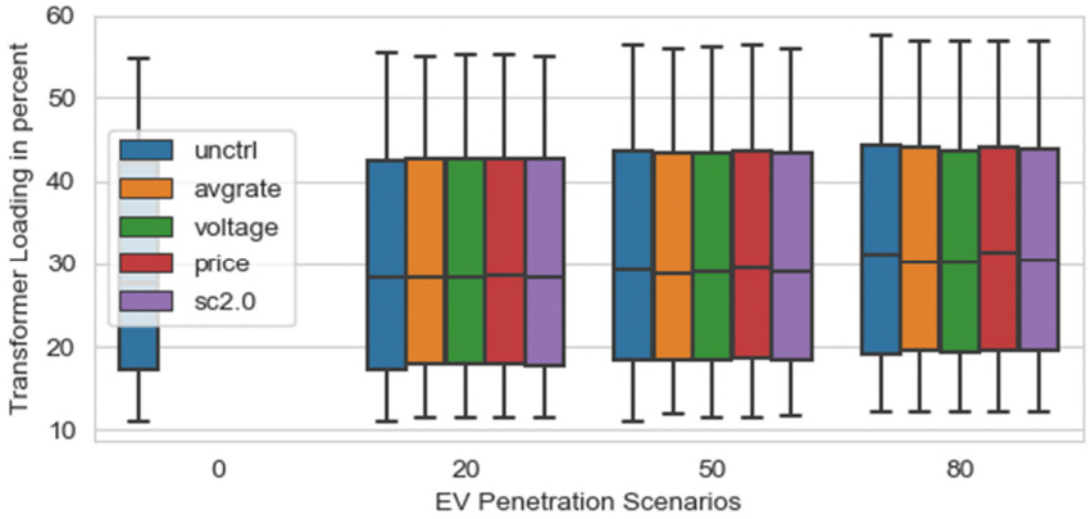

Figure 68: Comparison of transformer loading per simulation time step for all penetration scenarios and control algorithms Austrian Grid 6, winter.

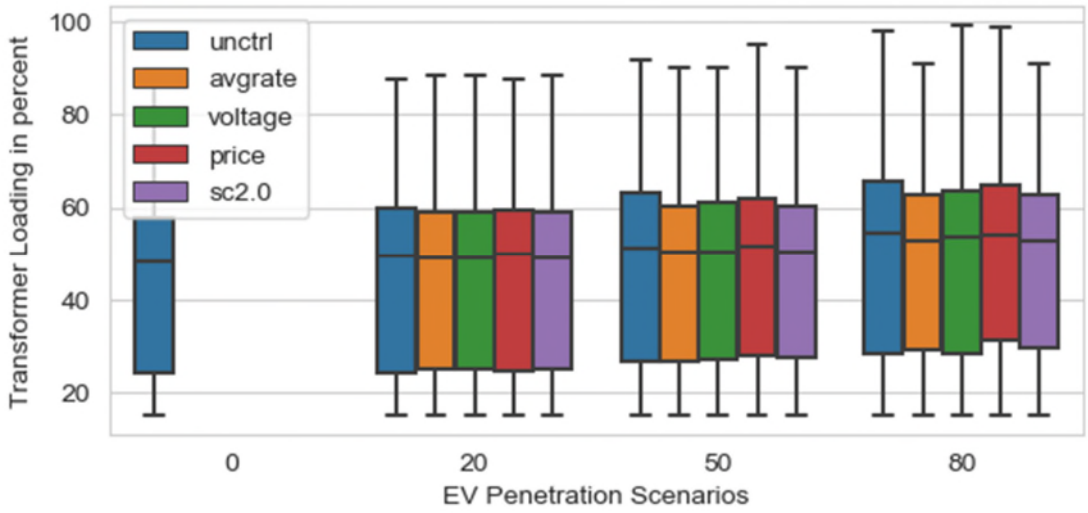

Figure 69: Comparison of transformer loading per simulation time step for all penetration scenarios and control algorithms Austrian Grid 7, winter.

Figure 70, Figure 71 and Figure 72 show the individual costs per charging event in € per kWh for all simulations conducted for Austrian Grid 5, 6 and 7 respectively. Like for the suburban and rural Austrian Grid simulations the prices seem to be very similar for all different smart charging schemes. Being able to buy energy through an aggregator at the intraday market will however provide a large improvement over standard energy procurement contracts as was explained in the previous sections.

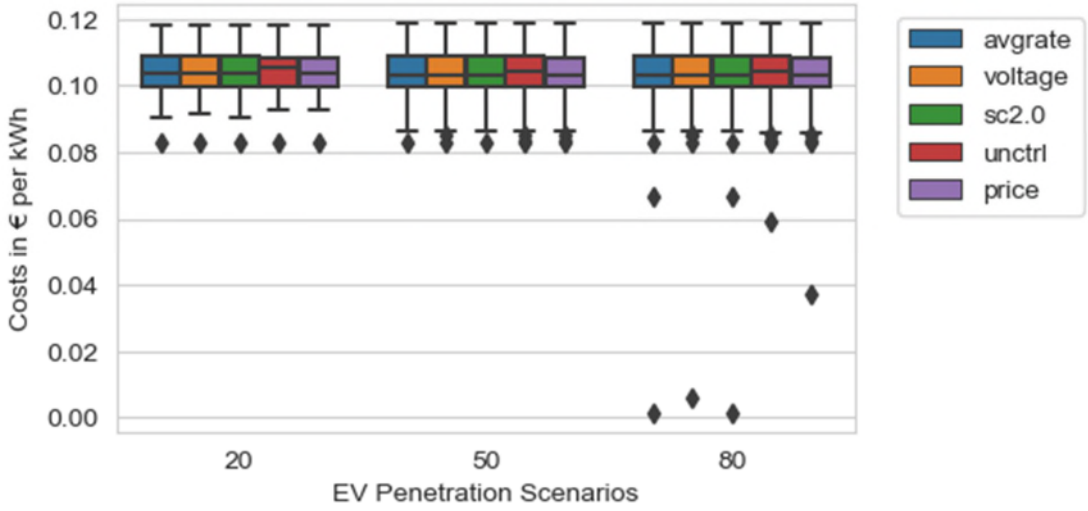

Figure 70: Comparison of charging costs per charging event for all penetration scenarios and control algorithms Austrian Grid 5, winter.

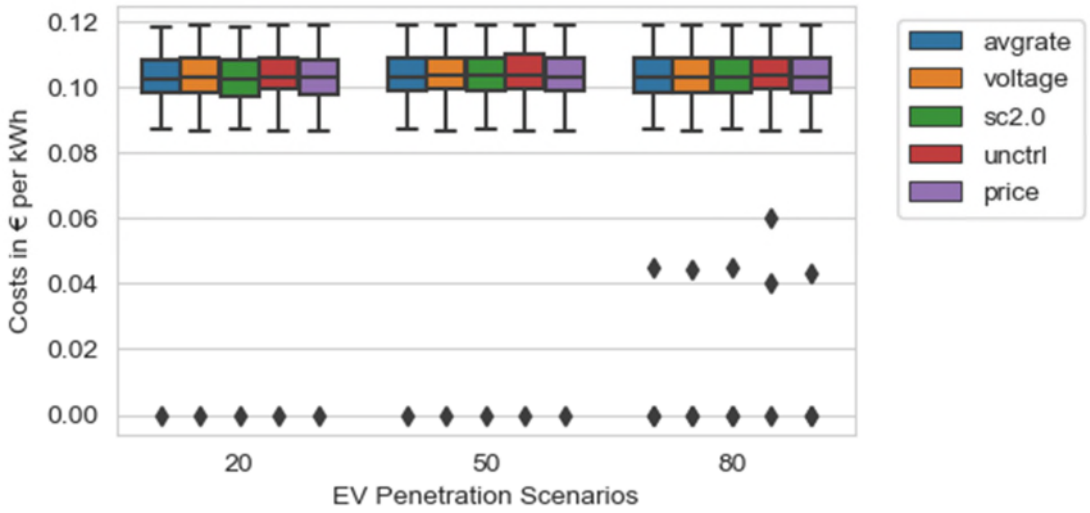

Figure 71: Comparison of charging costs per charging event for all penetration scenarios and control algorithms Austrian Grid 6, winter.

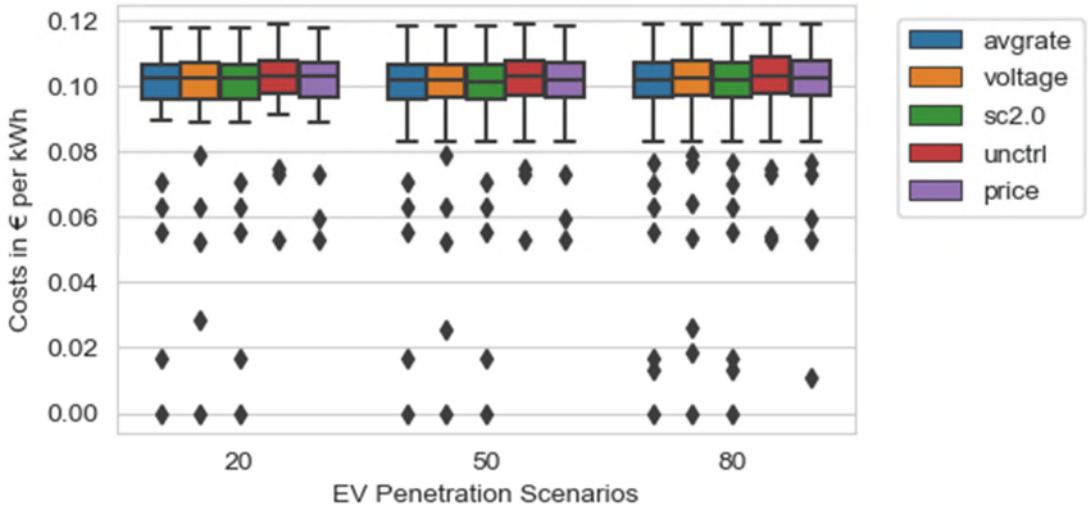

Figure 72: Comparison of charging costs per charging event for all penetration scenarios and control algorithms Austrian Grid 7, winter.

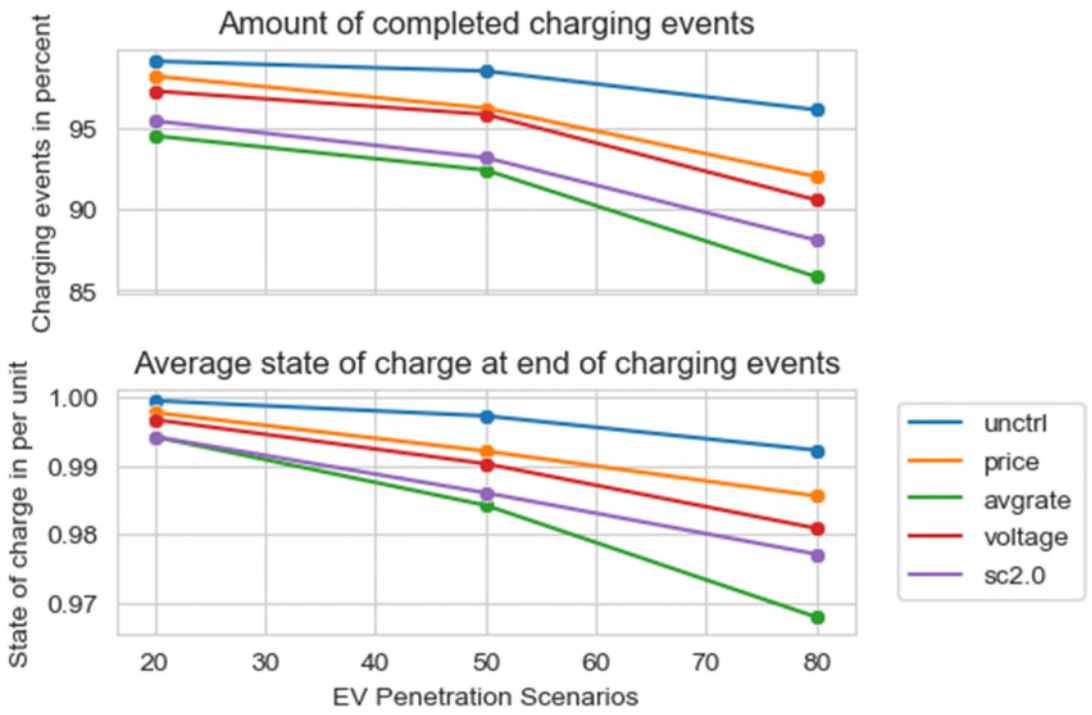

Figure 73: Comparison of completed charging events and average state of charge at the end of charging events for all penetration scenarios and control algorithms Austrian Grid 5, winter.

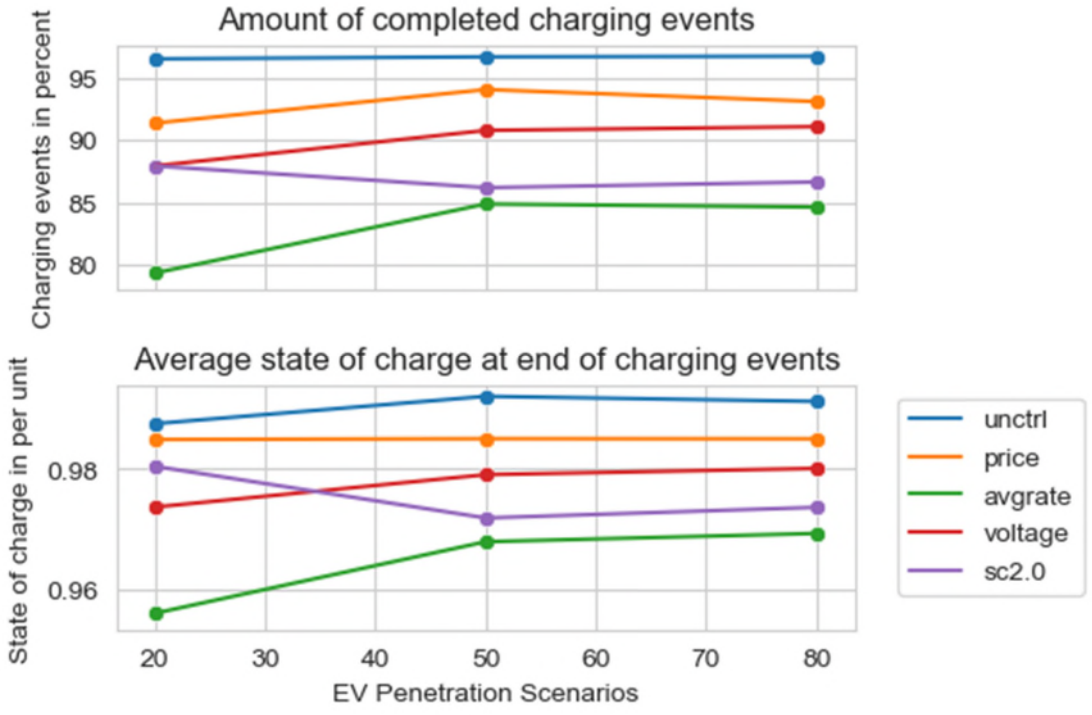

Figure 74: Comparison of completed charging events and average state of charge at the end of charging events for all penetration scenarios and control algorithms Austrian Grid 6, winter.

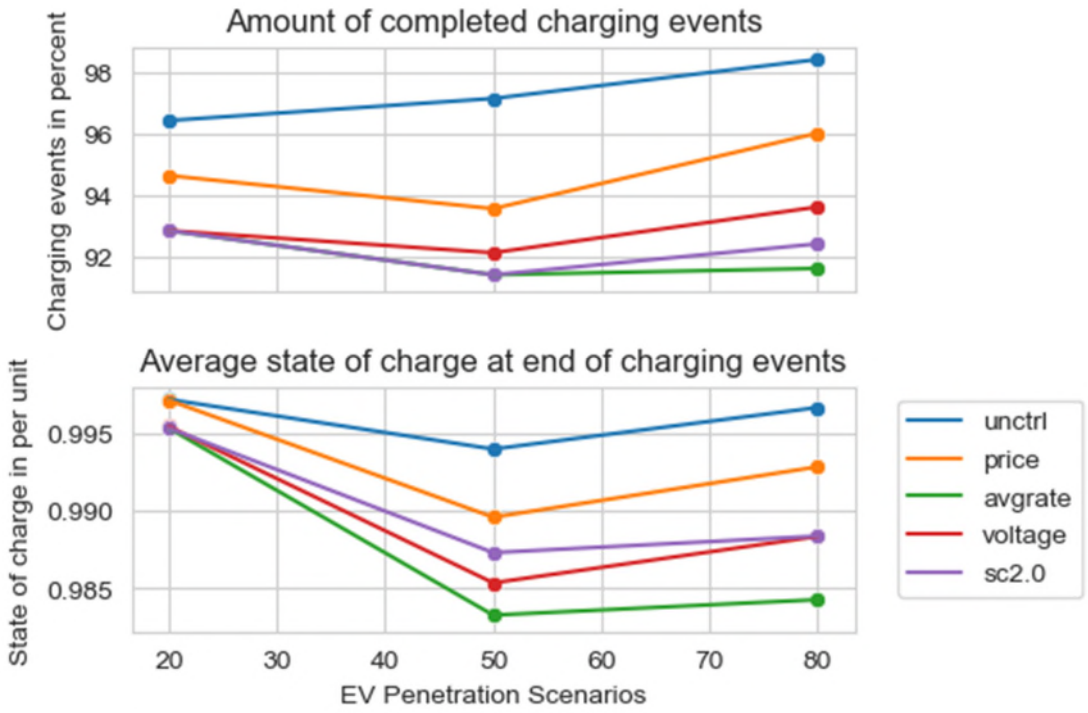

Figure 75: Comparison of completed charging events and average state of charge at the end of charging events for all penetration scenarios and control algorithms Austrian Grid 7, winter.

8. Simulation Results – Germany (AIT part)

To study the effects of the smart charging algorithm on typical German grids 6 different grids were modelled, 3 by the Technical university of Delft and 3 by AIT. As well as for the Dutch and Austrian Grids the Grids are separated into 3 categories, rural, suburban and urban grids.

8.1 Rural Grids

For the investigation of rural grids in Germany, one grid was modelled by AIT. The key facts concerning the grids are shown in the following table.

Table 4 Parameters of German rural grid with no expected problems

Rural German Grids	
Grid	German Grid 1
Problems expected	no
Transformer capacity	250 kVA
Annual electricity demand	42 MWh
Number of nodes	52
Number of households	12
Average line length	10 m

Figure 76 shows the minimum voltage throughout simulations for German Grid 1 with different charging controls implemented. The average rate charging scheme shows the best results, while none of the other charging controls ever reached a critical point throughout the simulations.

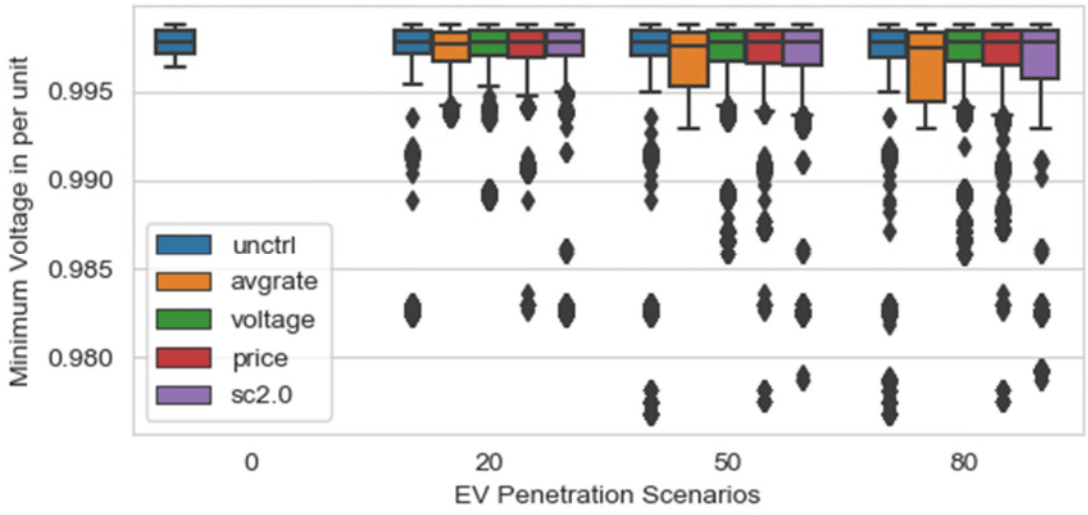

Figure 76: Comparison of minimum voltage per simulation time step for all penetration scenarios and control algorithms German Grid 1, winter.

The maximum line loading observed throughout simulations for different EV penetrations is visualised in Figure 77. As well as for the voltage level, the average rate charging shows the

least critical behaviour while no other control scheme results in any critical level throughout the simulations.

Figure 77: Comparison of maximum line loading per simulation time step for all penetration scenarios and control algorithms German Grid 1, winter.

In Figure 78 the results for the simulation for different EV penetrations with respect to transformer loading are shown. The average rate algorithm is also performing best here, while no critical situation can be seen at any time.

Figure 78: Comparison of transformer loading per simulation time step for all penetration scenarios and control algorithms German Grid 1, winter.